Master Thesis

DNV GL || Universitat Politècnica de Catalunya

Master in Energy Engineering

Harmonic Interactions in HVAC-Connected Offshore Windfarms

Author: Lara Depla

Supervisors:
Eduardo Prieto-Araujo
Roger Cremers
Konstantinos Velitsikakis

June 24, 2019

Acknowledgements

Special thanks to Eduardo Prieto, Marc Cheah, Ricard Ferrer San José and Carlos Collados of CITCEA-UPC for all the help and guidance over the course of this master thesis project. This project could be completed thanks to CITCEA-UPC. I would also like to express my gratitude to Roger Cremers and Konstantinos Velitsikakis of DNV GL for the daily supervision.

Harmonic Interactions in HVAC-Connected Offshore Wind Farms

Lara Depla
DNV GL
Universitat Politècnica de Catalunya || CITCEA-UPC

24-06-2019

Abstract

The connection of new Offshore Wind Power Plants (OWPP) in the existing Dutch transmission system gives rise to many technical challenges. For example, it is expected that harmonic issues will occur more frequently when the number of large offshore wind farms increases. Cases have already been reported in which resonances were triggered in HVDC- or HVAC-connected OWPPs and the wind farms had to be taken out of operation.

Recently developed offshore wind farms contain wind turbines which are connected to the system with a full-scale back-to-back Voltage Source Converter, which is responsible for inserting harmonics into the system. The onshore grid is also responsible for injecting harmonics. Since the wind turbine converter is an active element, where the control loops actively determine its electrical behaviour, it interacts with other converters and with the background harmonics inserted from the network. The initial harmonic emissions and the harmonic interactions can lead to an excitation of a resonance frequency. The cables, transformers, capacitor banks and filters are responsible for shifting the resonance frequencies. Especially a long HV export cable can strongly alter the resonance frequencies of the system.

To analyze the impact of connecting an increasing amount of wind farms to the same Point of Connection on the harmonic emission levels, a Harmonic Impact Assessment was performed for three offshore wind farms in the Dutch North Sea. Since the wind turbine converters are active elements, its electrical behaviour can be captured with an equivalent impedance, or Norton Equivalent. This Norton Equivalent was utilized in the Harmonic Impact Assessment to include the active behaviour of the converter. When comparing this novel approach to the conventional methodology, the expected peaks in the Total Harmonic Distortion (THD) are shifted. When an increasing amount of wind farms is connected, peaks in the THD shifted to lower frequencies. Then, depending on the specific profile of the background harmonics and the impedance profiles of the grid and the OWPP, this translates into the disappearance of appearance of an exceedance of the emission limits.

The effect of connecting two wind farms to the same Point of Connection instead of a single wind farm on the harmonic stability, was assessed. Frequency sweeps of the two assessed wind farms made clear that the presence of an additional filter in a wind farm leads to a small shift in the series resonance points. When multiple wind farms are connected instead of solely one wind farm, series resonance frequencies are shifted to lower frequencies and less damping appears to be present in the system.

Lastly, the postive-net damping criteria was applied to assess the stability of a system in which a varying number of wind farms is connected. Time-domain simulations in PSCAD were performed to varify the results. It can be concluded that a system becomes less damped, and therefore less stable, when an increasing amount of wind farms is connected. This effect arises since the various wind farms are placed in parallel and the total resistance of the wind farms becomes smaller than the sum of the resistances of each wind farm. Moreover, when less wind turbines are in operation, less damping is present in the system since the resistance of a single OWPP is then decreased.

Contents

List of Figures

List of Tables

List of Abbreviations

AC	Alternating Current
DC	Direct Current
FDNE	Frequency Dependent Network Equivalent
FFT	Fast Fourrier Transform
HVAC	High Voltage Alternating Current
HVDC	High Voltage Direct Current
HV	High Voltage
OWPP	Offshore Wind Power Plant
PCC	Point of Common Coupling
PI	Proportional Integral
PLL	Phase-Locked Loop
POC	Point of Connection
POE	Point of Evaluation
PSCAD	Power System Computer Aided Design
PWM	Pulse-Width Modulation
THD	Total Harmonic Distortion
TOV	Temporary Overvoltage
TSO	Transmission System Operator
VSC	Voltage Source Converter
WTG	Wind Turbine Generator
WT	Wind Turbine

1 Introduction

1.1 Background

The Dutch electrical power generation landscape is changing rapidly. The Dutch government intends to increase the amount of renewable energy sources significantly in the years to come. This objective partially includes the realization of a number of large Offshore Wind Power Plants (OWPP) in the Dutch North Sea. Several HVAC-connected offshore wind farms with a capacity of 700 MW will start operating by 2020. The Dutch Transmission System Operator (TSO) TenneT is developing several HVDC-connected wind farms with similar or even larger capacities [1].

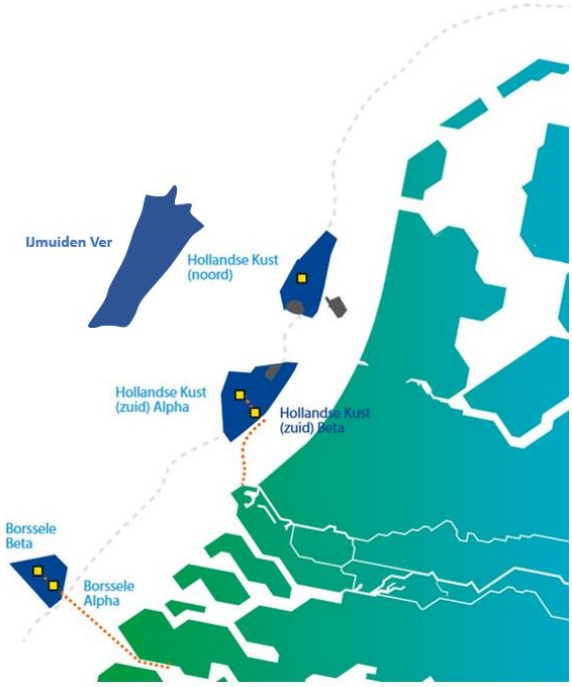

Figure 1: Several wind farms in the North Sea which are currently developed or which have already been developed [2].

The connection of such new offshore wind farms to the existing Dutch transmission system gives rise to many technical challenges. For example, TSOs have to cope with the impact of new wind farms on the harmonic behaviour of the power system. It is expected that the harmonic issues will occur more frequently if the number of large offshore wind farms increases. This increase will lead to a larger number of converters, a higher system capacitance due to the use of long HVAC cables, less inertia in the power system and more filter installations. An example of a failure incident due to harmonic interaction is the BorWin-1 installation [3]. Resonances in the offshore grid triggered

high frequency oscillations which had destructive effects and obliged to temporarily de-energize the HVDC link [4]. Moreover, harmonic resonance issues have also been present in HVAC-connected wind farms in Texas and China [5]. The latter seems to be related to the presence of series capacitive lines close to the wind farms in question. It can be very costly to take the wind farm temporarily out of operation. Therefore, the occurrence of harmonic resonance issues poses risks to wind farm developers and transmission system operators.

In theory, potential harmonic problems can be analyzed for each individual wind farm and solutions can be studied and evaluated to mitigate the potential problems related to an OWPP. However, the problem becomes much more complex when multiple wind farms need to be taken into account. Moreover, the effect of mitigation measures at one specific wind farm may be diminished by multiple wind farms connected to the same Point of Connection (POC). Concerns exist also with regards to the expected harmonic interactions between the wind turbines, filters, converters and the connection to the shore. Therefore, an increasing need for an integral approach for the execution of harmonic studies is expected.

1.2 Objectives and Scope

The overall objective of this research project is to study the consequences of connecting an increasing amount of wind farms at the same Point of Connection (POC) when considering harmonic issues and interactions.

This objective can be divided into the following sub-objectives:

- Identify the harmonic issues and interactions occurring within an HVAC-connected offshore wind farm.
- Assess the impact of the connection of multiple offshore wind farms at the same POC when considering harmonic issues and interactions.
- Identify the parameters which affect the identified harmonic issues and interactions.

In order to reach the project objectives, two methods for studying harmonic interactions in offshore wind farms have been selected: the Harmonic Impact Assessment and the Harmonic Resonance Stability Assessment. Consequently, performing a study of the effect of harmonic interactions on Temporary Overvoltages is not a part of this research project. Solely steady-state harmonics in the harmonic frequency range of 100 Hz up to half the switching frequency, were considered in this research project. Sub-synchronous oscillations and side-band oscillations of around the switching frequency were neglected.

Two case studies were performed. For each case study, several wind farms situated in the North Sea, which are connected at the same POC, were considered. Firstly, the impact of connecting an increasing amount of wind farms to the same POC on the harmonic emission levels was analyzed. In order to do so, a model incorporating the active behaviour of the wind turbine converters was implemented when performing a Harmonic Impact Assessment. Secondly, the impact of harmonic interactions on the harmonic resonance stability at the POC was studied. The control parameters of the wind turbine converters and parameters related to the OWPP configuration were taken into account for this stability assessment.

1.3 Project Description

Several tasks have been carried out for this research project:

1. *Assessing the impact of connecting an increasing number of wind farms at the same POC when considering harmonic emission levels*
   A Harmonic Impact Assessment was performed for three scenarios in which the number of connected wind farms increased for each scenario. Currently, in industry, the models which are utilized for the Harmonic Impact Assessments includes a harmonic constant current source to represent the wind turbine converters. For this project, a Norton Equivalent Impedance was added in parallel to the harmonic constant current source, representing the active behaviour of the converter. The results of the Harmonic Impact Assessment when utilizing a Norton equivalent, were compared with the outcomes of a conventional Impact Assessment.

2. *Studying the impact of connecting an increasing number of wind farms at the same POC by looking at resonance stability*
   A Harmonic Stability Assessment was performed for two wind farms in the North Sea. Three scenarios were assessed: (i) connecting OWPP I, (ii) connecting OWPP II, and (iii) connecting both OWPP I and OWPP II. The following sub-tasks were carried out:

   (a) The harmonic resonance points were identified by utilizing an impedance based method. Both an analytical model and a model in PSCAD/EMTDC were utilized. The PSCAD software was used for the frequency sweeps since it is very suitable for modelling the control structure of the wind turbine converters.

   (b) Performing a Stability Assessment by utilizing the positive-net-damping criteria at the bus where the wind farms are connected to the onshore network.

   (c) Verifying the results with time-domain simulations in PSCAD.

1.4 Master Thesis Outline

Chapter 1: Introduction

The background and the objectives of this research project are provided.

Chapter 2:HVAC-Connected Offshore Wind Power Plants

Firstly, HVAC-connected OWPPs are discussed. Most new offshore wind farms contain wind turbines which are connected to the system with a full-scale back-to-back Voltage Source Converter (VSC). Since these converters are a source of harmonic emissions and of vital importance when considering harmonic interactions in offshore wind farms, the VSC is described in detail. The control part of the converters is essential to the electrical behaviour of the VSC and therefore the control loops of the VSC are discussed as well. Moreover, the relation between the control loops and the different harmonic emissions is evaluated.

Chapter 3: Harmonics

This chapter discusses both the concept of harmonic emissions and harmonic resonance. It also provides a more detailed description of where harmonic emissions actually originate from. Moreover, the harmonic interactions occurring in an OWPP are outlined.

Chapter 4: Methods for Analyzing Harmonics in HVAC-Connected Offshore Wind Power Plants

Chapter 4 describes the three main methods which can be utilized to study harmonic issues and interactions in OWPPs.

Chapter 5: Methodology

Chapter 5 presents the methodology of this research project. Both case studies are outlined and the methods which are utilized to study the harmonic interactions are described in detail.

Chapter 6: Results and Discussion

The results of both analytical calculations and simulations are presented and discussed.

2 HVAC-Connected Offshore Wind Power Plants

Currently, a trend exists towards the installation of offshore wind turbines [6]. Offshore Wind Power Plants (OWPP) have several technical advantages over onshore wind power plants, such as higher average wind speeds, reduced visual impact and unlimited dimension of the blades of the turbine [7]. However, OWPPs have higher maintenance cost and more complex logistics with regards to installation and operation [6]. These conditions pose challenges for wind power manufacturers to develop offshore wind parks successfully.

An OWPP can be connected to the onshore network by utilizing either a High Voltage Alternating Current (HVAC) or High Voltage Direct Current (HVDC) transmission system. Power losses in a HVDC system are lower, leading to a higher efficiency for DC systems. However, DC systems usually have higher capital costs due to the immaturity of the technology [6]. On the other hand, HVAC systems require additional reactive power compensation, which increases the capital costs of the system with an increasing cable length [7]. Therefore, whereas HVAC systems are less expensive for shorter distances, around a distance of 100 km, the cost of an HVAC system becomes higher than the cost of an HVDC system, due to the losses and required reactive power compensation [6].

2.1 Topology of an HVAC-Connected Offshore Wind Power Plant

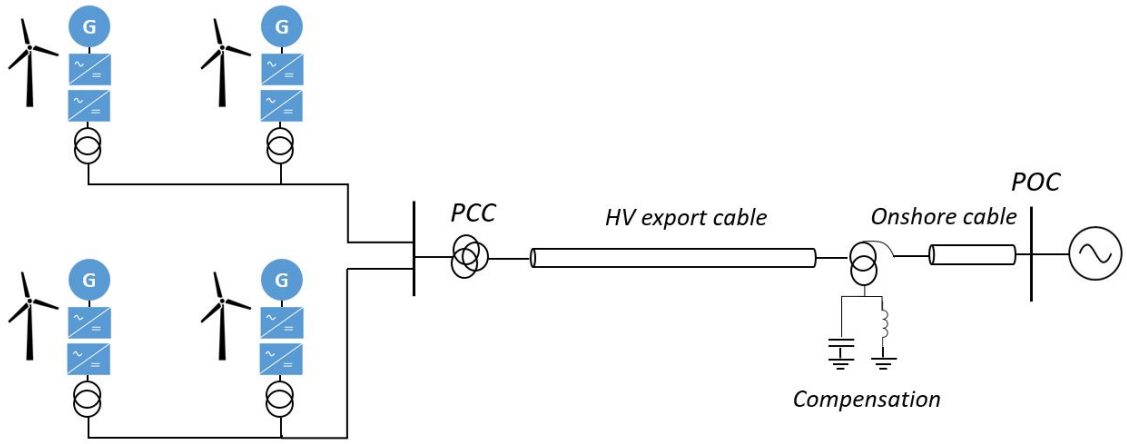

Figure 2: An equivalent model of the AC side of a VSC converter [8].

An HVAC-connected OWPP consists mainly of an AC collection grid that connects all the strings of wind turbines, and a high voltage submarine cable which is utilized to transport the electricity to the main grid [6]. Several electrical designs are possible for an offshore substation platform. Firstly, in the case of a radial collection configuration, one feeder connects one string of wind turbines. This configuration is the most simple and most common option, even though it is not the most

resilient option [6]. The ring configuration is more costly than the radial configuration, but has a higher reliability [6]. Cables have to be oversized in order to allow bidirectional power flow in this collection system. Lastly, the star configuration increases the reliability of the system. However, cable lengths are increased, which increases the losses and the costs [6]. All configurations are shown in Figure 3.

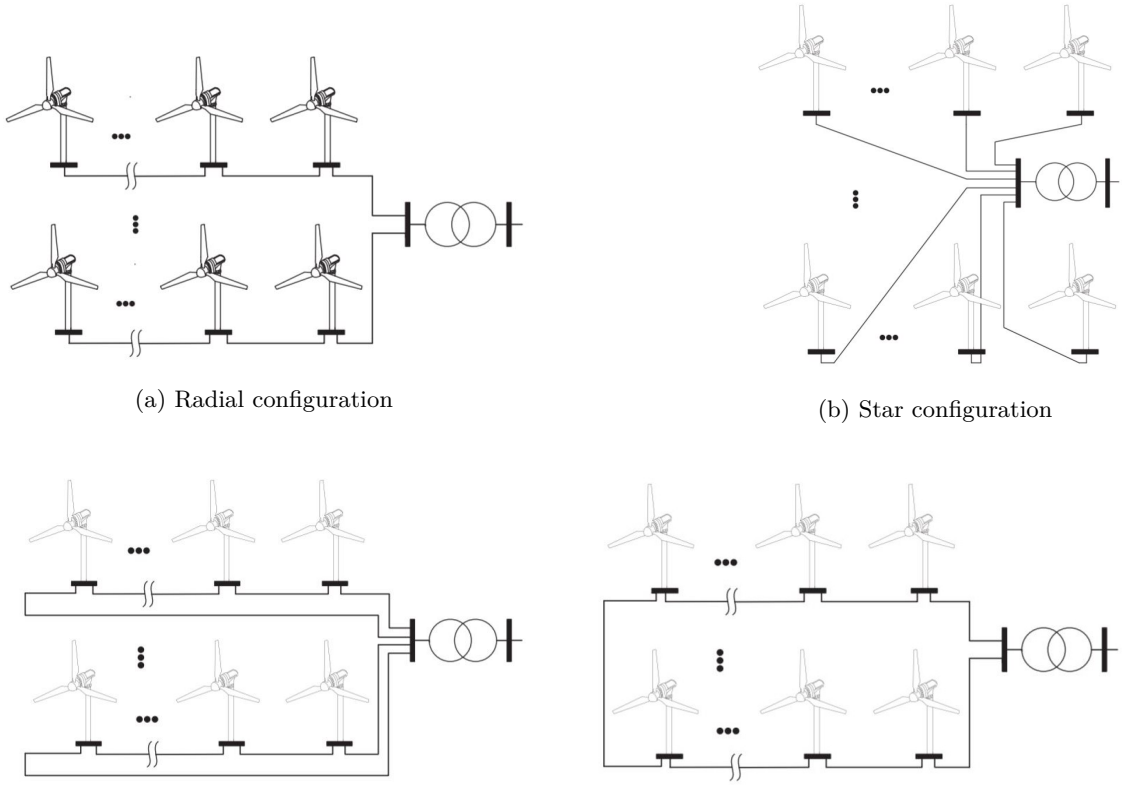

(a) Radial configuration

(b) Star configuration

(c) A Single-Sided Ring configuration

(d) A Double-Sided Ring configuration

Figure 3: Configurations of wind turbine strings [6].

In the case of a radial configuration, the collection networks of the wind turbines strings are connected at the Point of Common Coupling (PCC). A submarine cable then connects the OWPP to the onshore network at the Point of Connection (POC), as shown in Figure 2.

2.2 Wind Turbine Technologies

Modern Wind Turbine Generators (WTGs) can be categorized into four major types [9]. The following section provides an overview of this classification. Figure 4 shows each type as well.

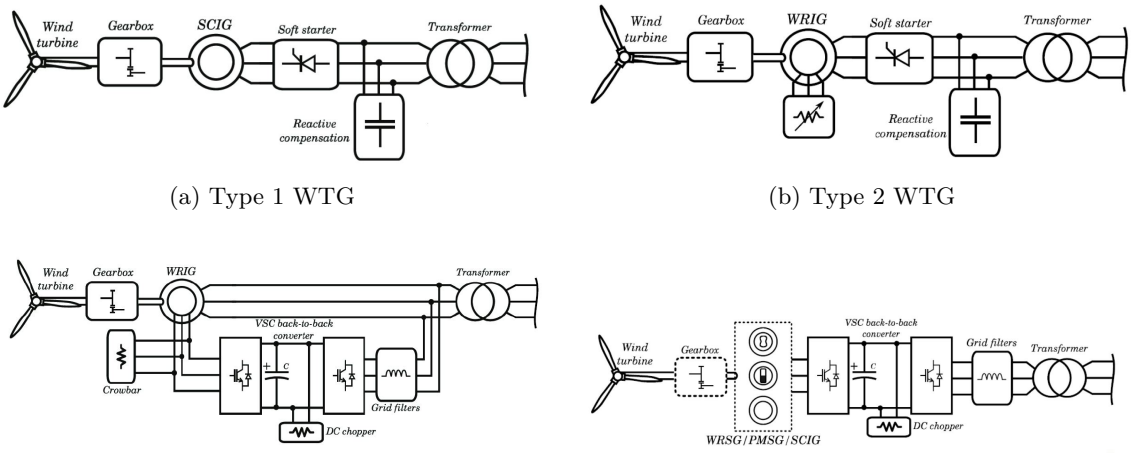

(a) Type 1 WTG

(b) Type 2 WTG

(c) Type 3 WTG

(d) Type 4 WTG

Figure 4: Classification of WTGs into the four categories [10], [6].

- **Type 1: Fixed Speed Wind Turbines with Squirrel Cage Induction Generator**
  This WTG type, also referred to as "the Danish concept", uses an asynchronous squirrel cage induction generator and it directly connected to the grid through a soft-starter and a step-up transformer [11]. The generator speed is merely fixed at the synchronous speed, allowing a variation of 1 percent [12]. The WTG absorbs reactive power from the grid and therefore reactive power compensation in the form of capacitor banks is required [6]. This configuration is related to a lower efficiency [11]. Moreover, any variation in the wind speed is reflected in the electrical output of the WTG [11].

- **Type 2: Limited Speed Wind Turbines**
  The type 2 configuration encompasses a Wound Rotor Induction Generator (WRIG) and enables a variable speed operation of typically up to 10 percent [6]. By adjusting the magnitude of the rotor resistance, the slip of the machine can be altered and the speed can be modified [6]. However, this results in losses in the rotor resistance,and a capacitor bank is still required for reactive power compensation purposes [11].

- **Type 3: Variable speed with partial-scale converter**
  This concept consists of a WRIG generator, directly connected to the grid through the stator and connected through the rotor by a partial-scale power converter, resulting in a Double-Fed Induction Generator [6]. The speed can now be varied between -40% up to +30% of the nominal speed [6]. The partial-scale converter enables reactive power control and a smoother grid connection [10]. This configuration is one of the dominant designs in industry [11]. However, the configuration has limited fault-ride through capabilities and the necessity of a gearbox increases the cost and maintenance requirements, making this type less appropriate for offshore applications [12].

- **Type 4: Variable speed with full-scale converter**
  Type 4 is a full variable speed WTG, which utilizes a synchronous generator and which is connected through a full-scale power electronic converter [11]. A Wound Rotor Synchronous Generator (WRSG), Permanent Magnet Synchronous Generator (PMSG) or a Squirrel Cage Inductor Generator (SCIG) is used [13]. The WTG allows independent active and reactive power control, doesn't require a gearbox and operates with a high efficiency. Lastly, the configuration also has fault-ride through capabilities [14]. Consequently, this configuration is very suitable for offshore applications [12].

It has to be noted that in order to enhance the controllability and to be able to operate at different speeds, mostly type 4 wind turbines are currently implemented in recent OWPPs. When studying an new OWPP, it is therefore important to obtain a deeper understanding of how the converter of the WTG type 4 is working. The behaviour of a power electronic component such as a converter is strongly dependent on how the converter is controlled. Therefore, the coming section will elaborate on the control of the type 4 WTG converter.

2.3 The Configuration of the Back-to-Back Voltage Source Converter

A WTG type 4 is connected with the grid through a full-scale converter, consisting of two VSC converters, which is referred to as a VSC back-to-back converter. The generator side converter maximizes the power extraction from the wind, controlling the reactive power and the active power and the voltage on the AC side. The grid-side converter controls the DC link voltage and manages the reactive power injection into the grid, as shown in Figure 5. The back-to-back VSC converter is connected through a coupling or LCL filter and a step-up transformer to the Point of Common Coupling (PCC).

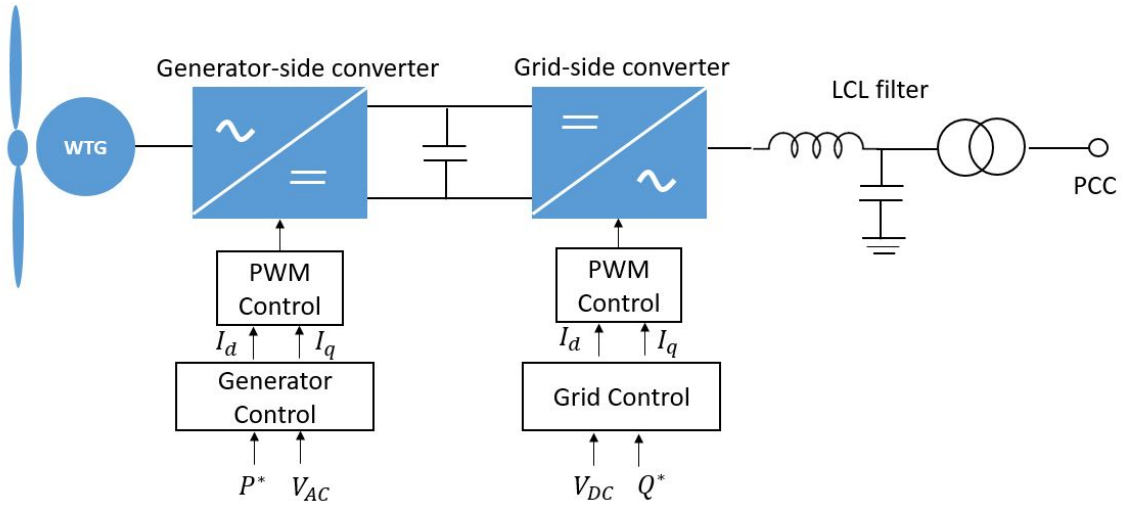

Figure 5: A back-to-back VSC converter.

A shown in Figure 5, a coupling inductance is utilized to smoothly connect the converter to the network. A filter capacitance is placed in parallel with this inductance as well. Naturally, the magnitude of the inductance and the filter capacitance are important for the impedance of the converter. The term LCL filter refers to the coupling inductance, the filter capacitance and to the equivalent inductance of the step-up transformer.

It has to be noted that in industry, when the wind turbines have a relatively large nominal power, usually two parallel converters are utilized [15] and [16]. For example, in the case of an 8 MW turbine, two 4 MW converters are placed in parallel, both having a coupling inductance, but sharing one filter capacitance and step-up transformer [5]. This configuration is shown in Figure 6.

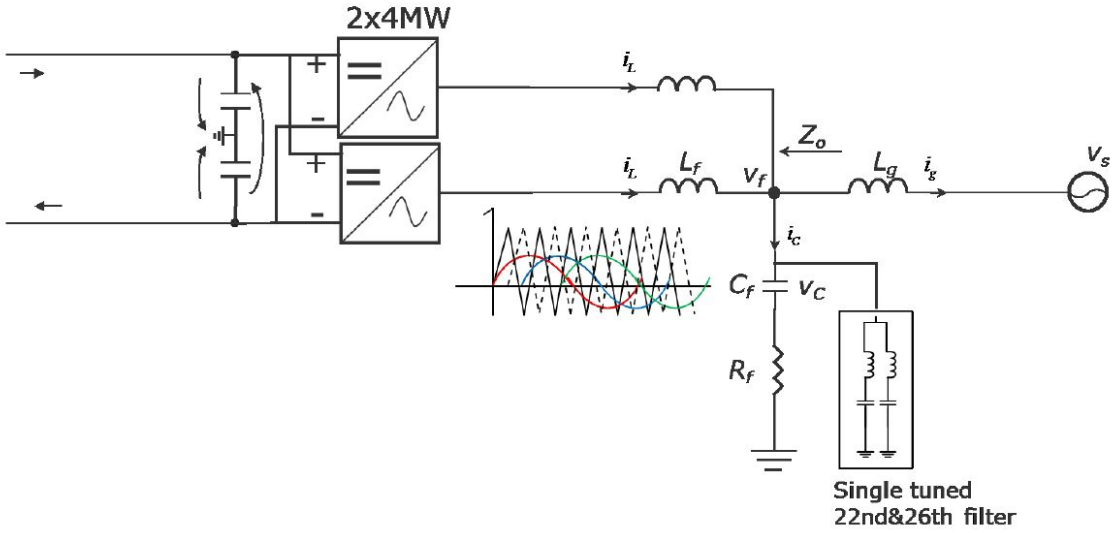

Figure 6: Configuration with two parallel VSCs [16].

2.4 Control of the Back-to-Back Voltage Source Converter

As shown in Figure 7, the Voltage Source Converter receives an AC side voltage set point and a reactive power set point. The VSC then applies a voltage in such way that in reality these reference values are obtained. In order to do so, the reference values of the AC voltage and reactive power have to be translated into the actual voltage the VSC has to apply. A current references calculation is performed which translates the reference values into reference values in terms of current. These current reference values are then translated in the inner current loop into the voltage the converter will have to apply.

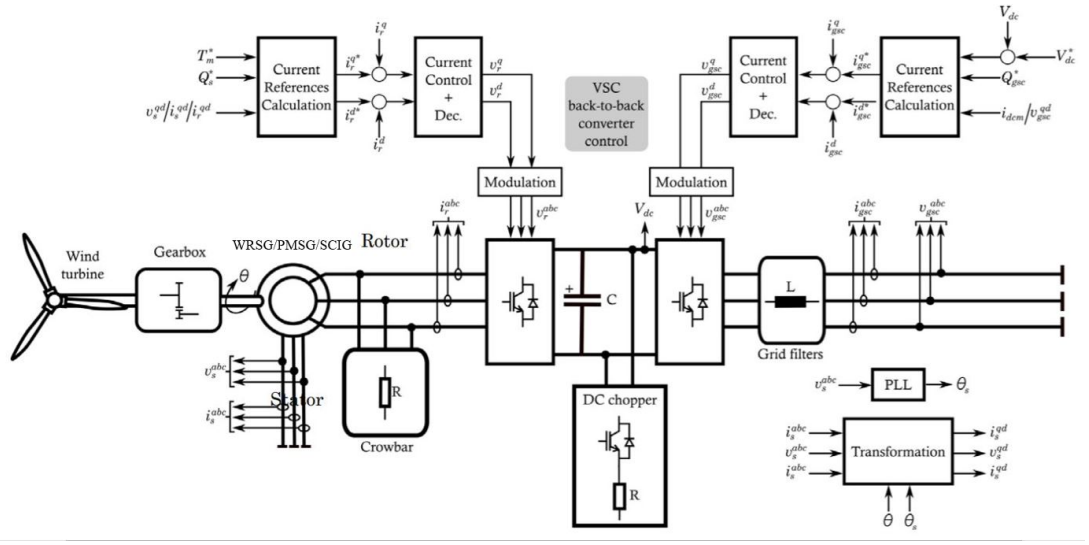

Figure 7: Control of a back-to-back VSC converter [17].

In order to track whether indeed the desired AC voltage and reactive power injection are obtained, the VSC is continuously comparing the reference current value with the actual current flowing through the system. Therefore, it utilizes a PI controller in the inner current loop control which ensures that the actual current is indeed equal to the current reference. Since it is difficult for a PI controller to deal with a sinusoidal signal, the current values are translated to current values in a rotating reference frame by applying a Park transformation [8]. The rotational angle of this so-called qd-reference frame is equal to the grid angle ω and a Phase-Locked-Loop is utilized to track this grid angle. The current references in the qd-frame are expressed into the voltage the converter will have to apply by utilizing a PI controller.
To summarize, the control scheme of the VSC consists of four main components: (i) an inner current loop, regulates the AC current in the d and q components, (ii) an outer current control loop, which regulates the AC voltage and reactive power injection [8]. A (iii) PLL is utilized to track the angle and (iv) a voltage modulator is utilized to apply the converter voltage. This way, the VSC ensures the desired AC voltage and reactive power injection are obtained. The generator side converter is responsible for ensuring a maximal power extraction from the turbine and a stable DC link voltage. The control schemes of the inner current loop and the PLL are given:

- **Phase-Locked Loop**
  The PLL block tracks the grid angle by ensuring that the d-component of the grid voltage is indeed equal to zero. It continuously applies a Park transformation and the error between the generated v_d with this Park transformation and the reference value, which equals zero, is then fed into the PI controller. Due to this PI controller, the Park transformation block is varying the frequency until the angle arrives at the angle at which the Park transformation

generates a v_d equal to zero. The PLL is initialized with an angle of 50 Hz, ω_0 to enhance a fast initialization of the PLL, as shown in Figure 8.

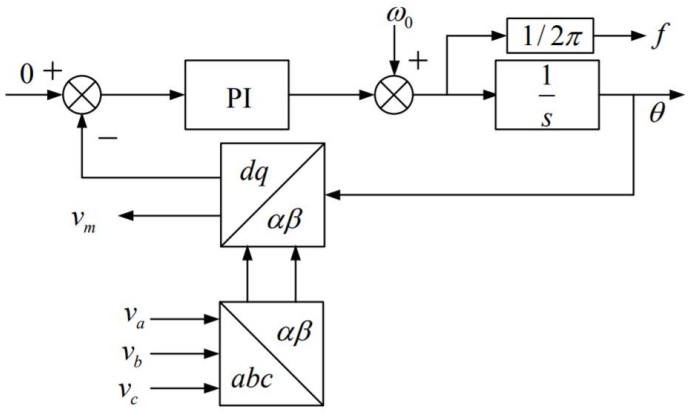

Figure 8: Control scheme of a synchronous reference frame PLL [18].

- **Inner Current Loop**
  The inner control loop translates the reference current values into the voltages which the converter has to apply. One PI controller is utilized per current component in order to do so. As shown in Figure 9, a decoupling loop, which adds the product of the grid angle w_e and the coupling inductance l_l to the voltage the converter has to apply, ensures that i_q and i_d can be controlled independently [8].

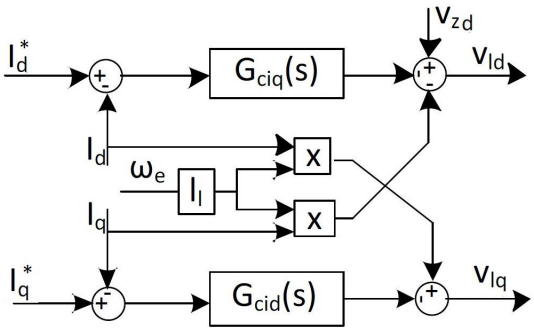

Figure 9: Decoupling loop of the inner current control loop, with $G_{ciq}(s) = G_{cid}(s) = \frac{K_p s + K_i}{s}$, grid angle w_e, coupling inductance l_l, converter voltages V_{lq} and V_{ld} and reference current values I_q anad I_d [8].

2.5 Analytical Description of the Voltage Source Converter

The behaviour of the VSC converter can be described analytically. In order to do so, the converter has to be described in a simplified manner. In essence, the VSC applies voltages in such a way, that the correct values for the AC voltage and reactive power flow are obtained. Consequently, the grid-side VSC can be modelled as a AC voltage source, as shown in Figure 10. The VSC will observed by the grid as a current source due to the presence of a coupling inductance, which makes it possible to connect the VSC to the grid [8]. Figure 10 shows the equivalent model of a VSC converter. The VSC converter is represented as a voltage source applying a voltage V_z, r_l and l_l are the coupling inductance and its equivalent resistance and the network is represented as a voltage source applying a voltage V_l.

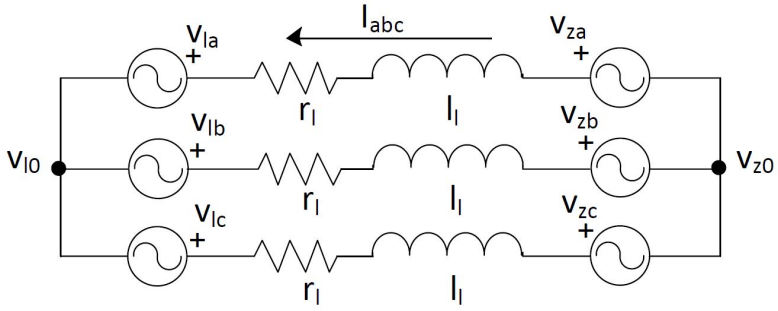

Figure 10: An equivalent model of the AC side of a VSC converter [8].

When a Park transform is applied to the current and it is taken into account that in a balanced three-wire system i_0 is equal to zero, the voltage equations of the grid side VSC can be expressed as [8], [19]:

$$\begin{bmatrix} v_g^d \\ v_g^q \end{bmatrix} - \begin{bmatrix} v_c^d \\ v_c^q \end{bmatrix} = \begin{bmatrix} R & L\omega \\ -L\omega & R \end{bmatrix} \begin{bmatrix} i_c^d \\ i_c^q \end{bmatrix} + \begin{bmatrix} L & 0 \\ 0 & L \end{bmatrix} \frac{d}{dt} \begin{bmatrix} i_d \\ i_q \end{bmatrix} \tag{1}$$

Where $v = v_d + jv_q$ and $i = i_d + ji_q$. With v_{zd} and v_{zq} the grid dq voltages, v_{ld} and v_{lq} are the converter dq voltages, i_d and i_q are the dq currents .

The system equation can then be written as [19]:

$$v_g - v_c = R\boldsymbol{i} + j\omega L\boldsymbol{i} + L\frac{d}{dt}\boldsymbol{i} = (R + j\omega L + sL)\boldsymbol{i} \tag{2}$$

(refeq:system) can be utilized to derive the expressions which further describe the behaviour of the converter, as elaborated on in Section 2.5.1.

2.5.1 Derivation of the Norton Equivalent Impedance

The control loops of the VSC are mainly build to operate at a balanced network voltage, and a VSC is not perfectly able to track an unbalanced voltage. Therefore, the disturbance from out the network will lead also to a disturbance in the injected current. So when an harmonic voltage is applied to the converter, it will 'respond' by injecting a certain current. When dividing the applied voltage by the injected current, an impedance value can be obtained which encaptures the interaction of the VSC with the network. The interaction of the wind turbine VSC converter with the network can thus be described with an impedance profile over a frequency range. Moreover, when studying the electrical behaviour of the VSC, it can be useful to describe the VCS as an impedance.

This impedance profile, or Norton Equivalent Impedance, can be derived analytically [20], [21], [22], [23]. Several approaches have been proposed in literature, however, most approaches are similar to the Unified Impedance Model approach presented in [20]. Firstly, similar to (2) the voltage balance across the converter filter is represented as:

$$v_{out} = (R_f^w + L_f^w s + jL_f^w \omega_1) \cdot \mathbf{i} + v_{wt} \tag{3}$$

With v_{out} the converter output voltage, L_f^w and R_f^w the coupling inductance and equivalent resistance, v_{wt} the voltage after the coupling filter and ω_1 the fundamental frequency in rad/s.

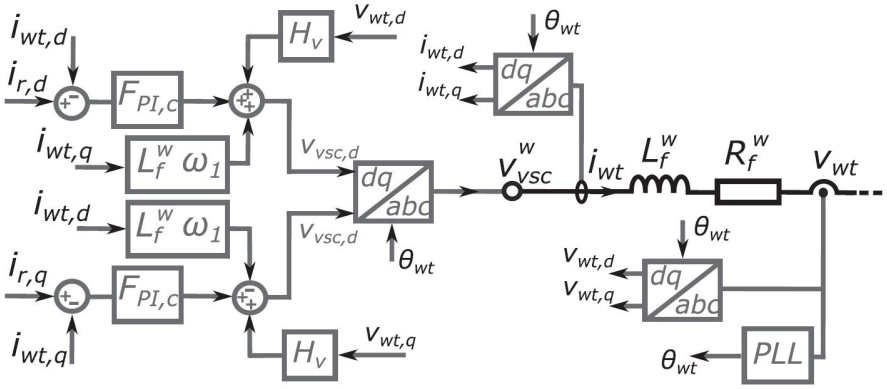

Figure 11: Control structure of the WT grid side converter [21].

When the control structure of the wind turbine grid side converter is taken into account as in Figure 11, the control of the converter can be described with the following expression [24]:

$$v_{ref} = F_{PI}(s)(i_{ref} - i_{wt}) + jL_f^w \omega_1 \mathbf{i} + H(s)v_{wt} \tag{4}$$

With converter voltage and current reference v_{ref} and i_{ref}, i_{WT} the grid current. F_{PI} is the transfer function of the PI controller of the inner current loop [24]:

$$F_{PI}(s) = k_p + \frac{k_i}{s} \tag{5}$$

With k_p and k_i the proportional and integral gains of the PI controller.

The grid voltage feed forward low-pass filter included in the control, $H(s)$ can be expressed as [24]:

$$H(s) = \frac{\alpha_f}{s + \alpha_f} \tag{6}$$

With α_f the low-pass filter bandwidth.

s represents a frequency vector in the complex plane, which mathematically is equal to a transfer function. The above equations are all expressed in the $\alpha\beta$-frame by performing a rotation of $s \rightarrow s - j\omega_1$ [21], which equals a phase shift of the fundamental frequency $omega_1$ or 50 Hz. By performing this rotation, values are translated from the dq-frame into the $\alpha\beta$-frame.

$$s = j\omega - j\omega_1 \tag{7}$$

With frequency in rad/s $\omega = 2\pi f$ and the fundamental frequency ω_1.

The output voltage of the converter can be related with the voltage reference value by taking into account the time delay T_d of the VSC:

$$v_{out} = e^{-sT_d} \cdot v_{ref} \tag{8}$$

The time delay is on its turn dependent on the sampling time T_s and a factor q_d which depends on the sampling technique and the computation time:

$$T_d = T_s q_d \tag{9}$$

When (3), (6) and (8) are combined,the converter can be described as [21] and [24]:

$$i_{wt} = i_{ref} \cdot F_c^{w,dq} - v_{wt} \cdot Y_c^{w,dq} \tag{10}$$

' With i_{wt} the current injected by the VSC, i_{ref} the control reference current, $F_c^{wt,dq}$ the closed loop transfer function, v_{wt} the voltage after the coupling filter and Y_c^w the VSC admittance.

$$F_c^{w,dq} = \frac{D^w F_{PI,c}}{R_f^w + sL_f^w + j\omega_1 L_f^w + D^w(F_{PI,c} - j\omega_1 L_f^w)} \tag{11}$$

$$Y_c^{w,dq} = \frac{1 - D^w H_v}{R_f^w + sL_f^w + D^w(F_{PI,c} - j\omega_1 L_f^w)} \tag{12}$$

$$D^w = e^{-sT_d^w} \tag{13}$$

This results in the final expression for the impedance of the grid side wind turbine converter:

$$Z_{wt} = -\frac{R_f^w + sL_f^w + j\omega_1 L_f^w + D^w(F_{PI,c} - j\omega_1 L_f^w)}{1 - D^w H_v} \tag{14}$$

It has to be noted that for this expression, the time delay, the dynamics of the inner current loop and the voltage feed forward term are taken into account. The PLL is not considered for

this expression since it mainly effects the impedance at sub synchronous frequencies and does not necessarily have to be considered when looking at frequencies of over two times the fundamental frequency (100 Hz) [25]. Outer control loops, DC voltage control or power control, are also not included in the VSC model since their dynamic response is slow and they interact with resonances near the synchronous frequency or below (sub-synchronous resonances) and will not impact the impedance of the converter at harmonic frequencies [21]. Section 3 describes in more detail for each component of the converter control at which frequencies oscillations are induced.

3 Harmonics

Two main harmonic concepts are relevant in the case of offshore wind power plants: harmonic emissions and harmonic resonance [26]. The term harmonic emissions refers to the injection of a periodic waveform distortion due to the switching of inverters, saturation of inductors or nonlinear behaviour [27]. The injection of these harmonics could lead to an exceedance of the limits imposed by the network operator. Moreover, when several harmonic emissions sources are present, these harmonics could accumulate, leading to a higher probability of surpassing the limits [26]. Even in the case the level of harmonic emissions is in compliance with the grid codes, under resonance conditions these harmonic emissions can be amplified significantly [28]. Resonance conditions can occur if an harmonic component of a certain frequency is present at the same frequency as a dip or peak in the impedance of the system. Harmonic emissions at a resonance frequency can then excite these resonances, leading to overvoltages or overcurrents, which in some situations can lead to damaging HV equipment or an instability of the system [29].

3.1 Harmonic Emissions

Harmonic emissions are often represented in terms of the Total Harmonic Distortion (THD) [30]:

$$THD = \frac{\sqrt{\sum_{n}^{\infty} V_n^2}}{V_1} \cdot 100\% \tag{15}$$

With V_1 the voltage at the fundamental frequency and V_n the voltage at the nth harmonic order, The harmonic emissions in an offshore wind power plant consist of power system background harmonics and emissions from the converters of the wind turbines [28]. The wind turbines inject harmonic currents to the collector due to the extensive use of power electronics [13]. Therefore, the presence of wind turbines is inherent to inserting harmonics into the system.

Firstly, the following section will elaborate on the impact of harmonic emissions on the system. Secondly, it will be described where the harmonic emissions of wind turbine converters exactly originate from.

3.1.1 Effects of Harmonic Emissions

The presence of harmonics can negatively effect the system. These negative effects of harmonics can be summarized [31]:

1. A reduced efficiency due to copper losses induced by the harmonic currents.
2. Harmonic amplification, due to series and parallel resonances, can cause excessive harmonic currents and voltages, which can lead to a costly system shutdown.
3. Premature aging of components due to voltage or temperature stresses.

4. Errors in the measurement devices since they are designed for sinusoidal voltages and currents.
5. Heating and vibrations of all power system components, which will especially be present in transformers and reactors.
6. Failure of protection devices.

Due to the negative impact of harmonics, Transmission System Operators (TSOs) have implemented limitations for the injection of harmonics into the grid. In order to comply with these grid codes, wind farm developers are responsible for the impact of its own harmonic sources, while the TSO takes responsibility for all other sources including their amplification [32].

3.1.2 Origin of Harmonic Emissions in Power Electronic Dominated Systems

Power electronic converters are widely used in modern power systems due to their relatively high efficiency and controllability [31]. Compared to synchronous and electrical machines, the timescale of the response of a VSC is significantly smaller. The bandwidth of the control dynamics ranges from synchronous frequencies for the outer power control loops, to frequencies of 100-1000 Hz for the inner control loops [33]. Due to the high frequency operation of the converters, interactions between the power grid and the converters can cause oscillations in a wide frequency range [33]. The usage of a VSC therefore leads to the unavoidable injection of harmonics into the system [34].

Moreover, the high frequency operation and steadily increasing bandwidth of their control loops leads to a power system with reduced damping [35]. Besides, LCL filters are often used to connect a VSC. These filters can add a resonant frequency to the system, which especially in the case of connecting multiple converters in parallel, can lead to power quality and stability issues [35].

The harmonics induced by the converter itself can be divided into characteristic harmonics and non-characteristics harmonics [36]. Characteristic harmonics depend on the converter topology and the applied switching pattern. These type of harmonics refers to the oscillations generated by the Pulse-Width Modulator of the converter or the sampling process [37]. The non-characteristic harmonics are depending on the operating point and control scenario [36] and are associated with the PLL and current control loops. As an example, the anti-wind up blocks lead to non-linearities in the control loops, which can induce non-characteristic harmonics. A brief overview of the oscillations induced by each component of the VSC' control is given, together with a visual representation, which is shown in Figure 12.

- **Pulse Width Modulation (PWM)**
  The PWM creates a sideband oscillation at the switching frequency [38]. It also has been reported that the PWM can be related to the creation of an additional sideband beyond the Nyquist frequency ($f_s/2$) [25]. Over-modulation of the PWM may also lead to the creation of non-characteristic harmonics [38].

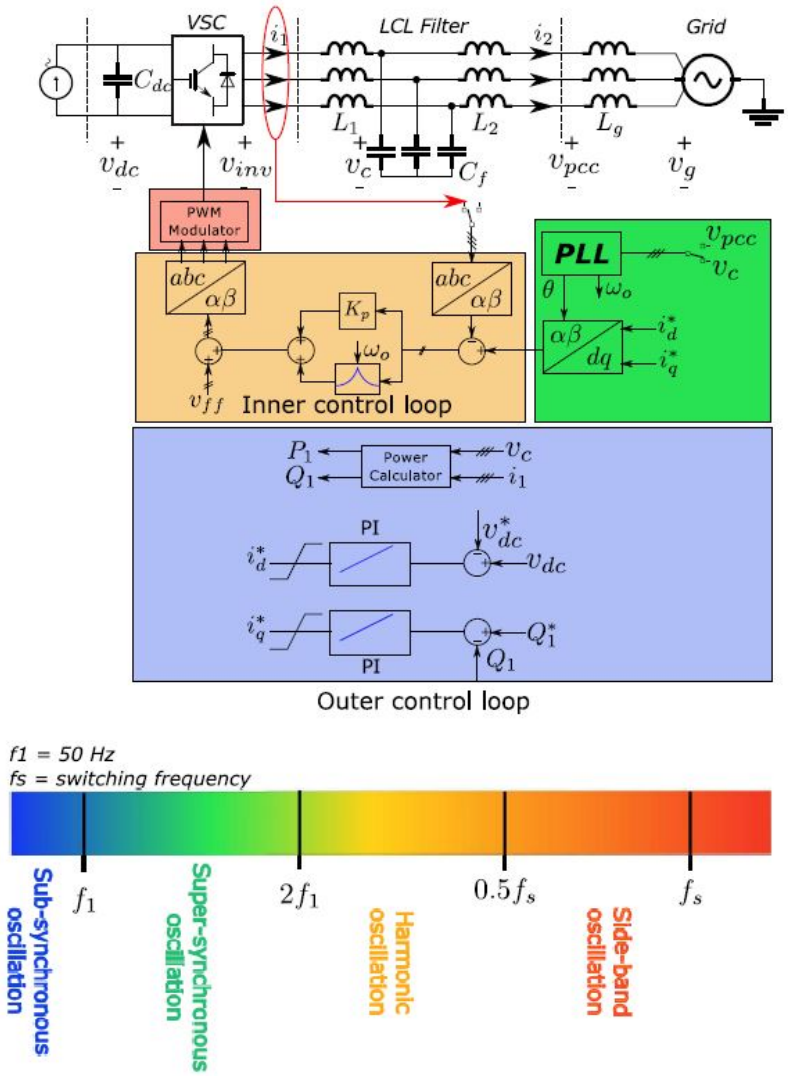

Figure 12: Frequency ranges of the power system oscillations induced by each component of the control of a VSC. [25]

- **Phase-Locked Loop**
  The PLL can make the inverter behave like a negative resistor at the PCC, which can create harmonics under week grid conditions [39]. In the case of dq-control, the PLL utilizes the q-axis voltage to perform phase synchronization, and consequently the negative damping is only introduced to the q-axis [38]. The side band oscillations introduced by the PLL are of around the fundamental frequency [38].

- **Inner current loop**
  The inner current control loop may cause high frequency oscillations, above the Nyquist frequency, in the case the equivalent negative resistance region caused by digital delay interferes with the network resonance point, where little damping is present [25]. The inner control loop might also interact with the lower frequency component of the sideband around the switching frequency, resulting in sideband-harmonic instability, which has especially been observed in parallel VSCs [38] [37].

- **Outer current loop**
  The outer current control loop can cause low frequency sub-synchronous oscillations, especially in the case the grid-side VSC is controlling the terminal voltage or is absorbing active power from the grid [25]. Lastly, the Direct Voltage Control of the grid-connected VSC adds a negative damping to the d-axis, causing sideband-oscillations around the fundamental frequency ($f_1 \pm f_{dq}$) [38], [27].

To summarize, two sideband-oscillations are induced by the VSC: (i) sideband-oscillations around the switching frequency induced by the PWM, and (ii) sub- and near-synchronous sideband oscillations induced by the PLL and outer control loops. It can also be said that the second sideband-oscillations are caused by the Park transformations and dc-ac conversion [38]. The inner control loop is responsible for creating harmonic oscillations.

The oscillations induced by the PLL and PWM are also related to a phenomena called frequency coupling [27]. Frequency coupling describes the process in which a perturbation in the system at a certain frequency provokes the appearance of other frequencies which on their turn induce new frequencies again. Due to non-linearities in the system, these new frequencies are also coupled to other frequencies [27]. Due to this frequency coupling effect, the PLL and the PWM can create additional non-characteristic harmonic emissions [27]. Moreover, other parts of the control of the VSC, such as the inner current loop, utilizes the angle tracked by the PLL. Therefore, the PLL will also have its effects on the harmonic emissions from the inner current loop.

In the case a voltage distortion propagates to the PCC voltage, the VSC will respond to this perturbation at the PCC with a component of the frequency of the perturbation, f_p and a component with a frequency of $f_p - 2f_s$ [40]. In the case the grid impedance is passive and balanced, the current at these two frequencies will solely induce similar frequency and sequence components at the PCC.

These two components induced at the PCC will create two components each again. The two newly created components will have a frequency of $-(f_p - 2f_1)$ and $-(-(f_p - 2f_1) - 2f_1) = f_p$, which are again the same components as created in the first response. Therefore, the voltage perturbation at the PCC doesn't create a current at new frequencies. However, in the case of a unbalanced grid impedance, a positive sequence current will create both a positive and negative sequence voltage. Moreover, the PCC will also again have a component created at $f_p - 2f_1$, which generates on its turn a current at $-(f_p - 4f_1)$ [40]. This sequence of events will not stop and frequency couplings will be created continuously [40].

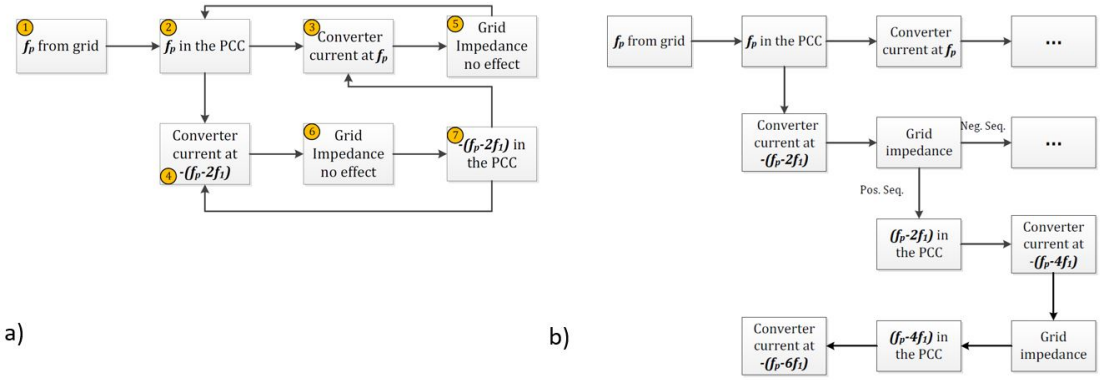

Figure 13: a) Frequency coupling under balanced grid conditions. b) Frequency coupling under unbalanced grid conditions [40].

3.2 Harmonic Resonance

An electrical system, which contains capacitance in the form of cables, overhead lines or capacitor banks, will have several frequencies where the reactance of the capacitors and the reactance of the system are equal, opposite and in parallel [29]. These parallel resonance points magnify voltages and can be characterized by peaks in the impedance [28]. In the case of series resonance points, the reactance of the capacitors and the reactance of the inductors are equal, opposite and in series, leading to dips in the impedance [29].

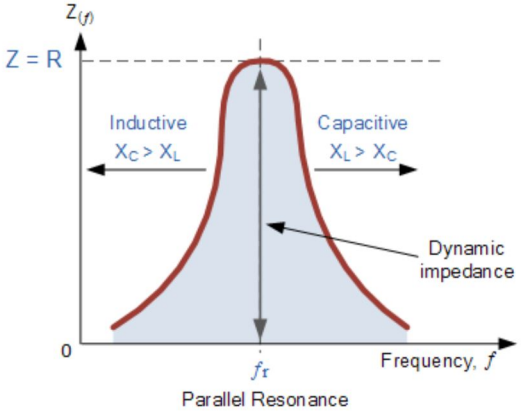

(a) The impedance at a parallel resonance frequency.

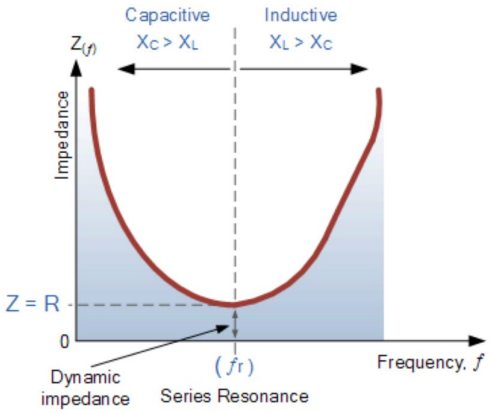

(b) The impedance at a series resonance frequency [41].

The resonance frequency is given by [42], [43]:

$$f_r = \frac{1}{2\pi\sqrt{LC}} \tag{16}$$

The resistive elements in the circuit strongly determine the bandwidth of the resonances. In the case of a series resonance, the bandwidth of the resonance peak, BW_s, can be determined by utilizing the quality factor Q [44]:

$$BW_s = \frac{f_r}{Q} = \frac{f_r R}{X} \tag{17}$$

In the case of a parallel resonance, the bandwidth, BW_p, also depends on the resistance:

$$BW_p = \frac{f_r}{Q} = \frac{f_r X}{R} \tag{18}$$

The resonance points in an OWPP depend on several fixed parameters, such as the inductance of the transformers and capacitance of the HV cable. The resonance frequencies are also sensitive to several variable parameters such as, but not limited to [13]:

1. Number of switched capacitor banks.
2. A change in the equivalent impedance of the collection network due to the connection or disconnection of a feeder.

The resistive elements in the system don't cause major shifts in the frequency points of the resonances [27]. However, these elements play an important role with providing damping to the system. In the case these elements are ignored, excessive corrective measures to mitigate harmonics might be applied [27].

In the case of a HVAC-connected OWPPs, the capacitances of the long HV cable and capacitor banks lead to a shift of the resonance points to lower frequencies, where harmonic emissions occur frequently [29]. A series or parallel resonance can then more easily be excited by harmonic components in the system. The occurrence of harmonic resonance conditions can lead to three different issues:

1. *Exceeding the harmonic limits by amplification of harmonics*
   The resonances might be excited by a distortion in the system or by an imbalance in the components and control of the converter [29]. It can occur that the harmonics inserted from the wind turbine excite the parallel resonance, leading to an oscillating current between the energy storage in the inductance and the energy storage in the capacitance and high harmonic voltages [45]. This could negatively affect the components of the OWPP and possibly damage the system [45]. A series resonance might be excited by a harmonic voltage from the grid, leading to a low-impedance path for the harmonic current, resulting in a high current. Figure 15 gives a visual representation of the series and parallel resonances in an OWPP. The OWPP then acts as a 'harmonic sink', amplifying the background harmonics in the grid [27]. The increased harmonic distortion due to an amplification of the background harmonics or wind farm harmonics can lead to higher energy losses and grid code compliance violation [32].

2. *Temporary Overvoltages (TOVs)*
   Resonances can also be excited by harmonic currents created by specific events in the system. For example, in the case a resonance point exists at 100 Hz, the frequency of the inrush current during the (re-)energization of a transformer can excite this resonance [46], [32]. This can cause Temporary Overvoltages, which can overstress the insulation, which can lead to insulation breakdown and catastrophic failure of equipment [32].

3. *Harmonic or Resonance Instability*
   Lastly, the system can become in stable due to harmonic resonance conditions [38]. For example, the interactions occurring between the resonances and the VSC control can destabilize the system due to VSC non-passivity [21]. The wind turbine VSCs are composed of the passive element, the LC filter, and the active element, the control output admittance in parallel with a current source [38]. The passive LC resonance can be triggered by the current source (parallel resonance) or the grid voltage (series resonance). Depending on the used controller, the control output admittance may have a positive, zero, or even negative real part in different frequency ranges. Consequently, damped/under-damped, critically damped, or exponentially amplified resonances might occur in the VSC system an the system can become instable It has to be noted that the harmonic instability concept differs from the passive harmonic resonance in since it is dependent on the control mechanism of the converters, whereas the passive harmonic resonance solely depends on the values of the passive elements [38].

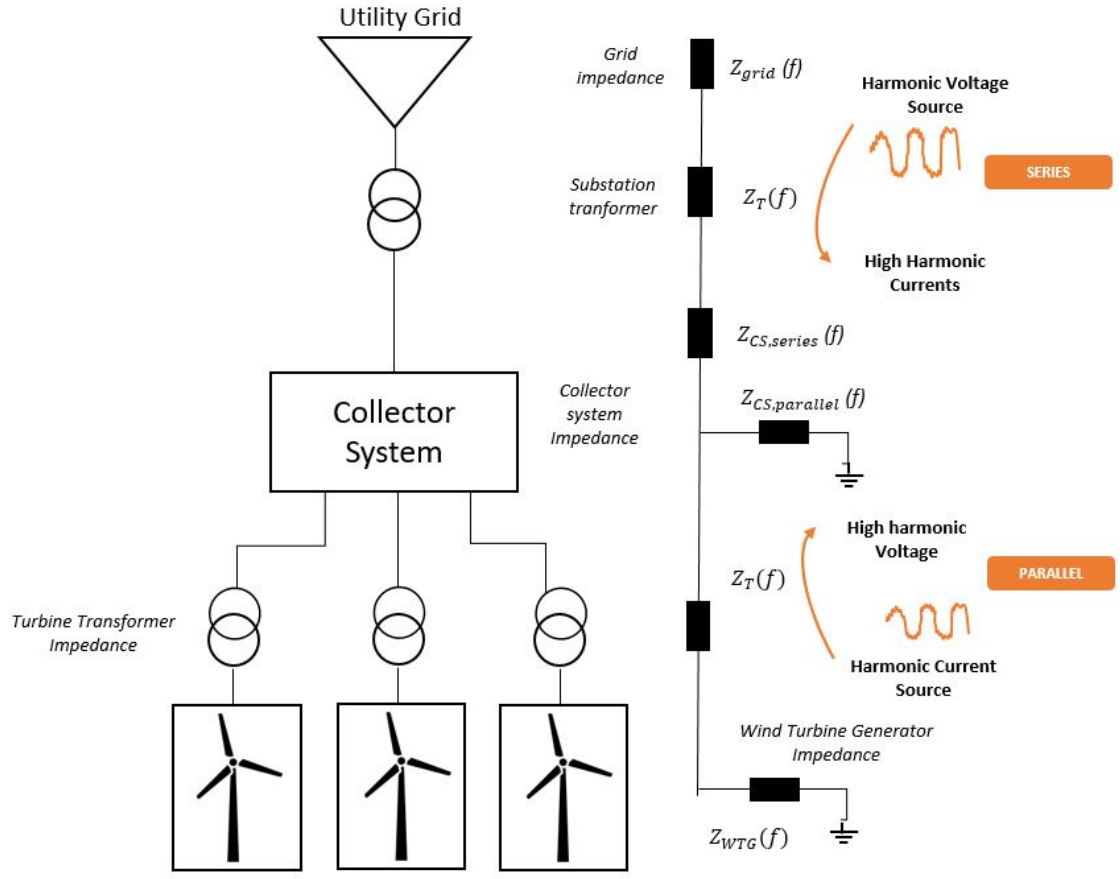

Figure 15: A Harmonic voltage source from the grid causing high harmonic currents due to a low-impedance path at a series resonance frequency and a harmonic current source from the wind turbines causing harmonic voltages due to a peak in the impedance at a parallel resonance frequency point.

3.3 Harmonic Interactions in Offshore Wind Power Plants

Elements such as wind turbine converters and transformer, but also the network itself, are responsible for the injection of harmonics. When considering harmonic interactions, several aspects have to be taken into account. Firstly, injected harmonics can have a certain interaction with the system at resonance frequencies. Passive elements can shift these resonance points and can therefore affect these interactions. Secondly, wind turbine converters are active elements, from which the current injection is dependent on the applied voltage. When an unbalanced voltage is applied, the converter will also respond with a certain harmonic current injection. Lastly, parallel converters can also have interactions with each other.

Consequently, the wind turbine converters, filters, cables and the network are each playing a role with regards to harmonic interactions in HVAC-connected offshore wind power plants. The following section summarizes the contribution of each of these elements to harmonic resonance Figure 16 provides a visual overview of all contributions.

- **Cables**
  The introduction of a long HVAC cable to connect an OWPP can lead to resonances in the lower frequency range [31], [27], [47]. Moreover, energization of the long cables could excite low resonance frequencies [47].

- **Transformers**
  During the energization of a transformer, several harmonic components are strongly present in the inrush current. These current harmonics can excite a resonance in the low-frequency range [47], [48], [44].

- **Passive filters**
  Frequently, LCL filters are utilized to connect VSCs [35]. These filters can add a resonant frequency to the system, which, especially in the case of several converters operating in parallel, can lead to power quality and stability issues [35], [27].

- **Capacitor banks**
  A change in the number of switched capacitor banks will lead to a shift in the resonance frequencies [13].

- **Converters**
  (i) The wind turbine converters will interact with the background harmonics from the grid. If a harmonic voltage is applied to the VSC, it will respond with an increased current, leading to negative damping.

(ii) The converters insert harmonics into the network due to its the high-frequency operation and can consequently excite resonances [31]. This can also be referred to as the interaction of the converters with passive elements [49].

(iii) The control loops of the converters can also interact with each other, possibly leading to an excessive amount of harmonic voltages and currents [40] [49].

- **The network**
  The network inserts background harmonics and these harmonics can excite resonances. Secondly, the background harmonics will have an interaction with the wind turbine converters, which can lead to an exceedance of the harmonic limits. In the case of a weak grid, the resonances are located at lower frequencies, leading to more possibilities of the excitation of a resonance [40].

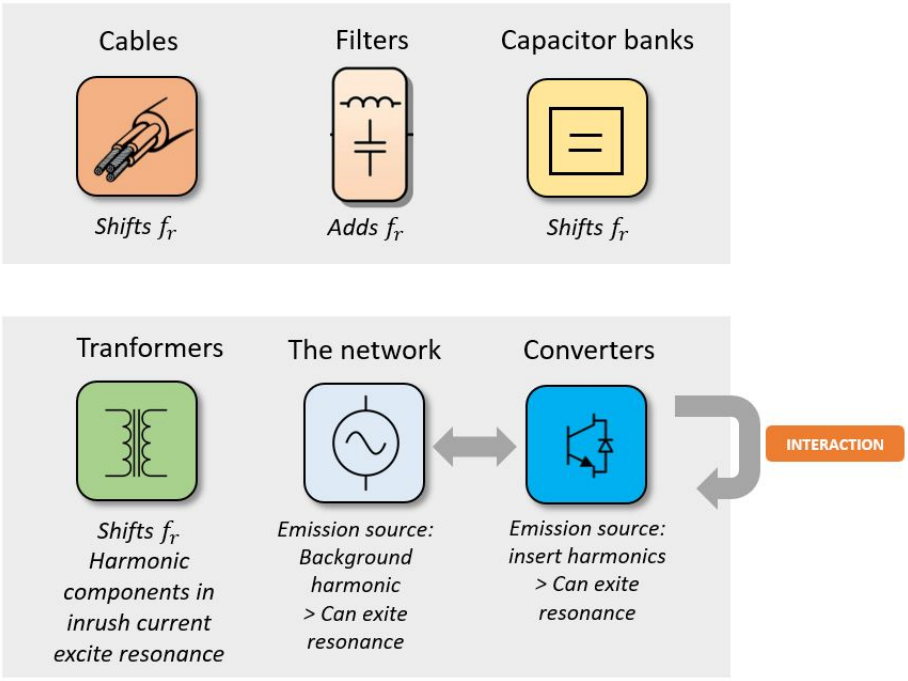

Figure 16: An overview of the impact of system components on the harmonic emissions and harmonic resonances [13], [31], [35], [47], [49].

4 Methods for Analyzing Harmonics in HVAC-Connected Offshore Wind Power Plants

As already mentioned, three main issues can arise when connecting an OWPP with a long HVAC cable to the onshore network. Firstly, the harmonic emissions of the OWPP or the background harmonics can excite the resonance frequencies, which may lead to an exceedance of the harmonic limits. Secondly, an event such as the (re-)energisation of an offshore transformer or one connected to the POC, can lead to TOVs. Thirdly, the harmonic emissions and interactions can lead to instability. In the first case, a harmonic impact assessment can be performed in order to verify whether harmonic limits are surpassed. Several methods to study these harmonic resonances in a system have been developed by TSOs [32]. The Dutch TSO TenneT and DNV GL utilize a harmonic impact assessment as described in [32]. In the case of assessing possible TOVs, a harmonic impedance analysis can be performed, followed by a time-domain transient study [47]. When studying harmonic stability, a variety of approaches is still utilized in literature. Section 4.3 will elaborate briefly on harmonic stability assessment methods. The Harmonic Impact Assessment, the TOVs study and the assessment of harmonic stability will each be described in the following sections.

4.1 Harmonic Impact Assessment

4.1.1 The Conventional Harmonic Impact Assessment Method

The harmonic impact of a new distorting installation can be assessed for a certain Point of Evaluation (POE) [32]. The new distorting installation can be represented by a current source with a current I_{WF} and a parallel impedance, Z_{WF}. Firstly, the amplification factor k, with represents the amplification of the background harmonic voltage by the new installation, has to be determined [32]:

$$k = \left| \frac{Z_{WF}}{Z_{WF} + Z_g} \right| \tag{19}$$

With Z_{WF} the impedance of the distorting installation, which can be the impedance of the wind farm in the case of an analysis of the harmonic impact of an OWPP, and Z_g the impedance of the grid. The harmonic emissions voltage of the new distorting installation $V_{h,WF}$ is given by [32]:

$$V_{h,WF} = \left| \frac{Z_{WF} \cdot Z_g}{Z_{WF} + Z_g} \cdot I_{WF} \right| \tag{20}$$

The post-connection harmonic voltage U_h can then be determined [32]:

$$U_h = \sqrt[\alpha]{(k \cdot V_{BCK,h})^\alpha + (V_{h,WF})^\alpha} \tag{21}$$

With background harmonic voltage $V_{BCK,h}$ and summation law exponent α. α is equal to 1 for $h < 5$, 1.4 for $5 \leq h \leq 10$ and 2 for $h > 10$ [50].

In order to determine the harmonic voltage of the OWPP, the impedance of the grid and the OWPP have to be determined with the frequency method. The frequency method, or current source method, represents a plot of the impedance at a certain point in the system for a range of frequencies [13]. By injecting an 1 A of sinusoidal current with a specific frequency at a certain bus, the corresponding voltage and impedance can be determined [13]. This frequency sweep for the grid impedance can be performed in a power system simulation tool such as PowerFactory.

The impact of the new distorting installation is dependent on the grid impedance. In order to verify whether the harmonic emissions for the new distorting installation don't exceed the limits, several grid topologies have have to be encountered. The harmonic impact can be calculated with the grid impedance in 'worst case scenarios', where one or two elements are out of service. Consequently, the grid impedance is determined for N, N-1 and N-2 conditions [32]. For each harmonic order, the grid impedances of all these network topologies can be represented in an R, X-diagram. A six-corner envelope or hexagon can then be constructed for each harmonic order h in $[1, 50]$. This envelope encompasses all possible grid impedances that might appear at a given frequency [27]. Afterwards, between five to seven groups of individual enveloped are created based on the degree of overlap of the envelopes [32]. For each group, the frequency range is determined by using the minimum frequency of the lowest order in the group and the maximum frequency of the highest order in the group. Lastly, the six-corner envelope is constructed for each group, based on frequency scans of the grid impedance within the frequency range of that specific group [32].

The harmonic impact analysis consists of performing two tests [32]. Firstly, it has be tested whether the harmonic voltage of the new distorting installation is exceeding E_{Uhi}, the maximum individual emissions limits specified in the connection agreement. Secondly, it can be checked whether the post-connection harmonic voltage exceeds the compatibility level for N, N-1 and N-2 (planning) network topologies [32]. These two tests can be performed for each point (R, X-coordinate) of the hexagon of each group.

4.1.2 A Novel Approach for Harmonic Impact Assessments

The typical harmonic analysis practice in industry is to consider the harmonic-generating devices as ideal current sources. The data sheet of the harmonic emissions as defined by the manufacturer of the converter is then used to identify the magnitude of the harmonic current injection by the converter [28]. The converters are thus treated as passive elements, whereas in reality they are interactive elements. The approach utilized in industry still originates from the time that line commutated harmonic-generating devices such as load-commutated converters and diode rectifiers, were dominating [25]. It has been proven that modeling a VSC as an ideal current source might have considerable inaccuracy [13], [25], [29], [51], [52]. Three main reasons for this inaccuracy can be pointed out [31], [25]:

- The measurements of the harmonic emissions are performed by the wind turbine manufacturers in a clean grid environment. In reality, background harmonic distortion exists and the

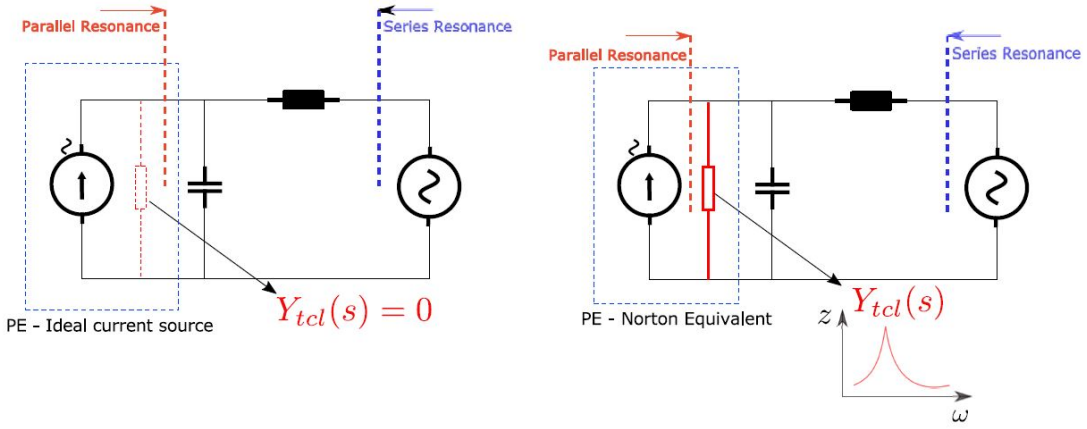

Figure 17: A wind farm modelled as a ideal current source (left) and the wind farm represented as a Norton equivalent, consisting of a current source and a Norton equivalent impedance in parallel (right) [25].

interaction of the converter with the background harmonics is therefore not included.

- An ideal current source model cannot capture the converter control reaction to the background harmonic voltage. Currently, the background harmonic voltage is solely added into (21) and are not implemented into the model of the network, thus neglecting the interaction of the converter with the background harmonics.
- During a frequency impedance scan, an ideal current source doesn't represent the frequency dependent inner current loop and the passive output filter, which can lead to an inaccurate estimation of the network resonance point.

To overcome the shortcomings of the approach of modeling the VSC as a current source, a Norton equivalent can be utilized [25]. A Norton equivalent encompasses a current source parallel to a Norton equivalent impedance [25]. The equivalent current source represents the disturbances which are caused by the PWM's switching, dead-time effect and the non-linear properties of the converter hardware and control [31]. The control output admittance in the model describes the converter interaction to the background harmonics [31] and can encompass the dynamics of the converter due to the oscillations induced by the PWM and the inner control loop. Since a harmonic voltage induces a certain current response of the converter, an impedance can capture all these dynamics. The control output admittance may have a positive, zero or even negative real part in different frequency ranges, which will lead to damped or amplified resonances in the system [38]. Figure 17 shows a Norton equivalent for a VSC, leading to an admittance varying over frequency.

As described in Section 2, each type 4 wind turbine is equipped with a back-to-back converter consisting of two VSC converters [53]. However, only the grid side VSC is represented in the Norton

Equivalent Impedance since the generator-side VSC is decoupled from the AC voltage dynamics by the DC link between the two converters [21], [53].

To summarize, when a Norton Equivalent Impedance is included in the conventional model to study harmonic emissions of wind farms, the dynamics of the wind turbine converters can be taken into account.

4.2 Transient Studies

The first step of an assessment of possible TOVs due to the installed OWPP is to perform several harmonic impedance scans at the POE. These scans can be performed for several cases that might lead to the lowest short circuit power at the POC, such as shunt compensation being out of service or decreased generation [47], [54]. Afterwards, a more detailed transient study can be carried out. Firstly, a simplified resonance analysis can be performed to identify the main components responsible for the resonances. Secondly, time-domain simulations can be carried out for several scenarios to verify whether overvoltages may occur [47], [52]. Performing a transient study to analyze TOVs is not part of the scope of this project.

4.3 Assessing Harmonic Stability

A third and relatively novel method to study harmonic interactions in OWPPs, is a stability assessment. Whereas a Harmonic Impact Assessment assess harmonic emission levels and a TOV study considers overvoltages, a stability assessment analyses the stability of the OWPP at a certain point in the system. Since recently issues have occurred with harmonic stability, such as in the case of BorWin-1 [3], it becomes increasingly interesting to perform stability assessments.
Two main methods are utilized for the analysis of harmonic interactions and instabilities in offshore wind power plants. Firstly, the state-space eigenvalue analysis can provide information about possible oscillations in a power system and to identify the assets which are part of this resonance [3], [53]. For this approach, detailed information and significant computational power is required [53]. The alternative is performing an analysis with the impedance-based method in the frequency domain. This method represents the frequency response of the grid and converters from their connection point [53]. The impedance-based method is suitable for modelling the converters of the wind turbines when detailed information is not available [53]. However, it is possible to include the effect of the controllers of the converter and stability assessments for impedance-based studies require less computational efforts [3], [53].
When assessing harmonic stability with an impedance-based method, two main tasks have to be carried out. Firstly, resonance frequencies have to be identified by utilizing an impedance-based representation of the system. Afterwards, at these resonance frequencies the stability can be analyzed. An additional advantage of this approach is that when identifying resonance points with the impedance based representation, the impact of both control parameters and of the OWPP configuration on the resonance frequencies can be exposed.

In order to identify resonance points, a specific location, either in the OWPP or at the onshore bus to which the OWPP is connected, has to be selected. Afterwards, the impedance observed from out that point in both upstream and downstream direction has to be determined.

After assessing the impedance observed from a certain point in the OWPP in both the upstream and downstream direction, the resonance frequencies can be determined. For example, when assessing stability at a converter, the intersections of the magnitudes of the converter impedance, Z_c and the equivalent grid impedance observed from the converter, Z_g approximately determine the resonant frequencies [21]. Series resonance points exist where $Z_c + Z_g$ has a dip or peak, which is approximately at the same frequencies as where $|Z_c| = |Z_g|$ [21].
The stability at the selected location in the OWPP at the identified resonance frequencies can be assessed by utilizing several different methods [53] (the example of assessing the stability at a converter is utilized to clarify each method):

- By analyzing the poles of T_h or the roots of $Z_g + Z_c^h = 0$. Where T_h is the closed loop transfer function of the wind turbine VSC:

$$T_h = \frac{1/Z_g}{1 + Z_c^h/Z_g} \tag{22}$$

- By applying the Nyquist stability criterion of Z_c^h/Z_g [55].
- By considering the passivity of T_h [56].
- By applying the positive-net damping criteria.

The positive-net damping criteria is a very straightforward and relatively simple method to assess the harmonic stability at harmonic frequencies [53]. Section 6.2.5 elaborates further on applying the positive-net damping criteria.

The outcome of the stability assessment can be verified by performing time-domain simulations in a power system analysis software tool such as PSCAD.

5 Case Studies

5.1 Case study I: A Harmonic Impact Assessment of three OWPPs in the North Sea

A Harmonic Impact Assessment for three OWPPs in the North Sea has been performed. The OWPPs are connected to the same PCC and it is assumed that the OWPPs are connected with HVAC cables. The impact of including a Norton Equivalent Impedance into the PowerFactory model for an Harmonic Impact Assessment has been studied for the OWPPs. The calculations have been performed for three different cases. In the first case, only one platform is operating, in the second case two platforms are operating, and in the third case all three OWPPs are operating. The harmonic amplification was first determined for case 1. Afterwards, the harmonic amplification by the first wind farm was included into the background harmonic distortion for the calculation of case 2, when the second wind farm also starts operating. The harmonic amplification from case 2 were then included in the background harmonic distortion when determining the added harmonic amplification of the third wind farm.

A PowerFactory model has been utilized to perform the required frequency sweeps of the OWPPs and of the network at the 380 kV busbar. As already mentioned, a comparison has been made between the results with a model including a Norton Equivalent Impedance for the wind turbines, and thus including harmonic interactions into the analysis, and a model solely including constant current sources. It was decided to not include a harmonic voltage source in the model representing the background harmonics. This was due to the fact that for the Harmonic Impact Assessment solely frequency sweeps had to be performed, and there was no necessity for load flow simulations in PowerFactory. Adding a harmonic voltage source would have not impacted the results of the frequency sweeps. Therefore, it can be concluded that for this Harmonic Impact Assessment, the interaction between the converters and the background harmonics were not taken into account in PowerFactory. However, in (21), the background harmonic distortion is taken into account for the post-connection harmonic voltage.

Electrical characteristic	**Value [unit]**
Rated grid voltage (phase to phase RMS)	0.69 [kV]
Rated Grid side inverter power	2 x 4 [MW]
AC Grid Frequency	50 [Hz]
DC link voltage	1.2 [kV]
Switching frequency	1200 [Hz]
L_{inv} (converter side inductor)	120 [μH[
C_f (Filter capacitor)	5200 [μF[
R_f (Filter damping resistor)	0.02 [mΩ]
α_f (Bandwidth low pass filter feed forward term)	50
q_d	1
T_s (sampling time)	0.01 [ms]

Table 1: 8MW Wind Turbine design parameters [16].

The Norton Equivalent impedance was formulated by utilzing the parameters shown in Table 1. The Norton Equivalent Impedance is determined according to (14), while adding the parallel impedance of the capacitive filter. The outer current loop is not represented in the Norton equivalent impedance since its dynamic response is slow and sufficient bandwidth separation exists with the inner current loop [53]. Since this study encompasses harmonic interactions and considers oscillations of frequencies in the range from 100 up to 2500 Hz, sideband-oscillations induced by the PLL and the outer current loop are not taken into account when determining the Norton Equivalent Impedance.

5.2 Case study II: Stability Assessment of two OWPPs in the North Sea

A harmonic stability assessment for two HVAC-connected OWPPs in the North Sea has been performed. The OWPPs consist each of 54 wind turbines of 8 MW, encompassing a total capacity of 864 MW. In order to simplify, 1x8MW WT converters were considered instead of a 2x4 MW configuration. Four high voltage export cables of 60 km are utilized to transport the electricity at 220 kV to the shore. In order to increase the offshore capacity compared to a 33 kV offshore network which is conventionally utilized in industry, a voltage of 66 kV is utilized [57]. The wind farm consists of 12 strings in a radial configuration, which are connected in equal groups to four rails. These rails are then connected to two collector transformers, two export cables and one offshore platform. Figure 18 provides a general sketch of the lay-out of the wind farm. Both a link cable between neighbouring rails and between the two OWPPs exists and the breakers of these link cables are during normal operations open. The 380 kV busbar was selected as the Point of Evaluation for the stability assessment. It has to be noted that since harmonic interactions are studied, this case study solely considered frequencies from 100 Hz to less than half the switching frequency.

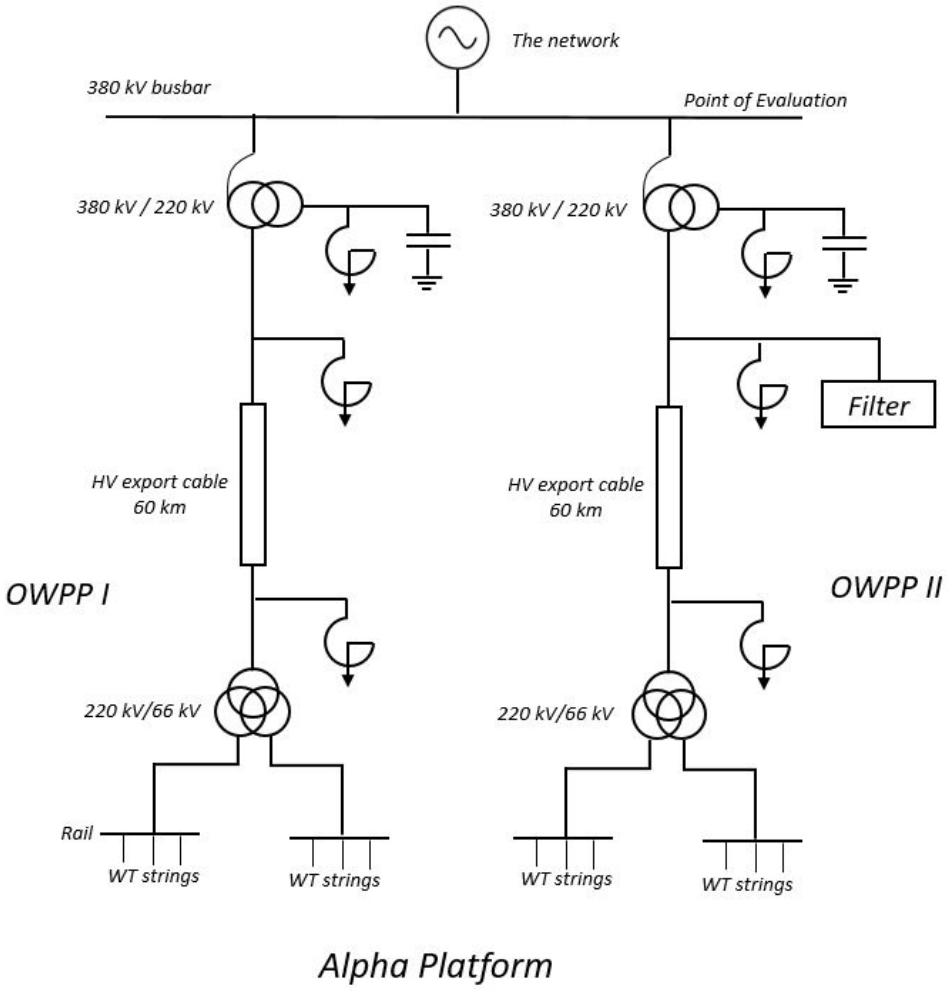

Figure 18: Configuration of OWPP I and OWPP II.

Since for this study solely harmonics in steady-state are considered, the impedance-based method is the most suitable approach for the stability assessment. Therefore, an impedance-based representation of the OWPPs was formulated. Secondly, resonance points were identified by comparing the network impedance and the wind farm's impedance and the positive net-damping criteria was applied. Lastly, time domain simulations were performed to verify the results.

The OWPP can be represented as a current source in parallel with the impedance of the Wind Turbines, together with an impedance representing the offshore grid ($Z_{OWPP,g}$). The Point of Evaluation (POE) is situated between the grid and the OWPP. Figure 20 shows that this can be simplified, when a constant power output of the wind turbines is assumed, to one impedance. For

the stability assessment, either a scenario where the grid and the OWPP are in parallel or a scenario where the impedances are in series, can be considered. Since the aim is to study the stability of the system when background harmonic voltages are coming fromout the network, the network is represented as a voltage source and an impedance. If the OWPP and the grid would be placed in parallel, and at a certain frequency the impedances of the grid and the OWPP are equal but opposite, no current would flow through the system. Whereas, in the case of a series circuit, when the impedances are equal but opposite, a large current will flow. Consequently, since in this case a voltage source is connected to the equivalent impedances, it makes sense to study the case in which the wind farm and the network are placed in series.

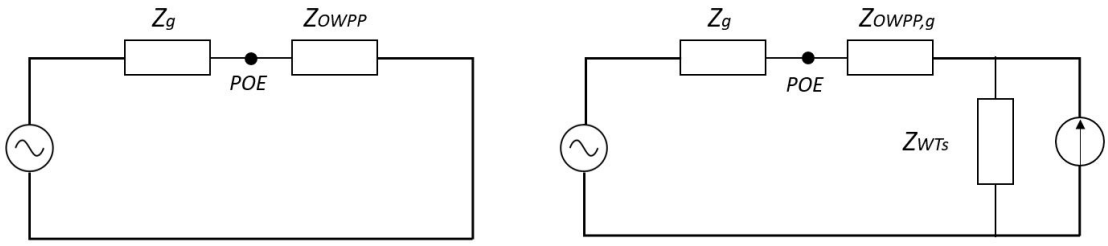

Figure 19: An equivalent circuits for a scenario where the OWPP and the grid are in series. The simplified equivalent circuit is displayed on the left.

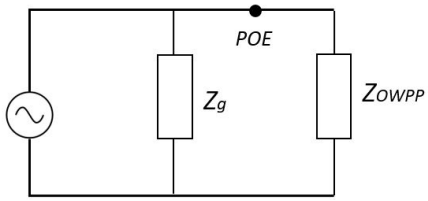

Figure 20: An equivalent circuit for a scenario where the OWPP and the grid are in parallel. A simplified equivalent circuit is displayed on the left.

The impedance-based representation of the OWPPs was made by both an analytical model and by performing frequency sweeps of a PSCAD model. The coming two sections will elaborate on these approaches.

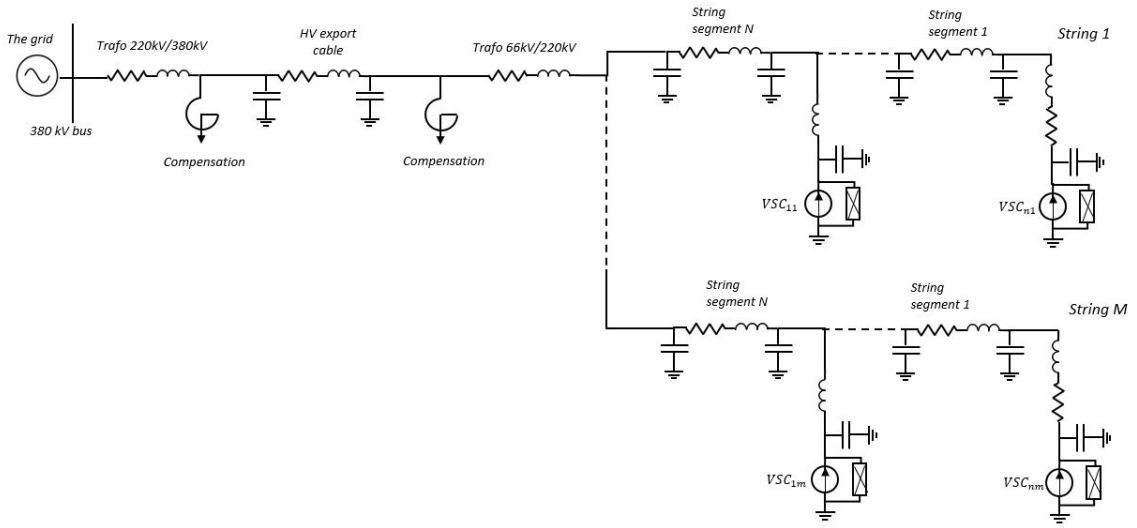

Figure 21: An impedance-based representation of the offshore network.

5.2.1 Analytical Model of the Impedance of the OWPPs

The analytical model describes the components of the offshore network solely as RLC elements, as shown in Figure 21.

The impedance of the transformers are translated into RL-equivalents and the export cable is represented by a PI-section. The filters and compensation in the OWPPs have been represented by RLC elements as well. Table 2 shows the utilized values for these components. The export cable data was obtained from [58], whereas the collector transformer data was obtained from [21].

Electrical Characteristic	**Value [unit]**
Export cables	
Length	60 [km]
C_{ec}	163 [μC/km]
R_{ec}	0.206 [Ω/km]
L_{ec}	0.428 [mH/km]
Collector transformers (66kV/220kV)	
L_{tr}^{cs} at 220 kV	20.6 [mH]
R_{tr}^{cs} at 220 kV	0.220 [Ω]
WT transformers (0.69kV/66kV)	
L_{tr}^{w} at 66 kV	0.124 [H]
R_{tr}^{w} at 66 kV	5.84 [Ω]

Table 2: Electrical characteristics of the OWPP which are utilized for the impedance based analysis [58], [21].

The analytical impedance of the converters has been modelled as a Norton Equivalent Impedance as in (14). The values which have been utilized for the VSC converter are shown in Table 3.

Electrical characteristic	**Value [unit]**
Rated grid voltage (phase to phase RMS)	0.69 [kV]
Rated Grid side inverter power	2 x 4 [MW]
AC Grid Frequency	50 [Hz]
DC link voltage	1.45 [kV]
Switching frequency	1200 [Hz]
L_{inv} (converter side inductor)	50 [μH[
C_f (Filter capacitor)	1 [mF[
R_f (Filter damping resistor)	0.02 [mΩ]
α_f (Bandwidth low pass filter feed forward term)	50
q_d	1
T_s (sampling time)	0.01 [ms]

Table 3: Electrical characteristics of the modelled wind turbine converter.

The impedance of the OWPPs was then studied using the Laplace transform, where the voltage is a Laplace transformed waveform. This voltage $V(s)$ is then dependent on the complex frequency s:

$$s = j\omega \tag{23}$$

With frequency in rad/s $\omega = 2\pi f$.

An expression can then be derived where the impedance of a certain RLC circuit is expressed as a transfer function:

$$V = RI + \frac{LdI}{dt} + \frac{1}{C}\int I \cdot dt \tag{24}$$

$$V(s) = R \cdot I(s) + Ls \cdot I(s) + \frac{1}{Cs} \cdot I(s) \tag{25}$$

$$V(s) = (R + Ls + \frac{1}{Cs}) \cdot I(s) \tag{26}$$

$$Z(s) = \frac{V(s)}{I(s)} = R + Ls + \frac{1}{Cs} \tag{27}$$

By utilizing (27), the equivalent impedance of the cables and transformers in an offshore network was determined. (14) was utilized to include the impedance of the converters. The impedance was displayed by creating a Bode plot, which is a common utilized method for RLC-circuits. The impedance is then expressed in dB's [59]:

$$Z[dB] = 20 \cdot log_{10}(Z[\Omega]) \tag{28}$$

Four different voltage levels are present in the OWPP: 0.69kV, 66kV, 220 kV and 380 kV. To convert the impedance value expressed at one voltage level to another voltage level, the following equation was utilized [60]:

$$Z_{V2} = \frac{Z_{V1}}{Z_{b,V1}} \cdot Z_{b,V2} \tag{29}$$

With the voltage level at the primary side V_1, the base of the impedance expressed at the primary voltage side $Z_{b,1} = U_1^2 S_b$, the voltage level at the secondary side V_2, and the base of the impedance expressed at the secondary voltage side $Z_{b,2} = U_2^2 S_b$.

5.2.2 PSCAD Model

A PSCAD model of both OWPPs has been created. The wind turbines have been modelled as AC voltage sources, representing the grid-side converter of the VSCs. Since the DC link electrically isolates the grid-side converter from the generator-side converter and the mechanical part of the VSC model, this representation is sufficient. The controls of the VSC were modelled as described in Section 2.4. PSCAD is mainly used since it allows implementing the controls of the WT converters into the model. Instead of utilizing the AC voltage reference, a power reference value of 8 MW was utilized to determine the q-component of the reference current value. The reactive power reference was set to zero and was utilized to calculate the d-component of the reference current [8]:

$$i_d^* = \frac{2}{3}\frac{P^*}{v_{zd}} \tag{30}$$

$$i_q^* = \frac{2}{3}\frac{Q^*}{v_{zd}} \tag{31}$$

With P^* and Q^* respectively the reference value of the active and reactive power, and with i_d^* and i_q^* respectively the reference value of the d-component and q-component of the reference current.

For simplification, an average model was created, without considering switching. The same values as in Table 3 were utilized. Figure 22 shows schematically the model of the VSC.

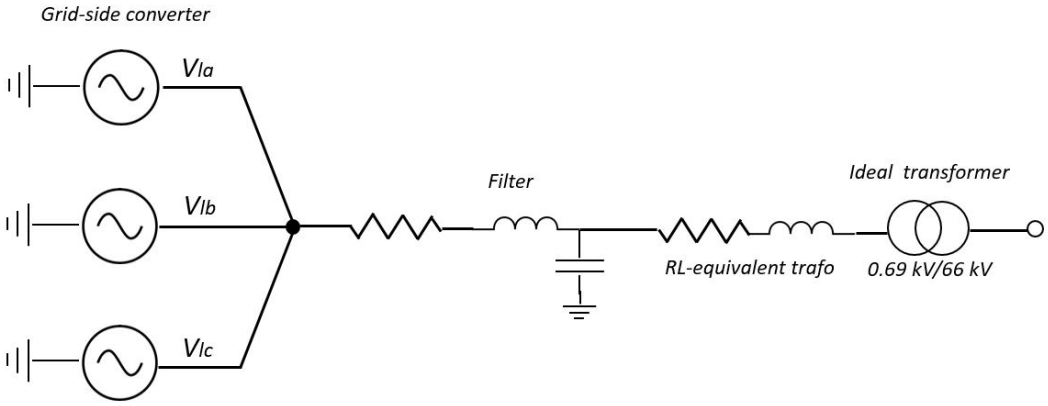

Figure 22: A schematic representation of the coverter model whcih was implemented in PSCAD. The control scheme is not visualized. V_{la}, V_{lb} and V_{lc} are the applied convertrer voltages, which result from the current loop.

The cable segments between the wind turbines have not been modelled in order to simplify the model. Section 6.2.2 elaborates on the justification of this assumption. Transformers were modelled as ideal transformer in series with a RL-equivalent. This was utilized instead of solely a non-ideal transformer model in order to simplify the comparison between the frequency sweeps performed in PSCAD and the analytical model. For the same reason, the export cable was modelled as a PI-section and no frequency dependent cable model from the PSCAD library was used. Consequently, the results from PSCAD can be more easily compared to the analytical model, however it leads to a certain error when comparing the results to reality. The same values as for the analytical model as in Table 2 were taken into account for the cables and transformers.

For a frequency sweep of the network at the 380 kV busbar, a PSCAD model of a large part of the Dutch network has been utilized. The Interface to Harmonic Impedance Solution (Frequency Scanner) block was implemented to obtain the impedance of the network.

The PSCAD model was utilized to perform frequency sweeps of the OWPPs. However, the Interface to Harmonic Impedance Solution component of PSCAD is solely able to measure the impedance profile of passive elements. When this component is connected, it grounds all voltage sources and injects a current of 1 A into the the system. Consequently, it cannot perform a frequency sweep for active elements such as a Voltage Source Converter. However, an alternative approach can be utilized for measuring the impedance of the VSC. The VSC can be connected to a voltage source which also applies the nominal voltage and a harmonic voltage of 1 percent of the nominal value. The Fast Fourier Transform (FFT) component of PSCAD can then identify the magnitude and the phase for each harmonic order when it receives instantaneous voltage and current measurements from a multi meter. For each harmonic order, the impedance can then be determined [21]:

$$|Z| = \frac{|V|}{|I|} \tag{32}$$

$$arg(Z) = arg(V) - arg(I) \tag{33}$$

The voltage and current in the dq-frame are fed into the FFT component. Since the dq-reference frame is shifted 50 Hz from the stationary-reference frame, the FFT has to measure at a frequency of 50 Hz above the frequency of the inserted harmonics in the stationary-frame.

As already mentioned, for every harmonic order, a harmonic voltage has to be applied, the harmonic voltage and current have to be measured and the impedance value for that specific harmonic order can be determined. In order to model a voltage source which consists of both a voltage at the nominal value and of a voltage at the harmonic frequency in PSCAD, three DC voltage sources were implemented. When the voltage applied by each DC voltage source is a cosine function, the DC source is converted into an AC source. Moreover, by utilizing this method, the voltage values of the DC sources can be a summation of a cosine function representing the nominal AC voltage and a cosine function representing the harmonic AC voltage. (34), (35) and (36) describe the values of the voltage in each phase (V_a, V_b and V_c) [61]:

$$V_a = |V_a| \cdot \cos(\omega t) + |V_h| \cdot \cos(n\omega t) \tag{34}$$

$$V_b = |V_b| \cdot \cos(\omega t - \frac{2\pi}{3}) + |V_h| \cdot \cos(n\omega t - \frac{2n\pi}{3}) \tag{35}$$

$$V_c = |V_c| \cdot \cos(\omega t - \frac{4\pi}{3}) + |V_h| \cdot \cos(n\omega t - \frac{4n\pi}{3}) \tag{36}$$

With harmonic voltage V_h, harmonic order n, time t and frequency in rad/s ω.

The tasks performed in PSCAD were automized by utilizing a Python script, as described in the appendix A.

6 Results and Discussion

6.1 Harmonic Impact Assessment

For the first case study, the effect of connecting an increasing amount of OWPPs on the harmonic emissions, was studied. Moreover, the impact of including a Norton Equivalent Impedance when performing a Harmonic Impact Assessment was analyzed.

6.1.1 Impedance profiles of the Wind Warms

Firstly, frequency sweeps were performed in PSCAD of the OWPPs. Figure 59, 60 and 61 show the result of these sweeps, including both the results of the case where a Norton Equivalent Impedance was utilized and of the conventional method. However, since for frequencies over 750 Hz, no differences can be observed between the two methods, solely the impedance of up to 750 Hz is displayed. Appendix B shows the impedance for frequencies up to 2500 Hz as well.

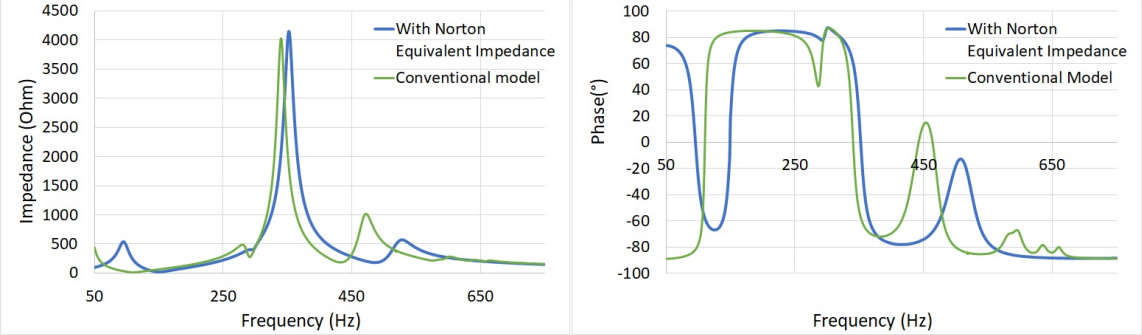

Figure 23: Impedance of wind farm 1.

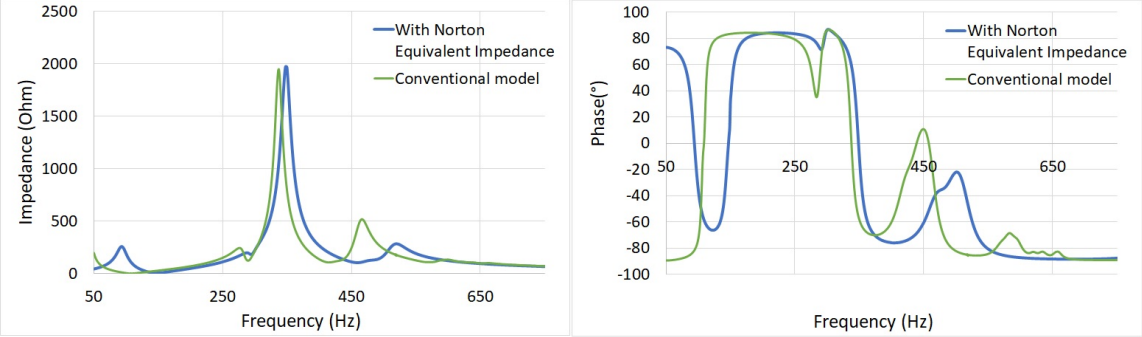

Figure 24: Impedance of wind farm 2.

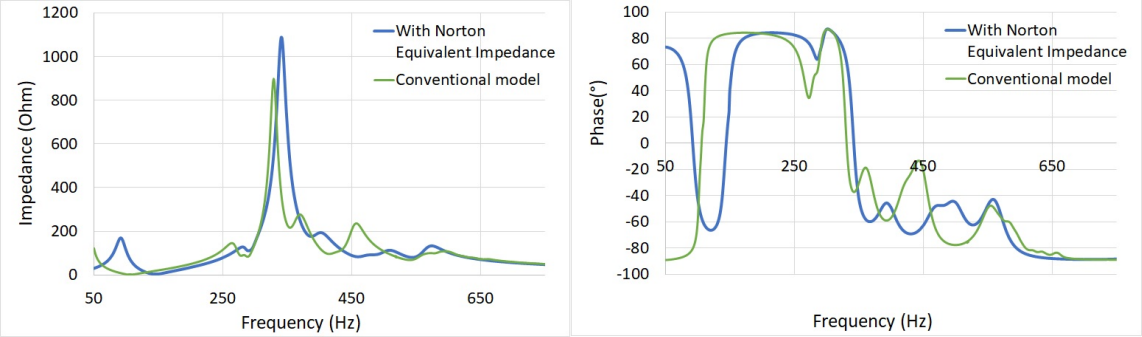

Figure 25: Impedance of wind farm 3.

It can be observed that when including a Norton Equivalent Impedance, both the series and parallel resonance frequencies of the wind farm are shifted. The magnitude of the peaks slightly differ as well, but no clear trend can be observed. However, the shift of resonance frequencies can be of significance for the harmonic levels at each harmonic order.

6.1.2 Impedance of the Network

For N-0, N-1 and N-2 topologies, the impedance of the network at the 380 kV busbar has been determined by utilizing a model of the network in Powerfactory. Figure 26, 27 and 28 show the R, X-diagrams for each of the three cases, including each the N-0, N-1 and N-2 topologies. It has to be mentioned that the hexagon of Figure 27 encompasses the impedance of the network which includes wind farm 1, whereas the hexagon of Figure 27 encompasses the impedance of the network which includes OWPPs 1 and 2.

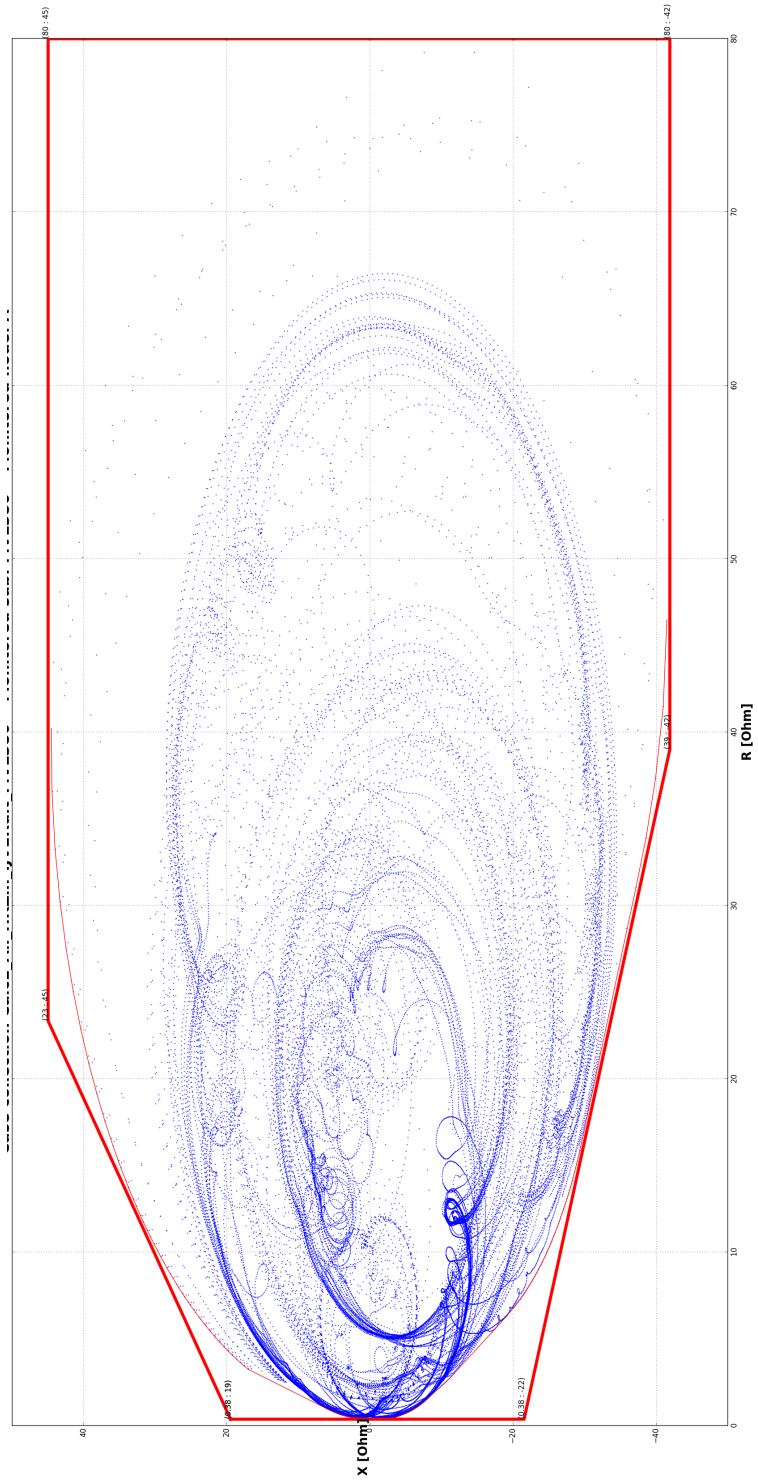

Figure 26: R, X values of the grid at the 380 kV busbar for case 1, with only one wind farm operating, for N-0, N-1 and N-2 topologies.

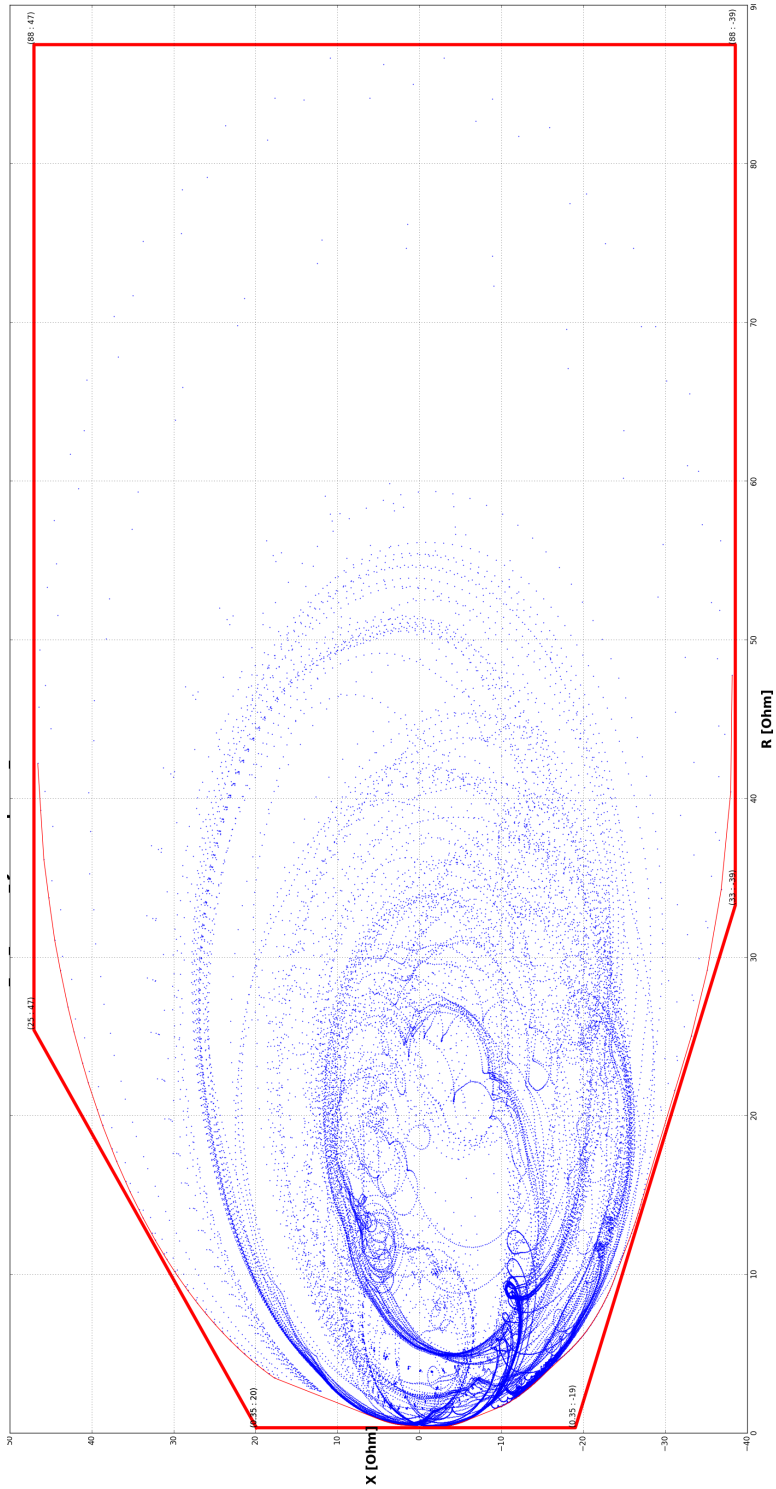

Figure 27: R, X values of the grid at the 380 kV busbar for case 2, with two OWPPs operating, for N-0, N-1 and N-2 topologies.

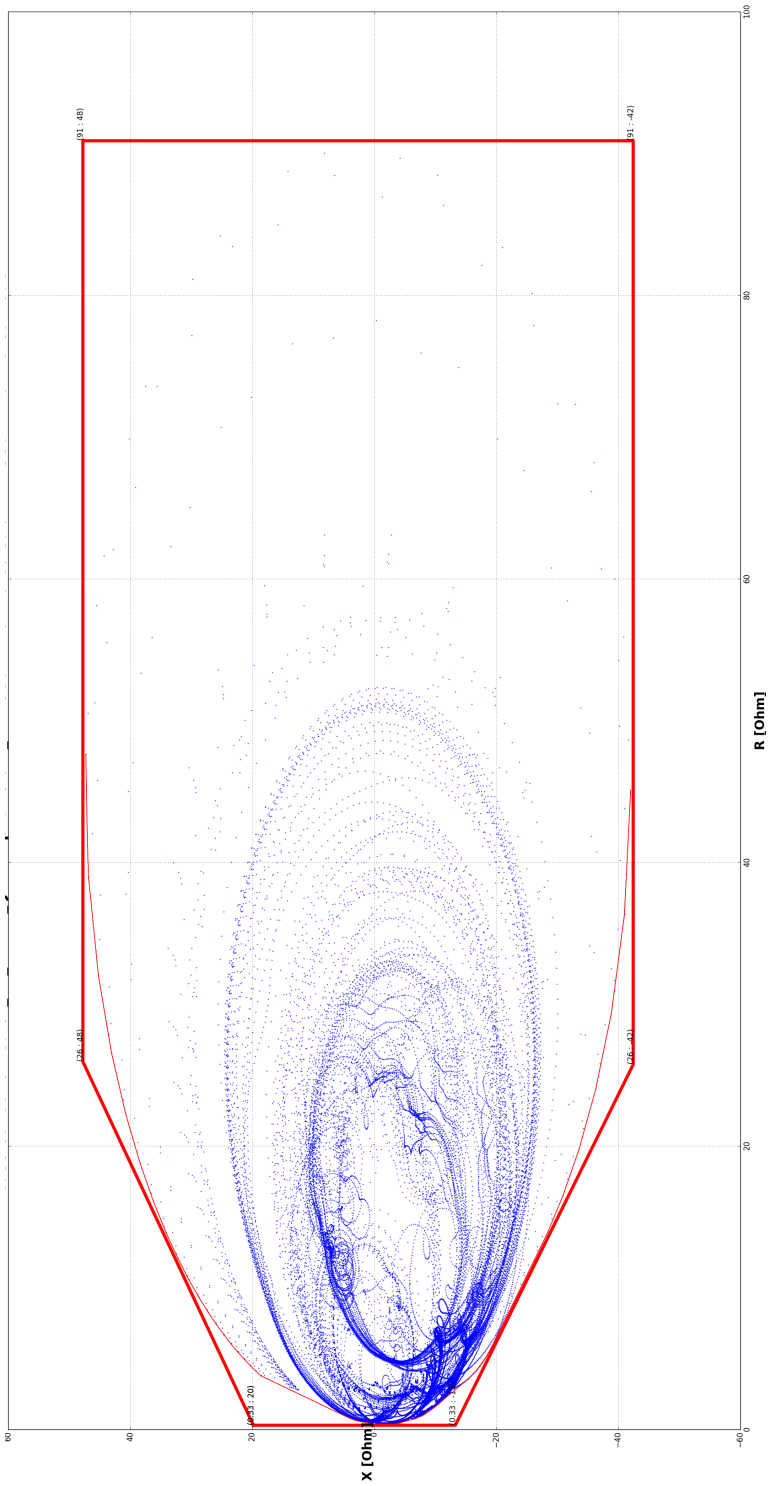

Figure 28: R, X values of the grid at the 380 kV busbar for case 3, with all OWPPs in operation, for N-0, N-1 and N-2 topologies.

6.1.3 Gain Factors

For each case, the gain factors were determined according to (19). Figure 29, 30 and 31 show the gain factors over a frequency range from 50 Hz op to 2500 Hz for both the model including the Norton Equivalent Impedance and the conventional model.

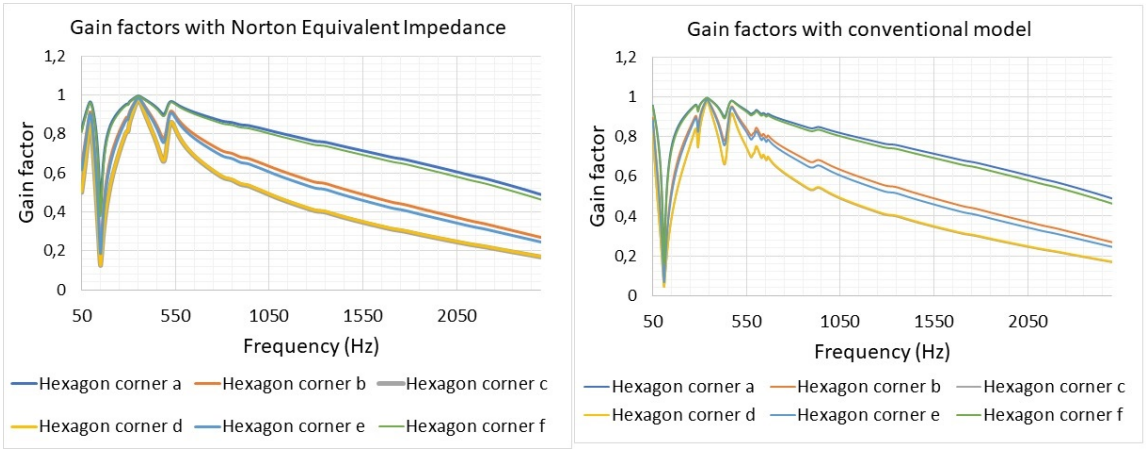

Figure 29: Gain factors determined with both the PowerFactory model including (left) and excluding (right) the Norton Equivalent Impedance for case 1, with only one wind farm in operation.

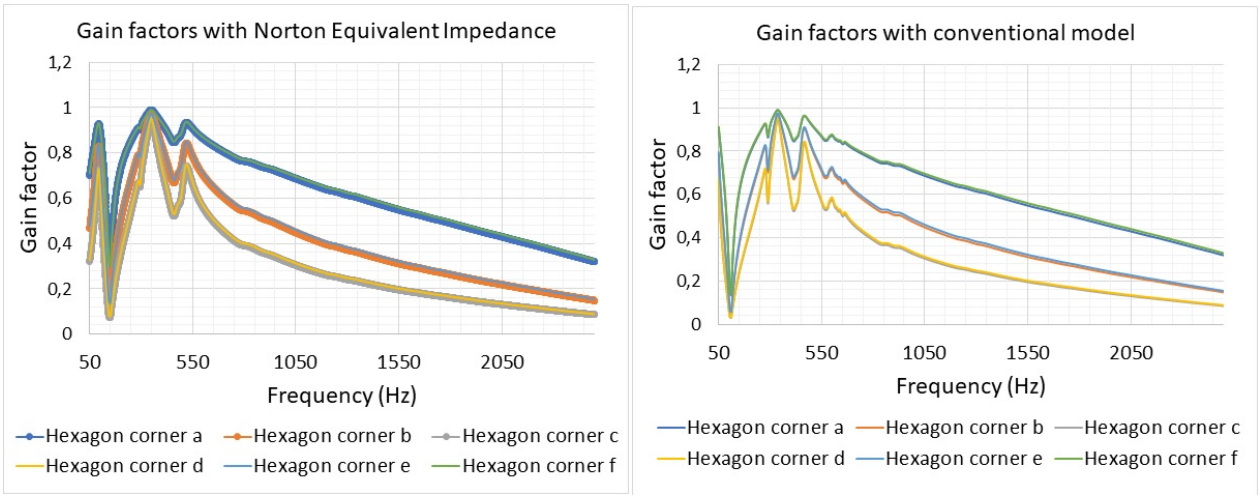

Figure 30: Gain factors determined with both the PowerFactory model including (left) and excluding (right) the Norton Equivalent Impedance for case 2, with two OWPPs in operation.

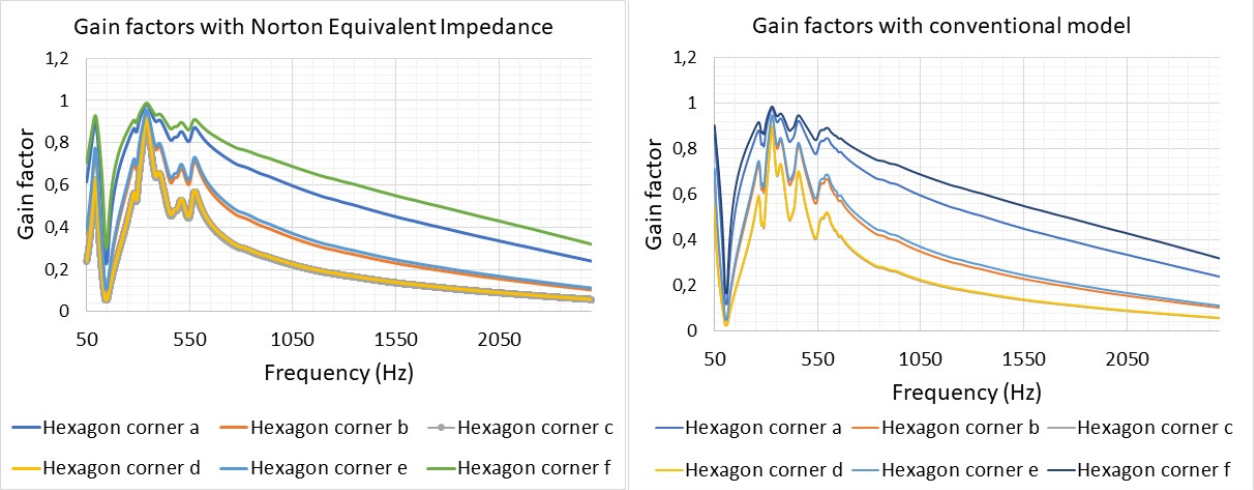

Figure 31: Gain factors determined with both the PowerFactory model including (left) and excluding (right) the Norton Equivalent Impedance for case 3, with all OWPPs in operation.

In general, it can be observed that when including a Norton Equivalent Impedance, the gain factor curves become smoother compared to the conventional case. Moreover, not necessarily the magnitude of the peaks change, but the peaks of the gain factor curves are shifted. For all cases, the peak of below 50 Hz with the conventional model, is shifted to a frequency of around 100 Hz. Naturally, a peak in the gain factor at 100 Hz can be troublesome, as it might affect transients such as the inrush current during the energisation of an offshore transformer. However, the gain factor doesn't provide a full picture yet and it is only a part of (21). Moreover, the effect of a transient event such as the energisation of a transformer is not within the scope of a harmonic Imapct Assessment where purely emission levels are assessed.

6.1.4 Total Harmonic Distortion

The post-connection harmonic voltage was determined for each case according to(21). This voltage was then translated into Total Harmonic Distortion values as a percentage of the maximum allowed value at each harmonic order. The 95 percent limit of THD as set by the TSO was utilized for when determining these values.

As shown in figures 32, 34 and 36, in the end, the peak in the gain factor at around 100 Hz, doesn't translate into an exceedance of the harmonic distortion. However, at higher frequencies the maximum value of the THD is exceeded. For these frequencies the grid impedance with the Norton Equivalent Impedance doesn't deviate from the impedance of the conventional case. For this specific case, including the Norton Equivalent Impedance doesn't yield different results when looking purely at where the harmonic distortion levels are exceeded.

When including more OWPPs at the POC, the largest peak of the THD shifts to lower frequencies. However, the magnitude of this peak also decreases when connecting more OWPPs. In general, all peaks in THD shift to lower frequencies when connecting more OWPPs. Some peaks shift more significantly than others. It varies whether the peaks in THD increase or decrease. It is very case dependent whereas the increase of the THD at a certain frequency when connecting more OWPPs is exceeding the limits. It is remarkable though that when more OWPPs are connected, an initial exceedance of the THD disappears.

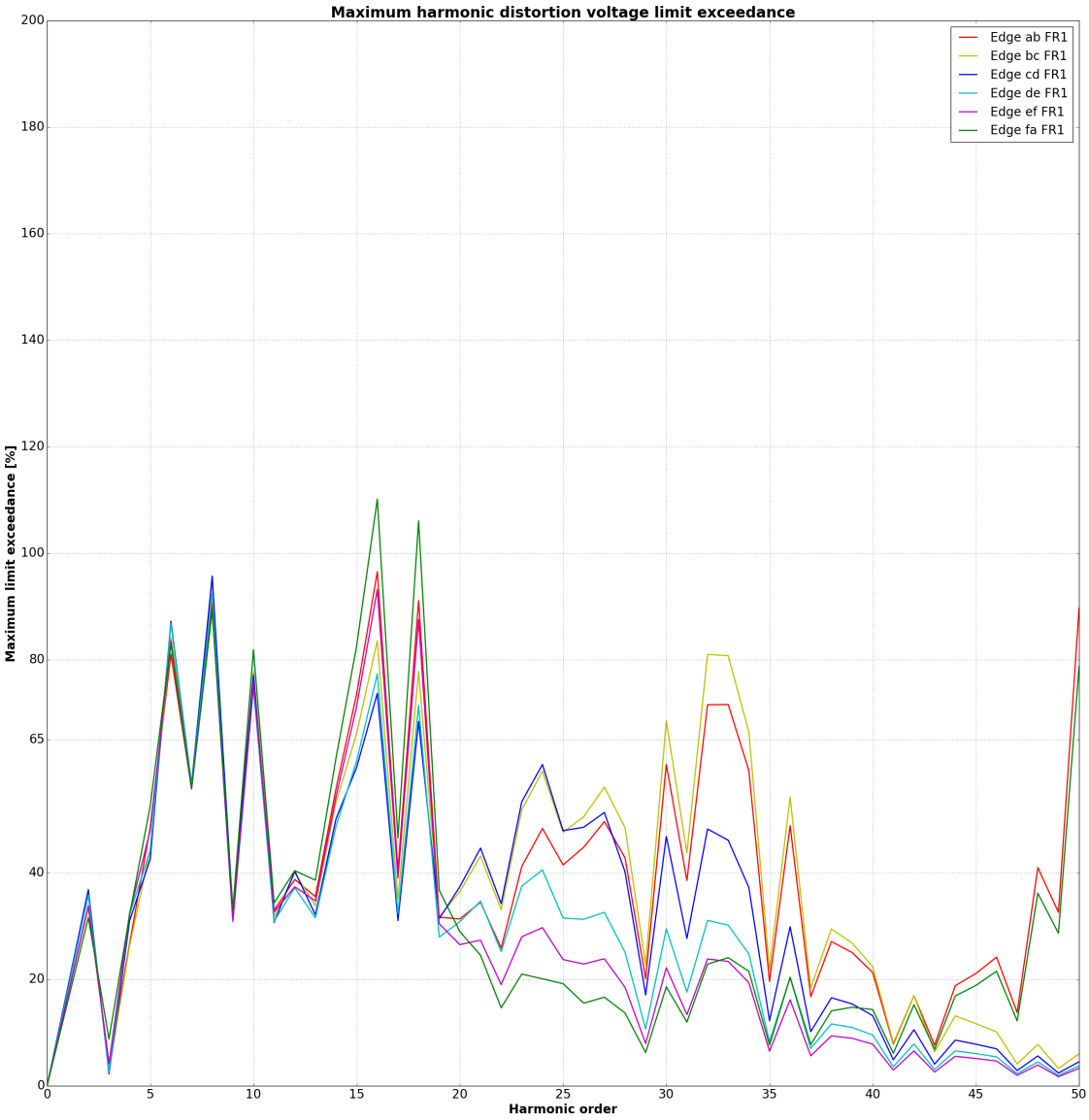

Figure 32: Total Harmonic Distortion of the voltage for case 1, after connecting one wind farm, as a percentage of the total allowed distortion. A Norton Equivalent is included for these calculations.

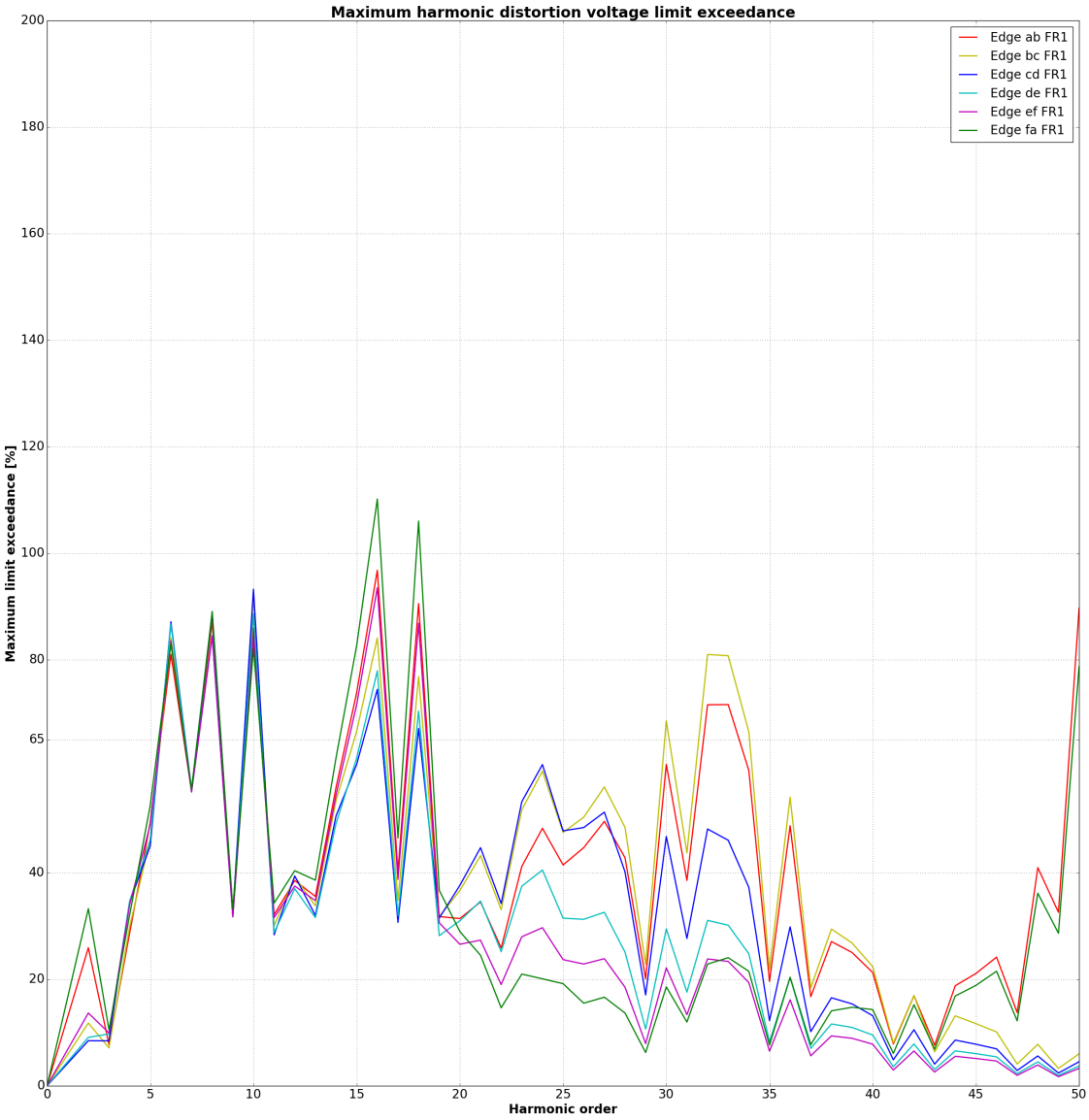

Figure 33: Total Harmonic Distortion of the voltage for case 1, after connecting one wind farm, as a percentage of the total allowed distortion, as determined with the conventional model.

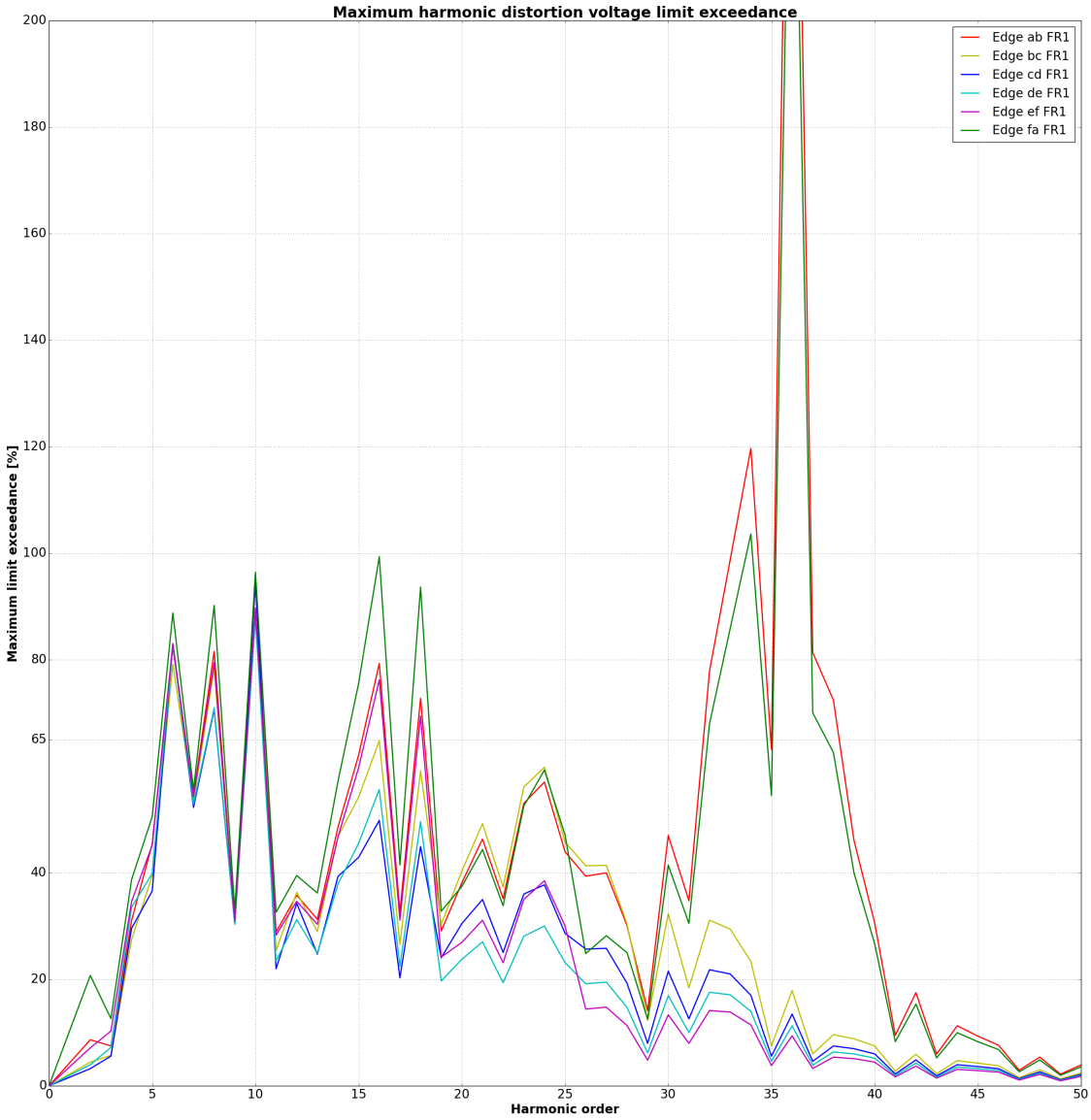

Figure 34: Total Harmonic Distortion of the voltage for case 2, after connecting two OWPPs, as a percentage of the total allowed distortion. A Norton Equivalent is included for these calculations.

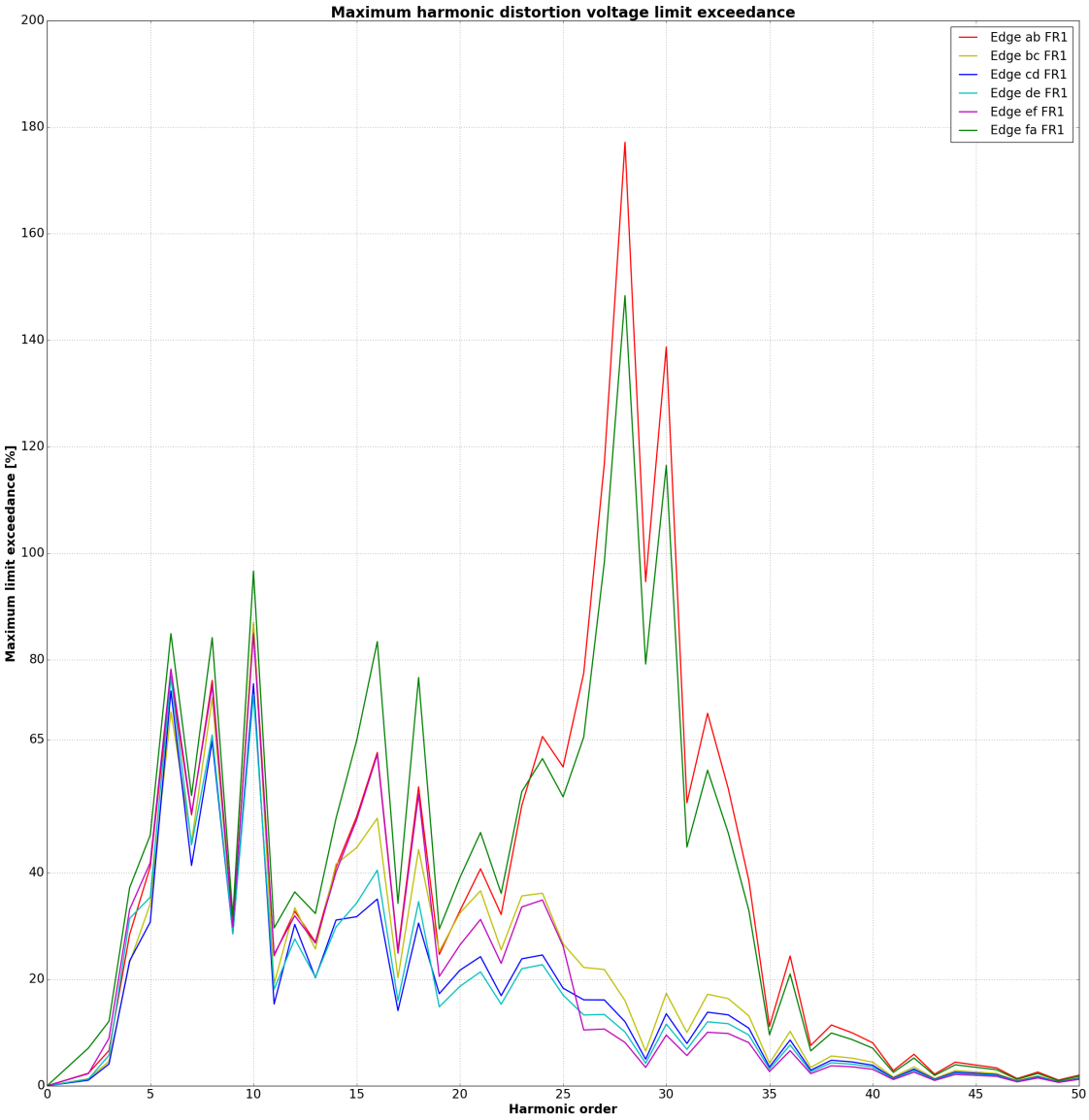

Figure 35: Total Harmonic Distortion of the voltage for case 2, after connecting two OWPPs, as a percentage of the total allowed distortion, as determined with the conventional model.

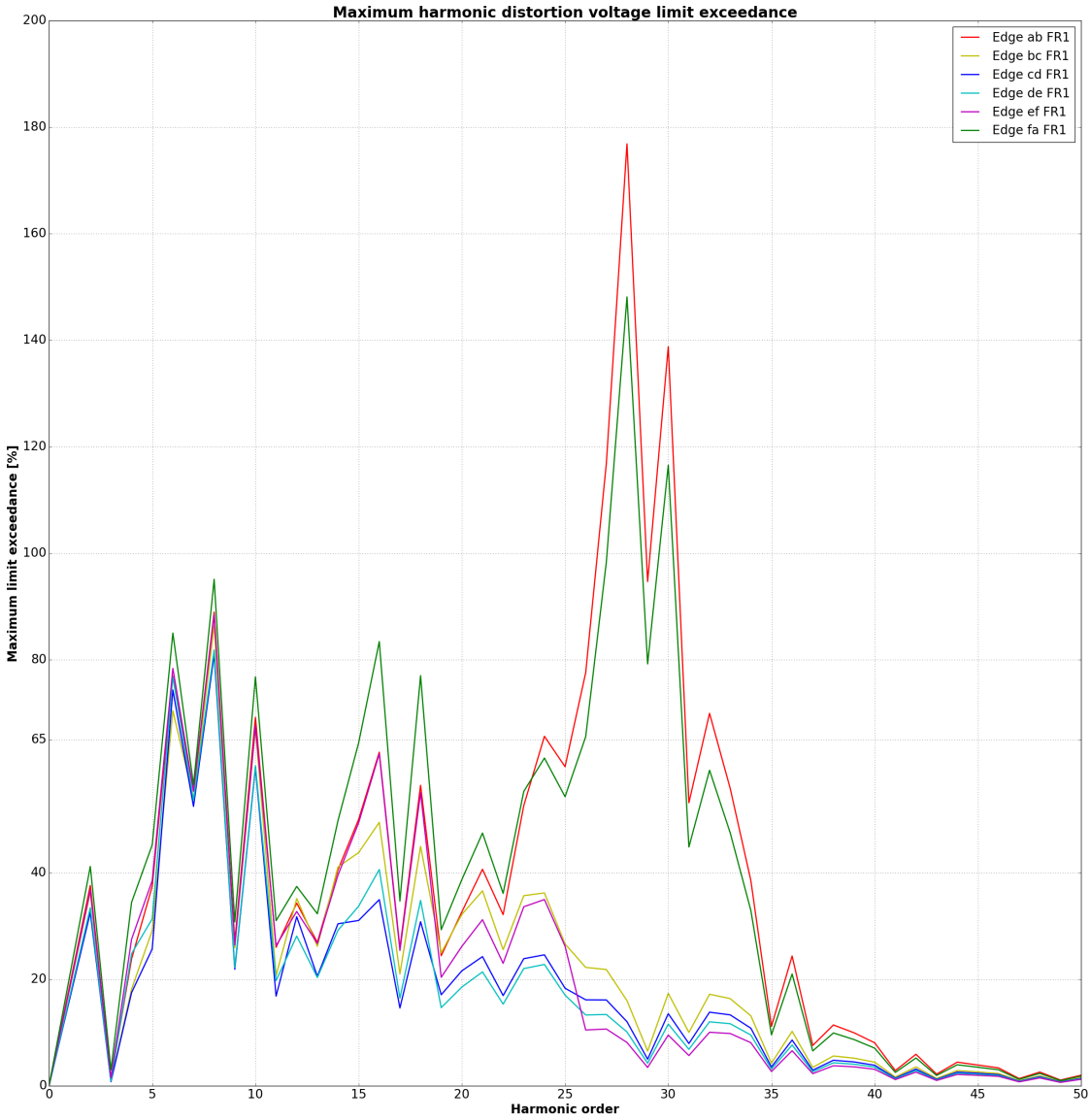

Figure 36: Total Harmonic Distortion of the voltage for case 3, after connecting three OWPPs, as a percentage of the total allowed distortion. A Norton Equivalent is included for these calculations.

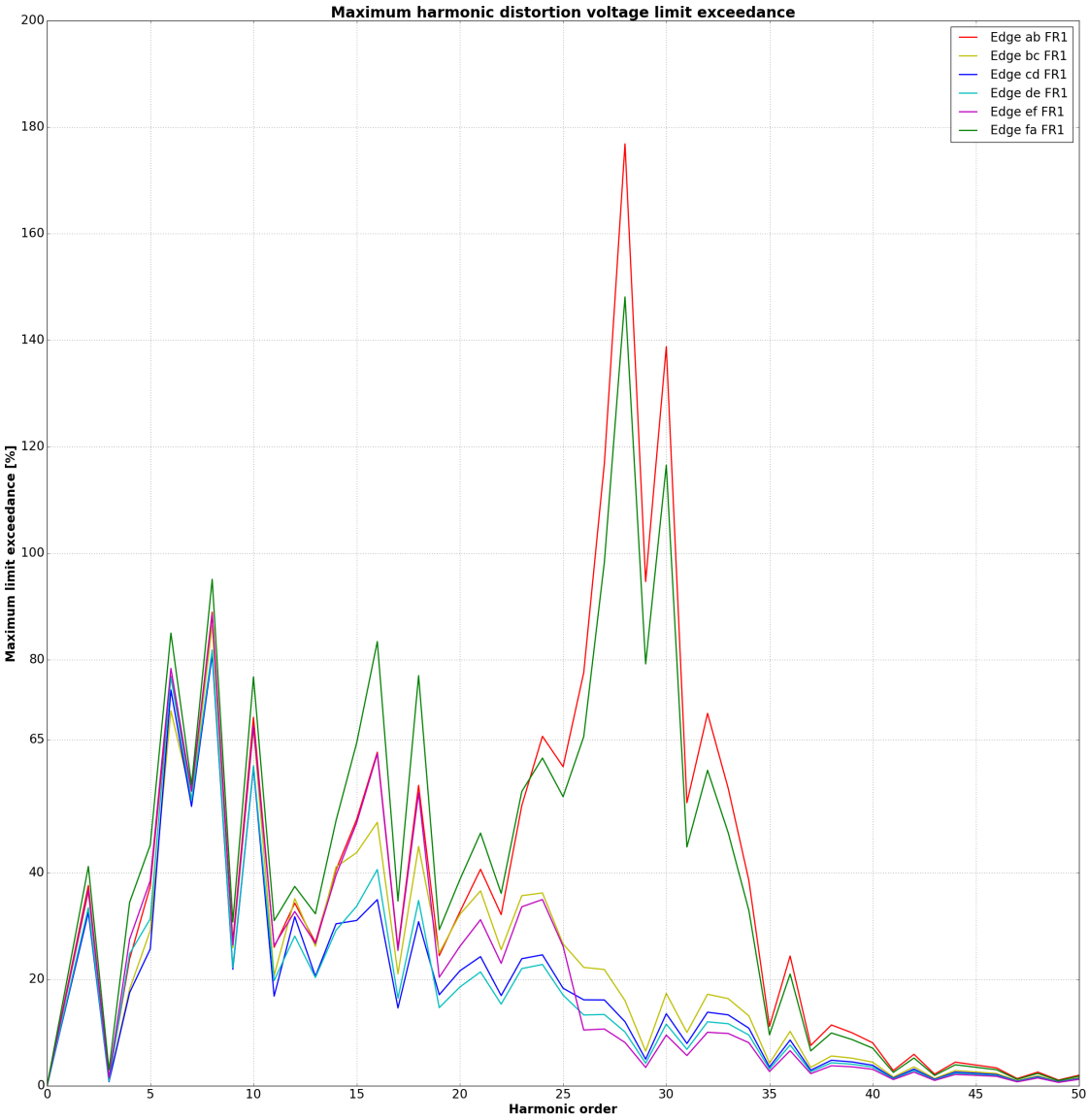

Figure 37: Total Harmonic Distortion of the voltage for case 3, after connecting three OWPPs, as a percentage of the total allowed distortion, as determined with the conventional model.

6.2 Harmonic Resonance Stability Assessment

6.2.1 The Impedance of a Single Wind Turbine converter

In order to perform the stability assessment of the wind farm of case study II, first the impedance profile of the wind farm had to be determined by utilizing both an analytical model and frequency sweeps in a PSCAD model. In order to do so, firstly for one single converter it had to be verified whether the analytical model and the PSCAD model were generating the same frequency profile. The most simplified model of the VSC solely considers the inner current loop and neglects the feed forward term H_v, the time delay Dw, the output filter capacitance and the step-up transformer. However, when no filter for the measured grid voltages is considered, the bandwidth of this filter approaches infinity. As can be seen in (6), when α_f approaches infinity, H_v becomes equal to 1. When the time delay is assumed to equal to zero, D^w becomes equal to 1 as well. Consequently, when both the feed forward term and the time delay are neglected, the impedance of the wind turbine approaches infinity. Therefore, the most simplified model of the converter which is considered, takes the inner current control loop, the coupling inductance and resistance and the voltage feed forward term into account. The impedance of the wind turbine can then be described with the following equation:

$$Z_{wt} = \frac{R_f^w + sL_f^w + F_{PI,c}}{1 - H_v} \tag{37}$$

Figure 38 shows the impedance of the converter including the low pass filter according to both the analytical model of (37) and frequency sweeps performed in PSCAD. The PSCAD model and the analytical model align, however, for frequencies towards 100 Hz, the analytical model becomes less accurate. A further decrease in the time step of the simulations could however also ensure that the curves align more for lower frequencies.

When a time delay is taken into account, the analytical expression for the impedance of the converter is equal to:

$$Z_{wt} = \frac{R_f^w + sL_f^w + j\omega_1 L_f^w + D^w(F_{PI,c} - j\omega_1 L_f^w)}{1 - D^w H_v} \tag{38}$$

Figure 6.2.1 represents the impedance of the converter including the time delay. It can be observed that the analytical model and the frequency sweeps performed in PSCAD are matching properly. Moreover, the time delay doesn't impact the impedance profile that much. This can be due to the fact that a relatively small time delay was selected.

Figure 6.2.1 shows the impedance of the converter when the capacitive filter is considered by utilizing (39). The capacitive filter has a relatively large effect on the impedance of the converter.

$$Z_{wt} = \frac{R_f^w + sL_f^w + j\omega_1 L_f^w + D^w(F_{PI,c} - j\omega_1 L_f^w)}{1 - D^w H_v} + \frac{1}{C_f s} \tag{39}$$

The step-up transformer, which increases the voltage from 690 V to 66 kV was also taken into account, as shown in Figure 41. This transformer was modelled as an RL-equivalent in series with an ideal transformer in PSCAD and the impedance was measured at 66 kV.

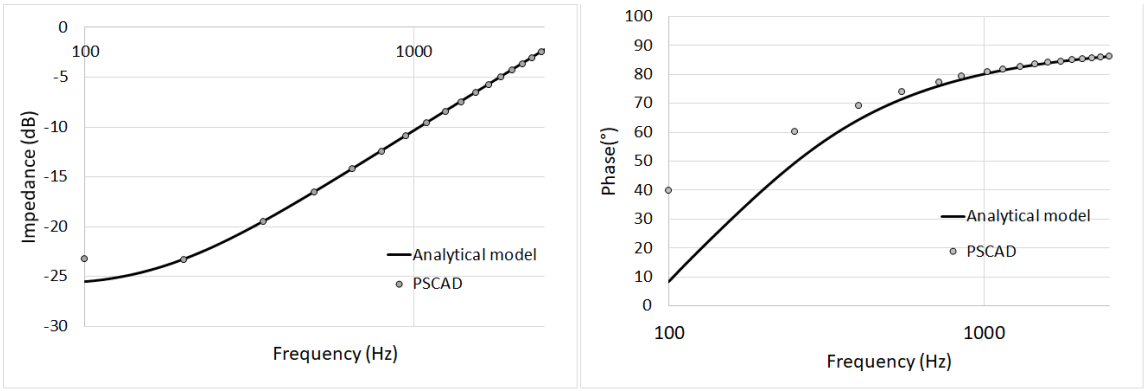

Figure 38: Magnitude and phase of the impedance of a single wind turbine converter at 690 V, when considering the current loop, the coupling inductance and resistance, and the low-pass filter of the voltage. The impedance is determine by both an analytical model and frequency sweeps in PSCAD.

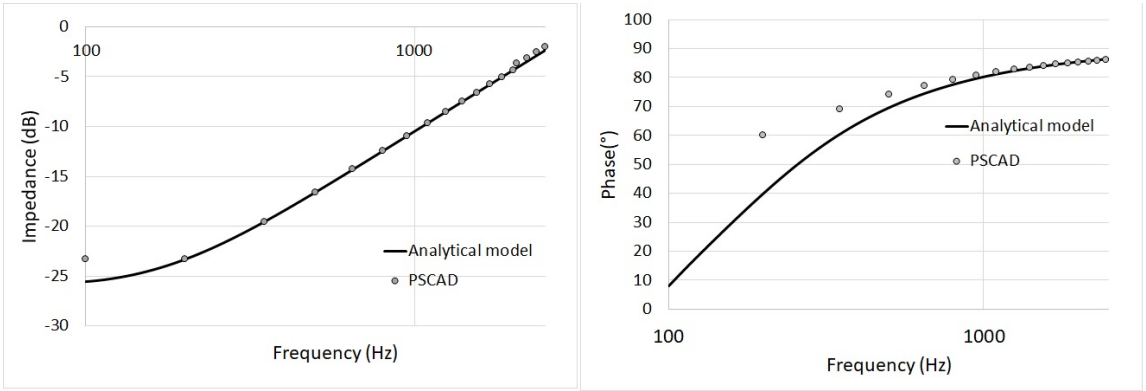

Figure 39: Magnitude and phase of the impedance of a single wind turbine converter at 690 V, when considering the current loop, the coupling inductance and resistance, the low-pass filter of the voltage and the time delay. The impedance is determine by both an analytical model and frequency sweeps in PSCAD.

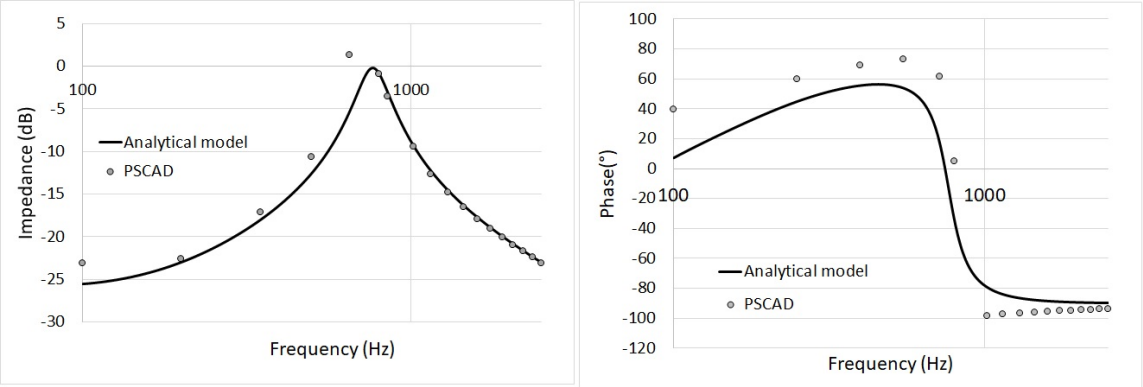

Figure 40: Magnitude and phase of the impedance of a single wind turbine converter at 690 V, when considering the capacitive filter. The impedance is determine by both an analytical model and frequency sweeps in PSCAD.

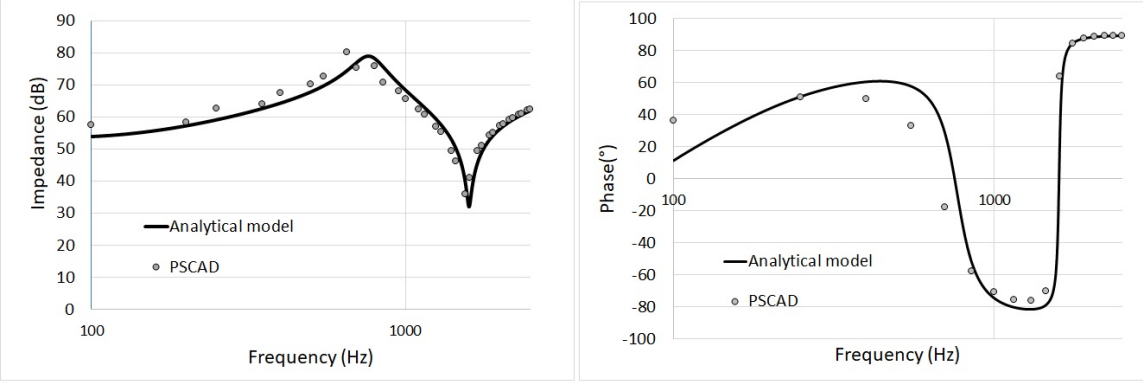

Figure 41: Magnitude and phase of the impedance of a single wind turbine converter at 66 kV, when considering the step-up transformer. The impedance is determine by both an analytical model and frequency sweeps in PSCAD.

It can be concluded that the analytical model can accurately describe the impedance of the wind turbine converter when comparing its results to frequency sweeps performed in PSCAD.

6.2.2 The Impedance of the Wind Farms

Both an analytical model and a PSCAD model were utilized to determine the impedance profile of the wind farm. Firstly, the impedance of one wind turbine string was determined. The impedances of the cable segments connecting the wind turbines was not taken into account. This assumption was justified by comparing analytically the impedance profile of string of wind turbines with a sweep of a string including cable sections between the wind turbines. As shown in Figure 42 the cable sections don't affect the impedance of the wind turbine string significantly. Consequently, the impedance of the string segments could be neglected.

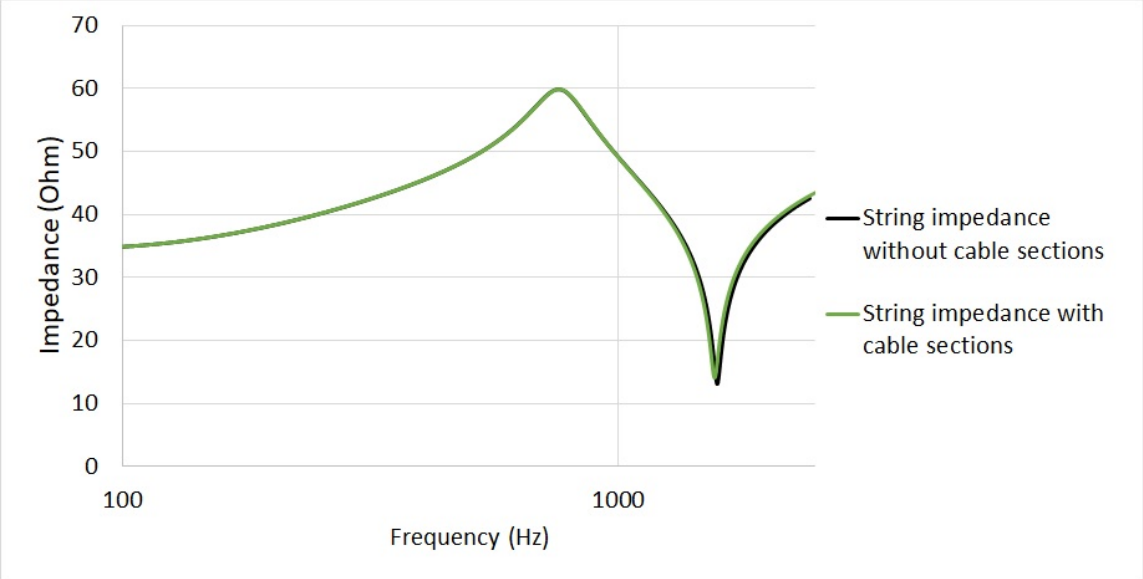

Figure 42: Impedance of one string of wind turbines, with and without cable sections, as determined with the analytical model.

The capacitance of the HV export cable shifts the resonance frequencies of the wind farm to smaller frequencies. Figure 43 shows the impedance of the wind farm as measured at the wind farm side of the HV cable ('before the cable'), and at the grid side of the HV cable ('after the cable'). It can be observed that due to the HV cable, the resonance frequencies shift to lower frequencies. Moreover, the system becomes less damped, which decreases the stability of the system.

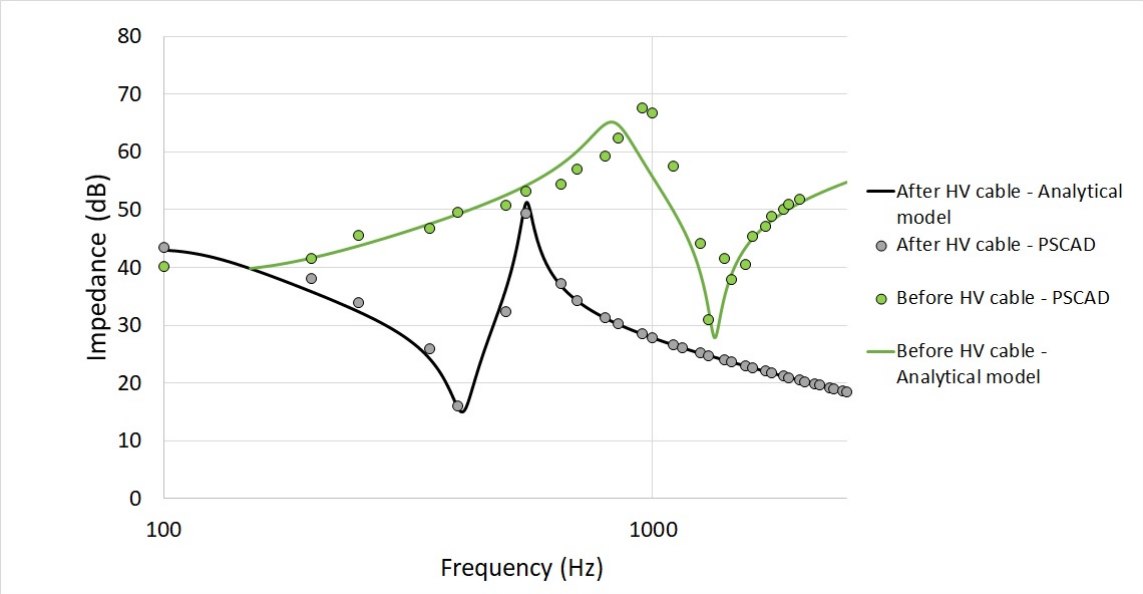

Figure 43: Impedance of the wind farm as seen from the wind turbine side of the HV export cable (before HV cable) and as seen from the grid side of the HV export cable (after HV cable).

Figure 44 shows the impedance of the entire first wind farm. The measurements of the impedance of the wind farm in PSCAD align with the analytical model. Again at frequencies close to 100 Hz, the analytical model deviates slightly from the PSCAD model.

Figure 45 shows the impedance of the entire second wind farm. The second wind farm has a parallel filter in this configuration, whereas the first wind farm has a configuration without containing this filter. The presence of this filter doesn't influence the parallel resonance points (impedance peaks). However, it does shift the series resonance points to slightly higher frequencies. This is due to the fact that it alters the series resonance point caused by the compensation.

When the two OWPPs are placed in parallel, the impedance of the entire Alpha Platform is obtained, as shown in Figure 46. The resulting impedance has smaller magnitudes than the OWPPs I and II have separately. Consequently, when instead of one wind farm, two OWPPs are connected, less damping is present in the system. Moreover, in this case, the resonance frequencies also shift to lower frequencies when both OWPPs are connected.

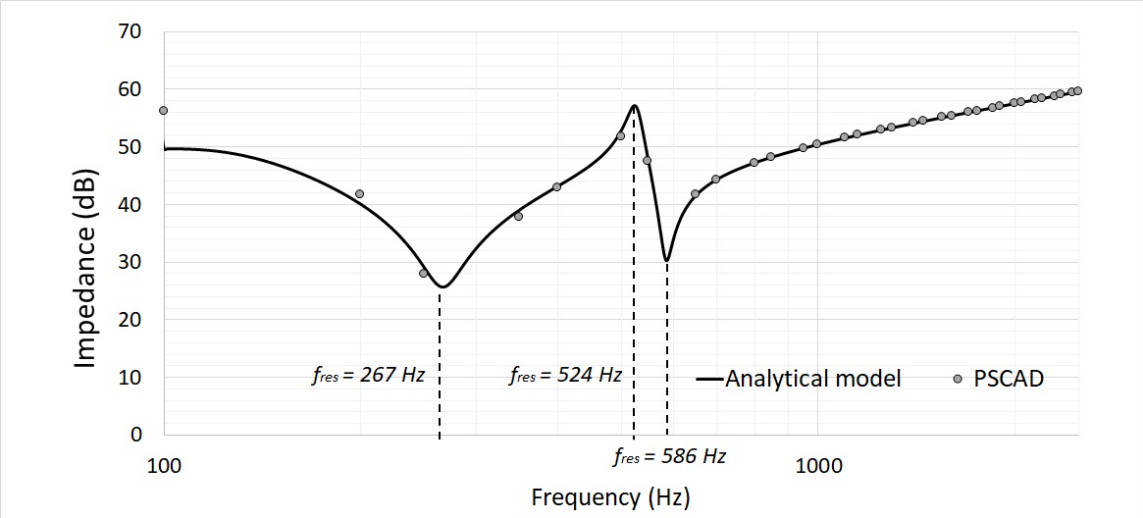

Figure 44: Magnitude of the impedance of the first OWPP at the Point of Connection to the onshore network at 380 kV.

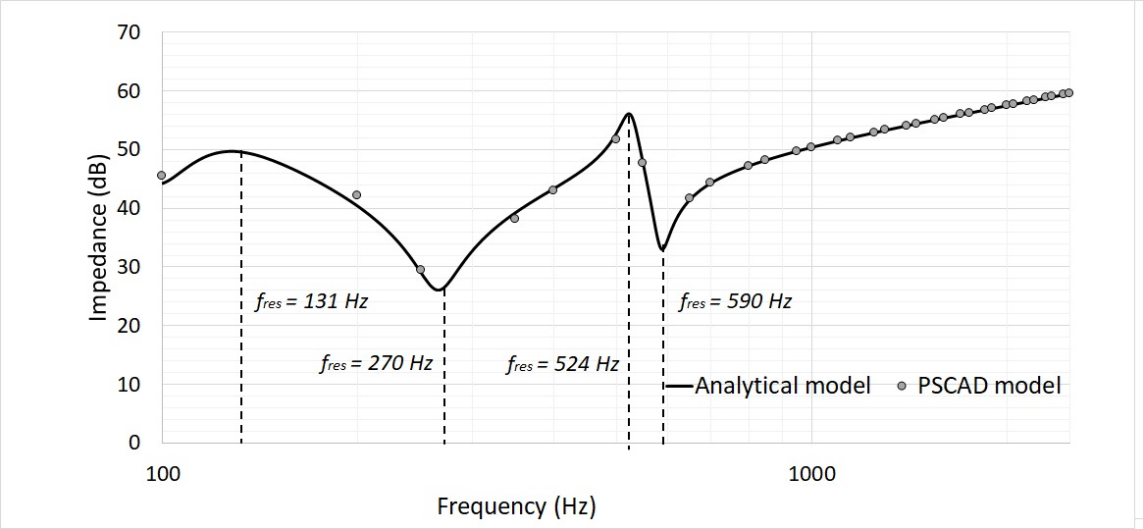

Figure 45: Magnitude of the impedance of the second OWPP at the Point of Connection to the onshore network at 380 kV.

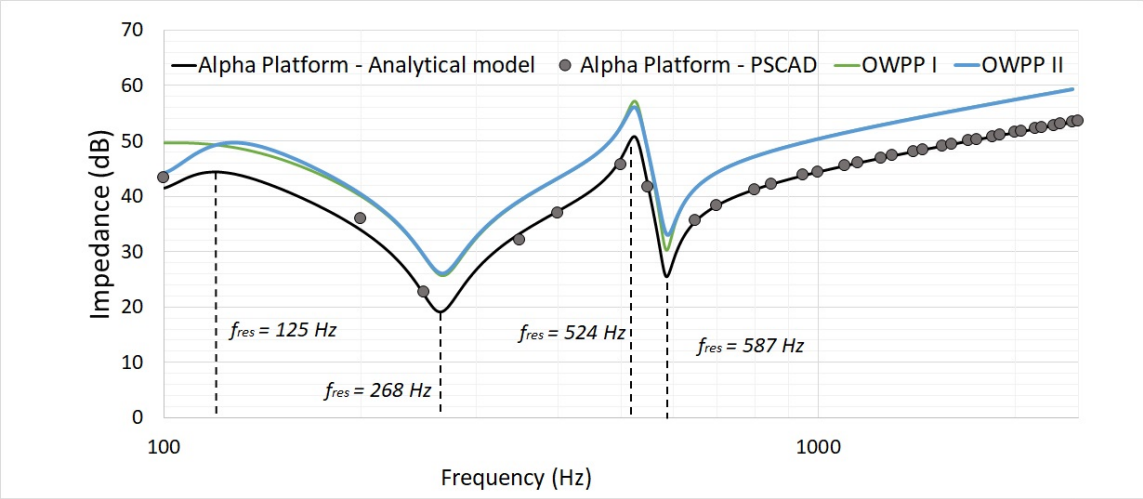

Figure 46: Magnitude of the impedance of the platform Alpha at the Point of Connection to the onshore network at 380 kV. The impedances determined with the analytical model of OWPPs I and II are also shown.

6.2.3 Impedance of the Network

The OWPPs are connected to an onshore network at a busbar at 380 kV. A model of a large part of the Dutch network, including this specific busbar, was available in PSCAD. For the stability assessment, the wind farm had to be connected to the onshore network model in PSCAD. This way, the real life case where the wind farm is actually connected to the network, could be studied. However, since connecting the wind farm to the onshore network requires a significant computational time, an equivalent for the network was utilized. First, a frequency sweep was performed of the network at the POE. Figure 47 shows this network impedance as measured with the Frequency Scanner in PSCAD. The Frequency Dependent Network Equivalent (FDNE) block of PSCAD could then be utilized to convert the output of this frequency sweep into an impedance block. Afterwards, it was verified with a FFT measurement whether the FDNE indeed represents the network impedance properly. Figure 47 shows the results of this frequency sweep with a FFT of the FDNE. It can be observed that the FDNE does not accurately represent the impedance of the network. Therefore, it was decided to utilize a simple RL-equivalent to represent the network at the Point of Evaluation (POE). The network equivalent, with an inductance of 0.0380 H and a resistance of 0.8204Ω, is also shown in Figure 47. The inductance and resistance were selected in such manner that the actual network impedance was represented mostly for frequencies of below 600 Hz, since that is also the frequency range where the resonance points of the OWPPs are situated.

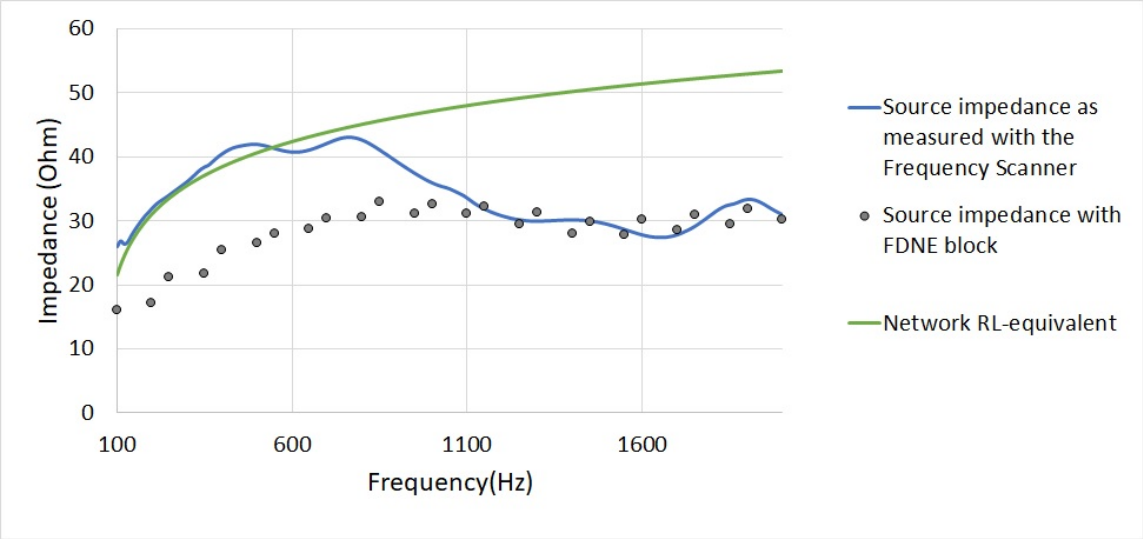

Figure 47: Impedance of the network at the POE and the impedance of the R-L network equivalent (L=0.0380 H and R=0.8204 Ohm)

6.2.4 Identification of Harmonic Resonance Frequencies

The OWPPs were placed in series with the network equivalent as explained in Section 5.2. Figure 48 shows the resulting impedance, which was determined analytically. Figure 49 shows the resulting impedance when the second OWPP is connected in series with the network.

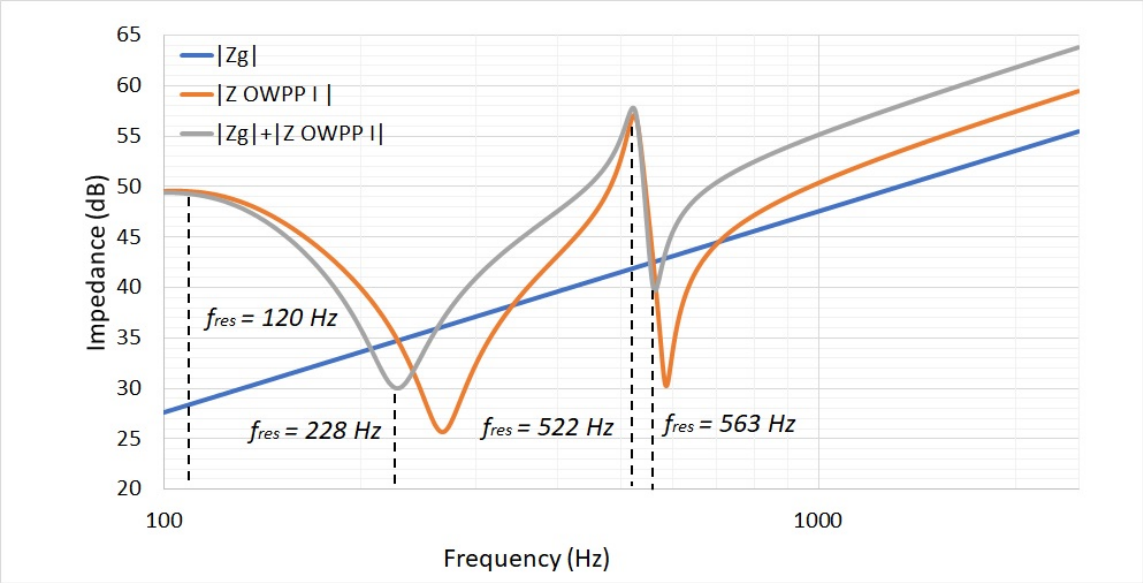

Figure 48: Impedance of OWPP I, the impedance of the network and the sum of the impedance of OWPP I and the network.

When both OWPPs are connected to the network, the series resonance frequencies shift to slightly lower frequencies, as can be seen in Figure 50. The parallel resonance frequencies don't show a continuous trend when moving from connecting one wind farm to connecting both to the network.

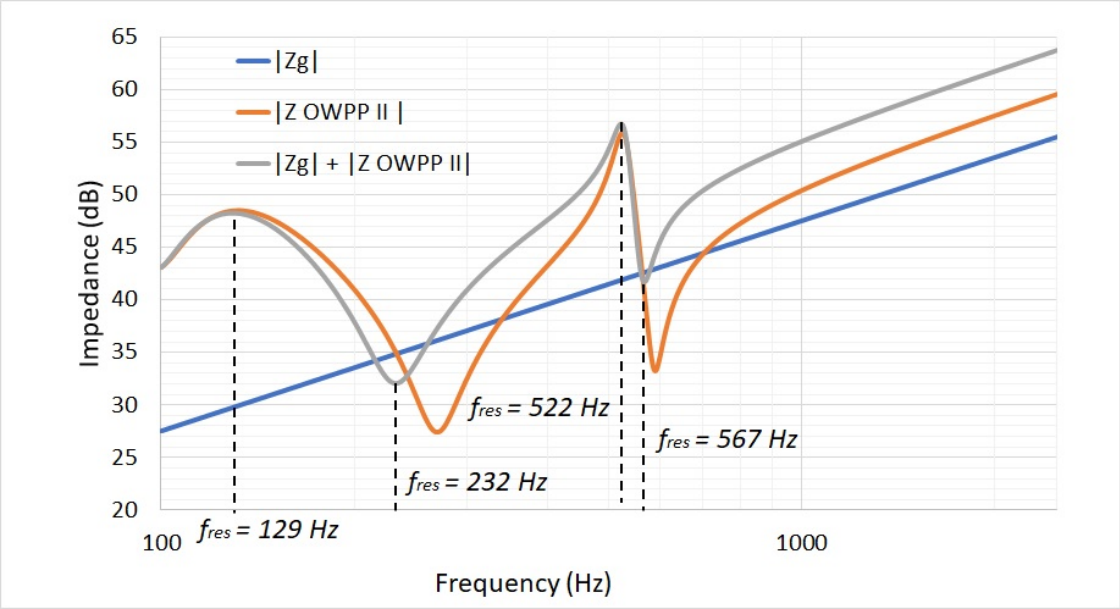

Figure 49: Impedance of OWPP II, the impedance of the network and the sum of the impedance of OWPP II and the network.

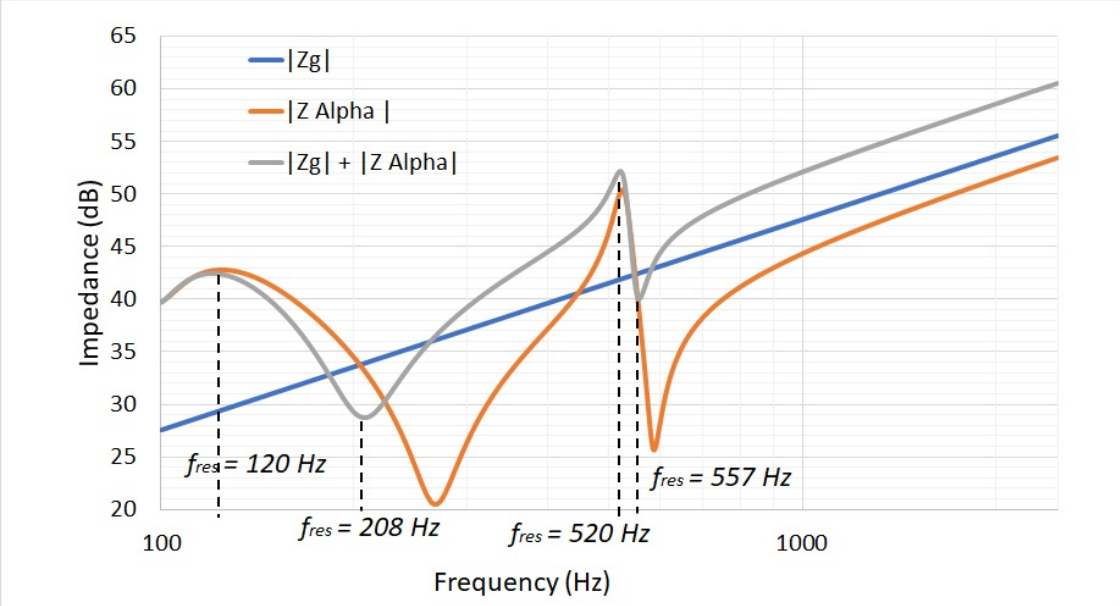

Figure 50: Impedance of the Alpha Platform, the impedance of the network and the sum of the impedance of the Alpha Platform and the network.

Resonance frequency	**Series resonance (Hz)**		**Parallel resonance (Hz)**	
OWPP I	267	586	125	524
OWPP + network	228	563	120	522
OWPP II	270	590	131	524
OWPP II + network	232	567	129	522
Platform Alpha	268	587	125	524
Platform aplha + network	208	557	120	520

Table 4: An overview of the resonance frequencies of the OWPPs separately, or when connected in series with the network.

Table 4 provides an overview of all the resonance frequencies of each configuration.

A scenario was studied in which the effect of the number of Wind Turbines (WTs) in operation on the damping in the system was assessed. Figure 51 shows that when less WTs are in operation in the case of OWPP I, the resistance decreases. Consequently, when less WTs are in operation, less damping is present in the system, and the system is more likely to become unstable when resonance frequencies are excited. Moreover, Figure 52 shows that the resonance frequencies also shift to lower frequencies when less WTs are in operation. The resonance frequency shifts with around 12 Hz when comparing the scenario of 30 WTs in operation and 54 WTs in operation.

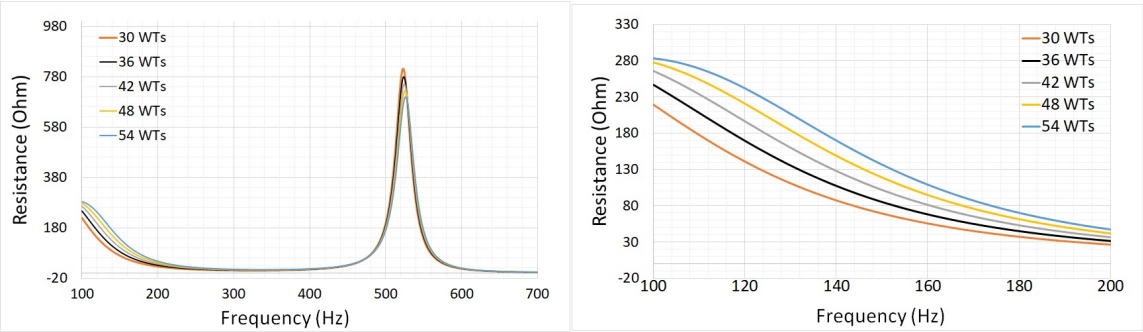

Figure 51: Resistance of OWPP I, when a varying number of Wind Turbines is in operation.

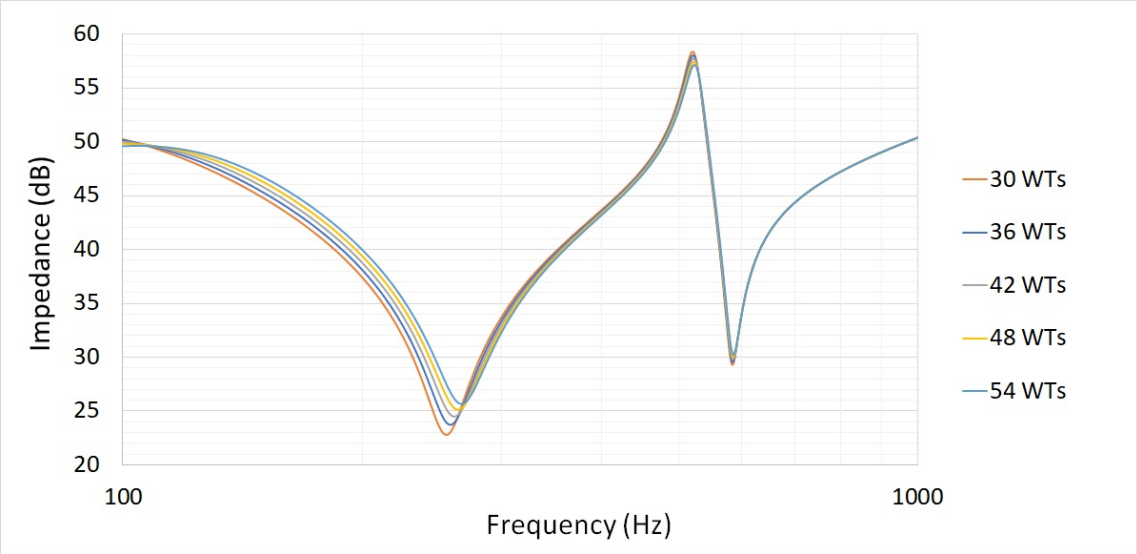

Figure 52: Resistance of OWPP I, when a varying number of Wind Turbines is in operation.

In general, it can be commented that both the control parameters of the wind turbines and the offshore wind farm configuration are influencing the harmonic interactions. Firstly, the selected values for the delay, the voltage feed forward term and the values of the PI-controller of the current loop, influence the impedance profile of the VSCs. It was observed that the impedance profile of the WTs matters, since when less WTs are taken into account, the resonance frequencies are shifted and the damping in the system is altered. The configuration of the OWPP also plays an important role when considering harmonic interactions. It was shown that the HV export cable shifts resonance points to lower frequencies. It would be expected that this effect is stronger when the cable length is increased. It was also shown that adding a filter to the OWPP, when comparing OWPP I and OWPP II, also alters the resonance frequencies slightly. This also proves that the wind farm configuration does matter for the resonance points.

6.2.5 Resonance Stability Assessment

For the identified resonance frequencies, the positive net-damping criteria was applied. By applying this criteria, it was verified whether the resonance points were stable.

The positive net-damping criteria was applied, where the sum of the real components of the impedances of the OWPP and the network at the resonance frequencies, have to be larger than zero. If the sum of the resistances is larger than zero, sufficient damping is present in the network for maintaining a stable system [21].

$$R_T(\omega_{res}) = R_{WF}(\omega_{res}) + R_g(\omega_{res}) > 0 \tag{40}$$

With total resistance R_T^w, the resistance of the wind farm R_{WF}, the resistance of the network R_g and the resonance frequency f_{res}.

The positive net-damping criteria was applied for the cases where solely OWPP I is connected to the grid, solely OWPP II is connected to the grid and when both OWPPs are connected to the grid. Table 5 shows the results resistances for each case.

OWPP I			
f_{res}	$R_g(\Omega)$	$R_{WF}(\Omega)$	$R_T(\Omega)$
120.00	0.82	241.96	242.78
228.00	0.82	29.83	30.66
522.00	0.82	647.95	648.95
563.00	0.82	79.59	80.62

Table 5: Resistance of the network R_g, the OWPP I (R_{WF}, and of the network and the OWPP I in series (R_T).

OWPP II			
f_{res}	$R_g(\Omega)$	$R_{WF}(\Omega)$	$R_T(\Omega)$
129.00	0.82	255.76	256.58
232.00	0.82	37.04	37.86
522.00	0.82	533.82	534.82
567.00	0.82	91.46	92.46

Table 6: Resistance of the network R_g, the OWPP II (R_{WF}, and of the network and the OWPP II in series (R_T).

Alpha Platform			
f_{res}	$R_g(\Omega)$	$R_{WF}(\Omega)$	$R_T(\Omega)$
120.00	0.82	131.13	131.95
208.00	0.82	23.94	25.21
520.00	0.82	296.73	270.01
557.00	0.82	63.76	64.58

Table 7: Resistance of the network R_g, the Alpha Platform (R_{WF}, and of the network and the Alpha Platform in series (R_T).

It can be observed that at each resonance frequency in each case, the total resistance is larger than zero. Consequently, all resonance points are stable. The series resonance points are less damped than the parallel resonance points, which is expressed in lower resistance values.

6.2.6 Verification with time domain simulations in PSCAD

The results were verified by performing time domain simulations in PSCAD. For each case, the wind farm was placed in series with the network RL-equivalent. In order to excite the resonance points, a network voltage step of 20 percent was performed. During this voltage step, the applied voltage inherently includes various harmonic components and consequently harmonic components were found in the measured current. The current was evaluated for one wave period after the voltage step. A time step of 10 seconds was utilized to be able to track the harmonic components in the current. A Fast Fourier Transform (FFT) was then applied in Matlab to measure the frequency of the harmonic components in the current.

For each evaluated case, as expected by applying positive net-damping criteria, the system remained stable after a significant voltage step. Figure 53 shows the current in the system when connecting OWPP I at the 380 kV level, after the voltage step at 0.4 seconds. It can be observed that indeed a distortion occurs in the waveform shortly after the voltage step. Figure 53 shows also the amplitudes of the harmonic components during the first time period after the voltage step. Naturally, the 50 Hz component is most present. Figure 54 provides an overview of at which other frequencies harmonic components were measured. It can be observed that at the expected series resonance points, the amplitude of the current is amplified. Whereas series resonance frequencies of 228 Hz and 563 Hz were expected, 237 Hz and 570 Hz are measured. However, since the choice of one wave period after the voltage step for this analysis is arbitrarily, a significant error margin exists for the time domain FFT measurements. Consequently, even though the measured resonance frequencies are not exactly the same as the expected frequencies with the frequency sweeps, it can still be assumed that the time domain simulation aligns to a certain extent with the analysis performed with the frequency sweeps.

It can be seen from Figure 54 that the current at the parallel resonance points is damped. At the parallel resonance points, the damping was expected to be larger and this is indeed observed with the time domain simulation.

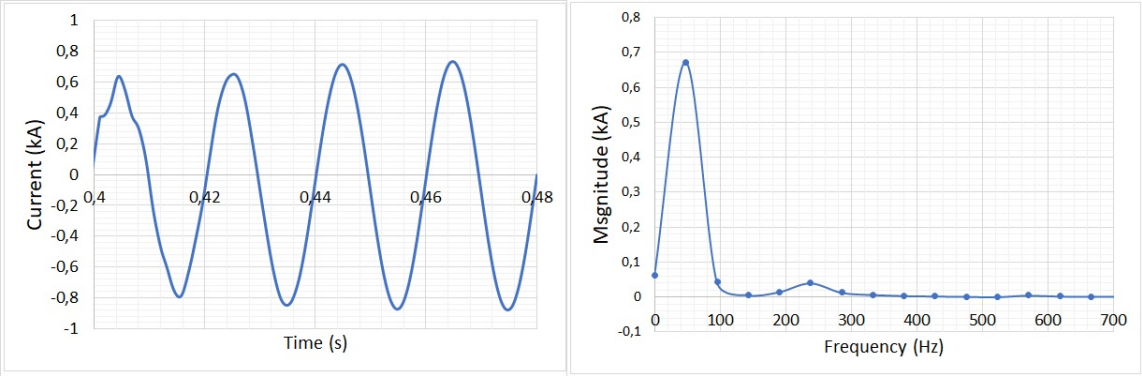

Figure 53: Grid current (left) after the voltage step and the magnitude of the currents at each frequency during the first time period after the voltage step for OWPP I.

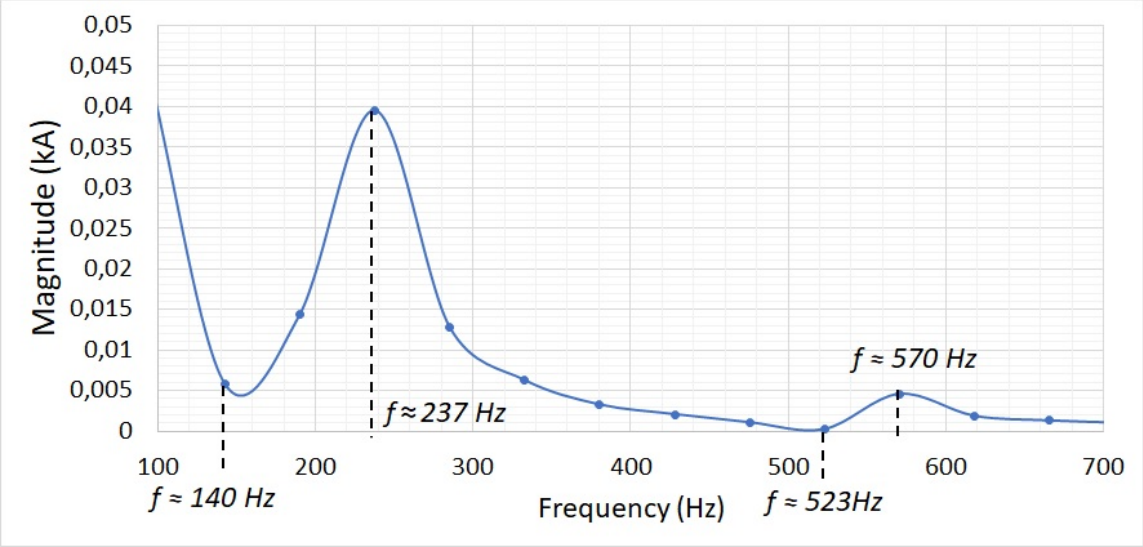

Figure 54: Magnitude of the current for frequencies between 100 Hz and 700 Hz during the first time period after the voltage step for OWPP I.

Figure 55 shows the current in the system when solely OWPP II is connected to the network after a voltage step of 20 percent. Again several harmonics are excited by this voltage step. Figure 56 shows again that the current is amplified at series resonance points and is damped at the parallel resonance points. As expected, the series resonance points have shifted to slightly higher frequencies than in the case of connecting OWPP I to the network.

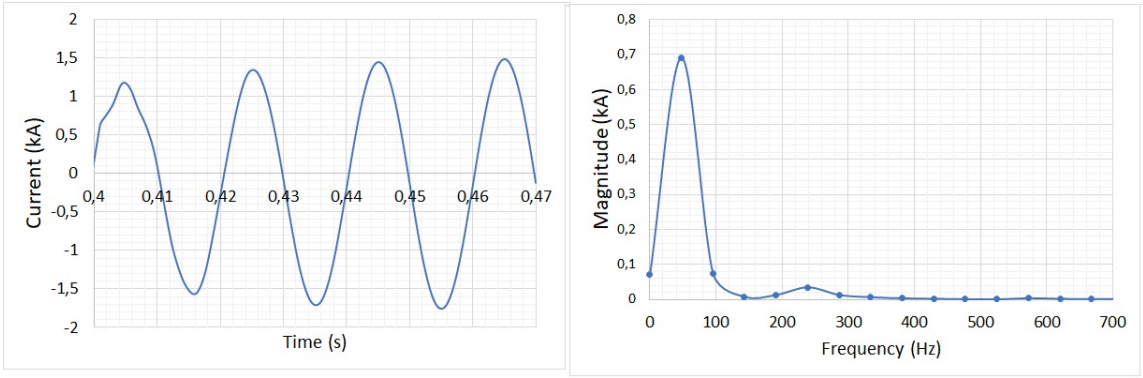

Figure 55: Grid current (left) after the voltage step and the magnitude of the currents at each frequency during the first time period after the voltage step for OWPP II.

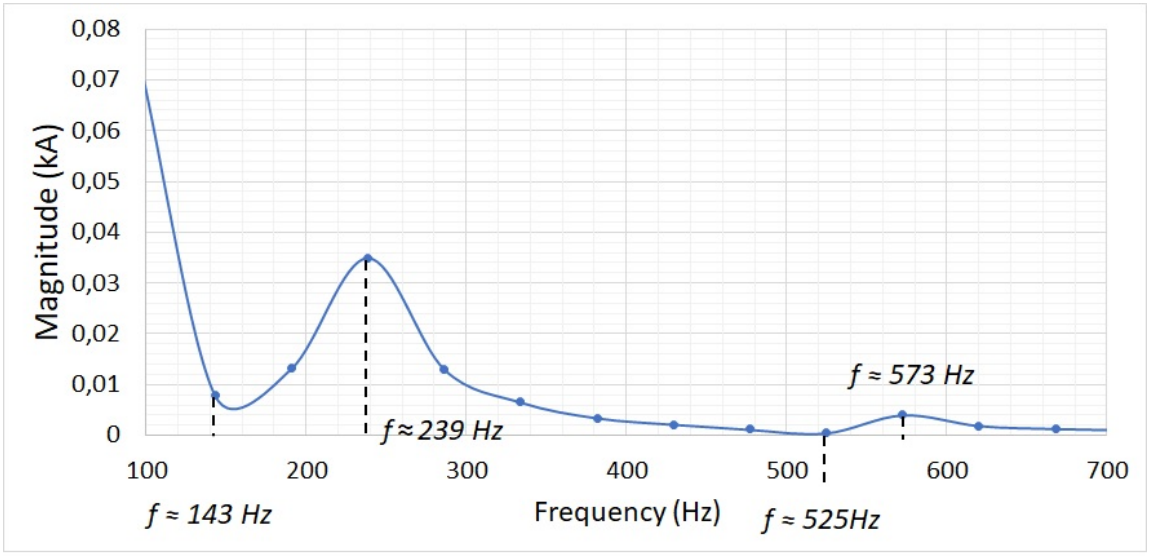

Figure 56: Magnitude of the current for frequencies between 100 Hz and 700 Hz during the first time period after the voltage step for OWPP II.

Figure 57 shows the current after a voltage step of 20 percent when both OWPP I and OWPP II are connected in series with the network. Indeed the first series resonance points is shifted significantly to a lower frequency, as expected from the frequency sweeps. Moreover, the series resonance points are also slightly less damped, current values of over 0.04 kA are reached in the case of the 194 Hz resonance point. Moreover, the parallel resonance points are less damped as well. This was already expected from the impedance profile, since when the entire Alpha platform is connected, less damping is present and the impedance reaches lower magnitudes.

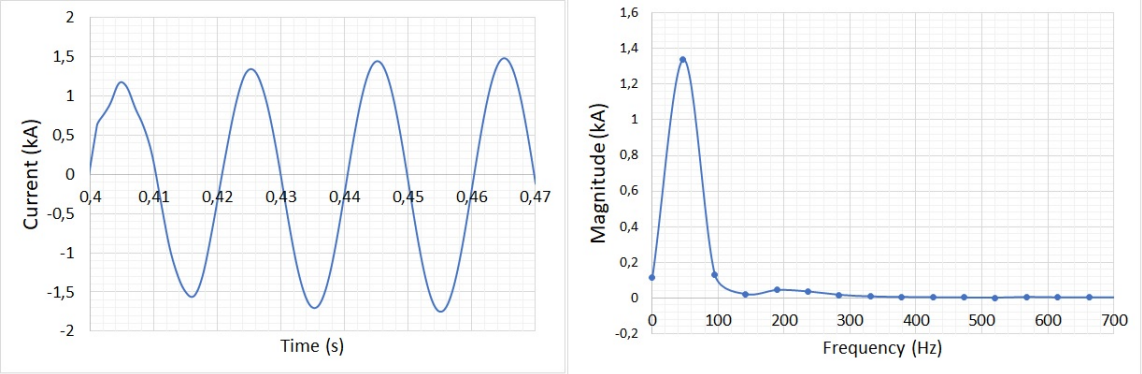

Figure 57: Grid current (left) after the voltage step and the magnitude of the currents at each frequency during the first time period after the voltage step for the Alpha Platform.

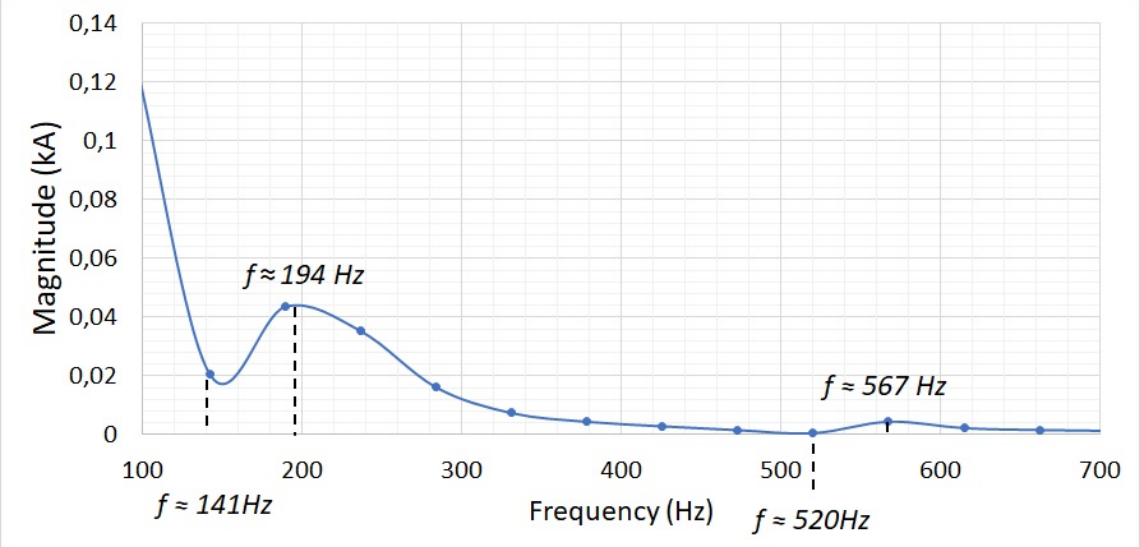

Figure 58: Magnitude of the current for frequencies between 100 Hz and 700 Hz during the first time period after the voltage step for the Alpha Platform.

In general, it can be observed that the time domain simulations confirm what was expected from the analysis in the frequency domain. The positive-net damping criteria predicts that the system will remain stable in each of the three scenarios, due to the relatively large damping present in the system, and this was indeed observed during the time domain simulations. When instead of one wind farm, two OWPPs are connected, series resonance frequencies shift to lower frequencies. Moreover, the damping decreases, which leads to a stronger amplification of harmonic currents at the series resonance frequencies.

7 Conclusion

The impact of connecting an increasing amount of wind farms to the same POC when considering harmonic interactions was analyzed. Firstly, two types of harmonic interactions were identified: (i) the interaction between the background harmonic voltage and the wind turbine converters, and (ii) the interaction between wind turbine converters. These interactions, together with the harmonic emissions from out the network and the WT converters, can create or excite resonances. The cables, filters and capacitor banks shift or add resonance frequencies to the system and therefore are also important to consider.

When considering the performed Harmonic Impact Assessment, including a Norton Equivalent Impedance alters the impedance profile of the OWPPs at frequencies below 700 Hz. Consequently, the peaks in the gain curves are shifted slightly, which could significantly impact the estimated THD profile. When connecting an increasing amount of wind farms to the same POC, the peaks in the THD are shifted to lower frequencies. The magnitude of the peaks in the THD are also altered. It could occur that when multiple OWPPs are connected, THD limits are not exceeded, whereas the limits are not exceeded when solely one OWPP is connected. It is depending on the specific profile of the background harmonics and the impedance profiles of the grid and the OWPP, whether an exceedance of the emission limits appears or disappears when an increasing amount of wind farms is connected.

In the case of the Harmonic Stability Assessment, frequency sweeps of the two assessed wind farms made clear that the presence of an additional filter in one of the wind farms leads to a small shift in the series resonance points. When multiple wind farms are connected, series resonance frequencies shift to lower frequencies and less damping appears to be present in the system. Consequently, a system becomes less stable when an increasing amount of wind farms is connected. It can also be concluded that when less wind turbines are in operation, less damping is present in a system, which makes the network less stable as well.

8 Environmental Impact

In the European Renewable Energy Directive, a binding target was set of 20 per cent of final energy consumption from renewable sources by 2020 [62]. In order to reach this objective, and to obtain a carbon neutral electricity mix, wind power generation is a necessity. Developing offshore wind farms can be an effective solution, since developing wind power onshore can be troublesome with regards to the limited availability of space onshore. However, the development of an offshore wind farm is capital intensive and can take many years. It is therefore important that when these wind farms are finally taken into operation, no issues occur and the initial investment can be recovered. However, when severe harmonic issues arise, a wind farm has to be taken out of operation. This is not only very costly, but it can also discourage future investments in OWPPs. This research project hopefully contributes to obtaining a better understanding when it comes to the risks related to harmonic emissions and interactions. When these issues are more deeply understood, OWPPs can be designed in such a way that these risks are mitigated. This on its turn can stimulate further investments in OWPPs, which will positively affect the carbon footprint of the electricity mix.

9 Cost of the project

Table 8 describes the estimated costs of this project. Around 840 hours were devoted to this project. An educational and professional license of PSCAD were utilized for the simulations. A return ticket from Amsterdam to Barcelona was required in order to be able to spend ten days at CITCEA-UPC after four months at DNV GL.

Item	**Estimated Cost ()**
Working hours (840)	0
PSCAD license	250
Return flight ticket AMS-BCN	220
Total	470

Table 8: The estimated cost of the project.

10 Suggestions for Future Work

This research project could be complemented by performing several additional tasks. Firstly, a sensitivity analysis could be performed by adjusting both the control parameters and the OWPP configuration. Consequently, the impact of these parameters on the magnitude of the resonance frequency and on the system stability could be assessed. For example, it would be interesting to assess the effect of an even longer HV export cable on the stability. Moreover, the stability assessment could be performed at other points in the system as well. For example, the stability could be assessed at a point in the 66 kV offshore network, or even at a wind turbine converter at the end of a string. This could provide more insight into what is exactly happening with regards to harmonic interactions and stability within the offshore network. Moreover, it would also be interesting to assess for different scenarios the resonance stability. For example, a scenario could be assessed where the link cable between two OWPPs is closed due to the failure of one offshore transformer.

Thirdly, for the stability assessment, the RL-equivalent which was utilized for the network could be replaced by a model of the actual network in PSCAD. This would increase the simulation time significantly, however, it would definitely be possible. It would also be interesting, especially when facing a large simulation time, to study the effect of aggregating the wind farm on the results the impedance profiles and the resonance frequencies. Besides the effect of aggregating the wind farm, the impact of including a frequency dependent cable model on the impedance profile. This could display the error margin between the approach where the focus is on aligning the analytical model and the PSCAD model, with the reality.Within this research project, it became clear that the number of wind turbines in operation influences the damping in the system. It would also be interesting to assess the actual impact on the system stability when less wind turbines are in operation.

Lastly, it would be beneficial to study the impact on the harmonic emission limits and the resonance stability, when even more wind farms are connected to the network. For this research project, solely scenarios with up to three wind farms were assessed. This could be expanded to studying cases with more than three wind farms connected as well.

A Automation Library PSCAD

PSCAD offers a library which can be utilized for automating several power system analysis tasks. The utilization of the so-called the Automaton Library can be mainly useful when the results of a simulation have to be post-processed. An example of a Python script utilized to perform a frequency sweep in PSCAD is given. It has to be noted that PSCAD Automation Library utilizes ID numbers for each individual component. IThese ID numbers can be called upon from out Python. Parameters of these components can then be altered from out Python [63].

```
import pandas as pd
import sys
import os
import logging
import mhrc  # import automation library
import mhrc.automation
import numpy as np
import matplotlib.pyplot as plt #for plotting

# Import other utilities to perform cool stuff
from win32com.client.gencache import EnsureDispatch as Dispatch
from mhrc.automation.utilities.word import Word
from mhrc.automation.utilities.file import File

import win32com.client
import shutil

print("Automation Library version:", mhrc.automation.VERSION)

pscad_version = 'PSCAD 4.6.2 (x64)'
fortran_version = 'GFortran 4.6.2'
fortran_ext = '.gf42'
project_name = '\project_name'
library = '\project_name'

# Working directory
working_dir = r"C:working_directory"
project_name2 = 'project_name'

# ------------------------------------------------------------------------
# Main script
# ------------------------------------------------------------------------
```

```
# Source and destination folders for output data
src_folder = working_dir + project_name + ".if12"
dst_folder = working_dir + "POW_output"

# Clear the ouput folder
try:
    shutil.rmtree(dst_folder)  # de
except Exception as ignored:
    pass

os.mkdir(dst_folder)

# Launch specific PSCAD and Fortran version
pscad = mhrc.automation.launch_pscad(pscad_version=pscad_version,
fortran_version=fortran_version, certificate=True)

# Load the project
pscad.load([working_dir + library + ".pslx"])
pscad.load([working_dir + project_name + ".pscx"])
project = pscad.project(project_name2)
project.focus()

#Set parameters# Get the "Main" canvas
main = project.user_canvas('Main')

##Get all components # Nh_list = [1,2,3,4,5,6,7]
FFT_block = main.user_cmp(826885555)
Harmonic_order = main.user_cmp(774078530)
ZM_dB_list = []
Zph_list = []

for f in range (2000,2550,50):
    N=f/50
    if N%3>0:
        FFT_block.set_parameters(F=f+50)
        Harmonic_order.set_parameters(Nh=N)
        print("Parameters are set")
        print("The project is running")
        project.run()
```

```
        file = r"C:wokring_directory+project_name.gf46\FFT_01.out"
        df = pd.read_csv(file, sep='\s+', header=None)
        ZM_dB=(df.loc[:,5])
        ZM_dB2= ZM_dB.loc[4100:5000].mean()
        Zph=(df.loc[:,7])
        Zph2 = Zph.loc[4100:5000].mean()
        print(N)
        print(ZM_dB2)
        print(Zph)
        ZM_dB_list.append(ZM_dB2)
        Zph_list.append(Zph2)
        #print(ZM_dB_list)


with open('VSC_BCN_VSC_BCN_without_cable2.txt', 'w') as f:
    for item in ZM_dB_list:
        f.write("%s\n" % item)

with open('VSC_BCN_VSC_BCN_without_cable_phase2.txt', 'w') as f:
    for item in Zph_list:
        f.write("%s\n" % item)
```

B Harmonic Impact Assessment with Norton Equivalent Impedance in PowerFactory

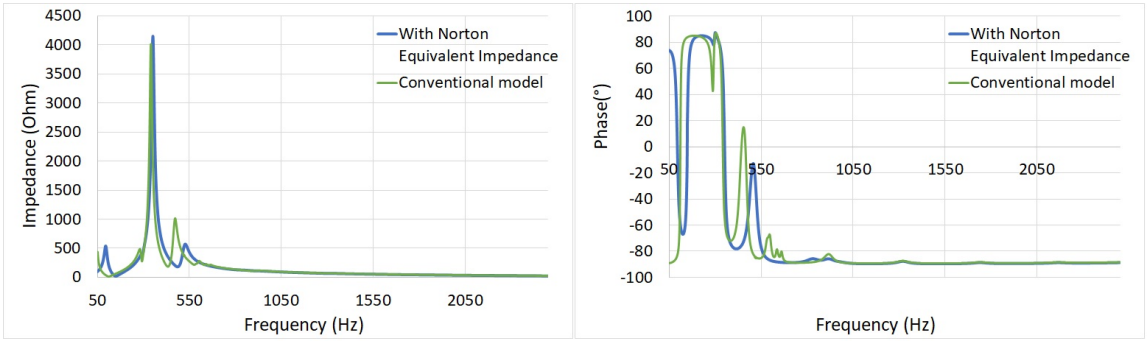

Figure 59: Impedance of wind farm 1 of case study I over the full measured frequency range.

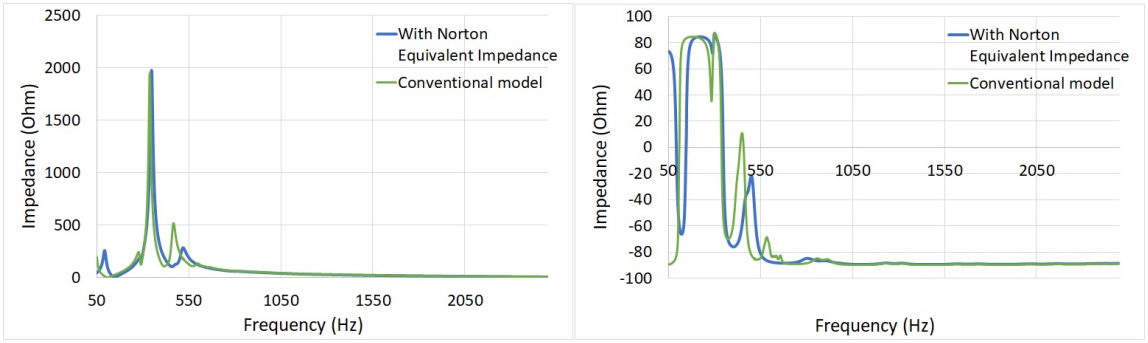

Figure 60: Impedance of wind farm 2 of case study I over the full measured frequency range.

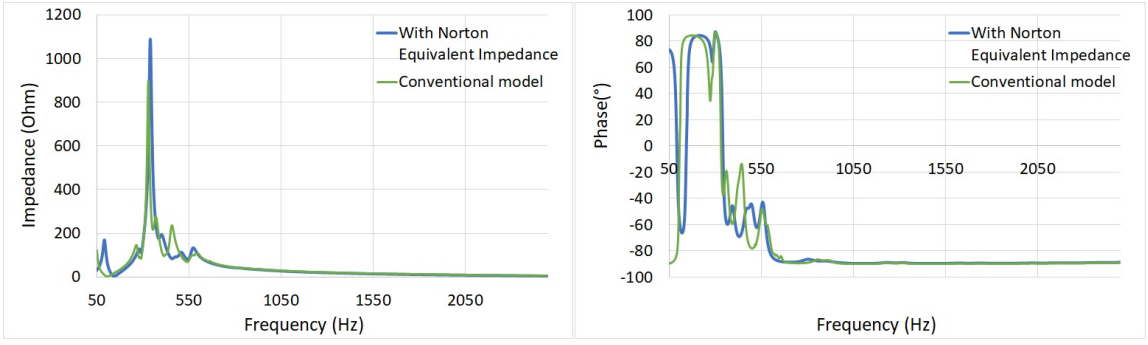

Figure 61: Impedance of wind farm 3 of case study I over the full measured frequency range.

References

[1] "Net op zee borssele. retrieved at: https://www.tennet.eu/nl/ons-hoogspanningsnet/net-op-zee-projecten-nl/net-op-zee-borssele/."

[2] "Programma 2023. retrieved at:https://www.tennet.eu/nl/ons-hoogspanningsnet/net-op-zee-projecten-nl/programma-2023/. , url=https://www.tennet.eu/nl/ons-hoogspanningsnet/net-op-zee-projecten-nl/programma-2023/, journal=TenneT."

[3] C. Buchhagen, C. Rauscher, A. Menze, and J. Jung, "Borwin1-first experiences with harmonic interactions in converter dominated grids," in *International ETG Congress 2015; Die Energiewende-Blueprints for the new energy age*, pp. 1–7, VDE, 2015.

[4] N. A. Cutululis, *MEDOW - Multi-terminal DC Grid for Offshore Wind, Final report.* 2018.

[5] "Conversation with yin sun," May 2019.

[6] D. Van Hertem, O. Gomis-Bellmunt, and J. Liang, *HVDC grids: for offshore and supergrid of the future*, vol. 51. John Wiley & Sons, 2016.

[7] N. B. Negra, J. Todorovic, and T. Ackermann, "Loss evaluation of hvac and hvdc transmission solutions for large offshore wind farms," *Electric power systems research*, vol. 76, no. 11, pp. 916–927, 2006.

[8] A. Egea-Alvarez, A. Junyent-Ferré, and O. Gomis-Bellmunt, "Active and reactive power control of grid connected distributed generation systems," in *Modeling and control of sustainable power systems*, pp. 47–81, Springer, 2012.

[9] V. Preciado, M. Madrigal, E. Muljadi, and V. Gevorgian, "Harmonics in a wind power plant," in *2015 IEEE Power & Energy Society General Meeting*, pp. 1–5, IEEE, 2015.

[10] T. Ackermann, *Wind power in power systems.* John Wiley & Sons, 2005.

[11] A. Nikolopoulou, "Wind turbine contribution to ancillary services under increased renewable penetration levels," 2017.

[12] V. Yaramasu, B. Wu, P. C. Sen, S. Kouro, and M. Narimani, "High-power wind energy conversion systems: State-of-the-art and emerging technologies," *Proceedings of the IEEE*, vol. 103, no. 5, pp. 740–788, 2015.

[13] J. Li, N. Samaan, and S. Williams, "Modeling of large wind farm systems for dynamic and harmonics analysis," in *2008 IEEE/PES transmission and distribution conference and exposition*, pp. 1–7, IEEE, 2008.

[14] L. Freris and D. Infield, *Renewable energy in power systems.* John Wiley & Sons, 2008.

[15] F. Blaabjerg and K. Ma, "Wind energy systems," *Proceedings of the IEEE*, vol. 105, pp. 2116–2131, Nov 2017.

[16] Y. Yang, *OWA Dynamics and harmonics in 50 Hz AC Offshore Networks (DH50Hz) - Harmonics Studies*. 2017.

[17] O. Gomis and E. Prieto, "V3 principles for power electronics based generation," 2018.

[18] X.-Q. Guo, W.-Y. Wu, and H.-R. Gu, "Phase locked loop and synchronization methods for gridinterfaced converters: A review," vol. 87, pp. 182–187, 01 2011.

[19] O. G. Enric Sánchez, Eduardo Prieto, "Interacciones de la red ac con electrónica de potencia [powerpoint slides]," 2017.

[20] X. Wang, L. Harnefors, and F. Blaabjerg, "Unified impedance model of grid-connected voltage-source converters," *IEEE Transactions on Power Electronics*, vol. 33, pp. 1775–1787, feb 2018.

[21] M. Cheah-Mane, L. Sainz, E. Prieto-Araujo, and O. Gomis-Bellmunt, "Impedance-based analysis of harmonic instabilities in hvdc-connected offshore wind power plants," *International Journal of Electrical Power & Energy Systems*, vol. 106, pp. 420–431, 2019.

[22] M. Cespedes and J. Sun, "Impedance modeling and analysis of grid-connected voltage-source converters," *IEEE Transactions on Power Electronics*, vol. 29, pp. 1254–1261, March 2014.

[23] Y. Sun, E. De Jong, J. Cobben, and V. Cuk, "Offshore wind farm harmonic resonance analysis—part i: Converter harmonic model," in *2017 IEEE Manchester PowerTech*, pp. 1–6, IEEE, 2017.

[24] L. Sainz, M. Cheah-Mane, L. Monjo, J. Liang, and O. Gomis-Bellmunt, "Positive-net-damping stability criterion in grid-connected vsc systems," *IEEE Journal of Emerging and Selected Topics in Power Electronics*, vol. 5, pp. 1499–1512, Dec 2017.

[25] Y. Sun, "The impact of voltage-source-converters' control on the power system: the stability analysis of a power electronics dominant grid," 2018.

[26] R. Zheng, M. H. Bollen, and J. Zhong, "Harmonic resonances due to a grid-connected wind farm," in *Proceedings of 14th International Conference on Harmonics and Quality of Power-ICHQP 2010*, pp. 1–7, IEEE, 2010.

[27] L. BeloquiLarumbe, Z. Qin, and P. Bauer, "Introduction to the analysis of harmonics and resonances in large offshore wind power plants," in *2018 IEEE 18th International Power Electronics and Motion Control Conference (PEMC)*, pp. 393–400, IEEE, 2018.

[28] M. Bradt, B. Badrzadeh, E. Camm, D. Mueller, J. Schoene, T. Siebert, T. Smith, M. Starke, and R. Walling, "Harmonics and resonance issues in wind power plants," in *PES T&D 2012*, pp. 1–8, IEEE, 2012.

[29] L. H. Kocewiak, J. Hjerrild, and C. L. Bak, "Harmonic analysis of offshore wind farms with full converter wind turbines," in *8th International Conference on Large-Scale Integration of Wind Power into Power Systems*, pp. 1–6, Energynautics GmbH, 2009.

[30] I. V. Blagouchine and E. Moreau, "Analytic method for the computation of the total harmonic distortion by the cauchy method of residues," *IEEE Transactions on Communications*, vol. 59, pp. 2478–2491, 2011.

[31] M. K. Bakhshizadeh, J. Hjerrild, Ł. Kocewiak, B. Hesselbæk, T. Sørensen, F. Blaabjerg, C. L. Bak, and F. F. da Silva, "Harmonic modelling, propagation and mitigation for large wind power plants connected via long hvac cables: review and outlook of current research," in *2016 IEEE International Energy Conference (ENERGYCON)*, pp. 1–5, IEEE, 2016.

[32] R. de Groot, "Method for harmonic and tov connection impact assesment of offshore wind power plants," in *17th Int'—Wind Integration Workshop Stockholm Sweden*, TenneT TSO BV, 2018.

[33] L. Harnefors, X. Wang, A. G. Yepes, and F. Blaabjerg, "Passivity-based stability assessment of grid-connected vscs—an overview," *IEEE Journal of emerging and selected topics in Power Electronics*, vol. 4, no. 1, pp. 116–125, 2016.

[34] E. Ebrahimzadeh, F. Blaabjerg, X. Wang, and C. L. Bak, "Harmonic stability and resonance analysis in large pmsg-based wind power plants," *IEEE Transactions on Sustainable Energy*, vol. 9, no. 1, pp. 12–23, 2018.

[35] X. Wang, F. Blaabjerg, and M. Liserre, "An active damper to suppress multiple resonances with unknown frequencies," in *2014 IEEE Applied Power Electronics Conference and Exposition-APEC 2014*, pp. 2184–2191, IEEE, 2014.

[36] L. H. Kocewiak, *Harmonics in large offshore wind farms*. Department of Energy Technology, Aalborg University, 2012.

[37] D. Yang, X. Wang, and F. Blaabjerg, "Sideband harmonic instability of paralleled inverters with asynchronous carriers," *IEEE Transactions on Power Electronics*, vol. 33, no. 6, pp. 4571–4577, 2018.

[38] X. Wang and F. Blaabjerg, "Harmonic stability in power electronic based power systems: concept, modeling, and analysis," *IEEE Transactions on Smart Grid*, 2018.

[39] B. Kroposki, B. Johnson, Y. Zhang, V. Gevorgian, P. Denholm, B.-M. Hodge, and B. Hannegan, "Achieving a 100% renewable grid: Operating electric power systems with extremely high levels of variable renewable energy," *IEEE Power and Energy Magazine*, vol. 15, no. 2, pp. 61–73, 2017.

[40] M. K. Bakhshizadeh, F. Blaabjerg, J. Hjerrild, X. Wang, Ł. Kocewiak, and C. L. Bak, "A numerical matrix-based method for stability and power quality studies based on harmonic transfer functions," *IEEE Journal of Emerging and Selected Topics in Power Electronics*, vol. 5, no. 4, pp. 1542–1552, 2017.

[41] "Parallel resonance and parallel rlc resonant circuit. retrieved at: https://www.electronics-tutorials.ws/accircuits/parallel-resonance.html," Oct 2018.

[42] A. Holdyk, J. Holbøll, E. Koldby, and A. Jensen, "Influence of offshore wind farms layout on electrical resonances," in *45th Session of the International Council on Large Electric Systems*, International Council on Large Electric Systems, 2014.

[43] J. H. Enslin and P. J. Heskes, "Harmonic interaction between a large number of distributed power inverters and the distribution network," *IEEE transactions on power electronics*, vol. 19, no. 6, pp. 1586–1593, 2004.

[44] F. De La Rosa, *Harmonics and power systems*. CRC press Boca Raton, 2006.

[45] A. Baggini, *Handbook of power quality*. John Wiley & Sons, 2008.

[46] P. van Oirsouw and J. Cobben, *Netten voor distributie van elektriciteit*. Phase to Phase, 2011.

[47] K. Jansen, B. Van Hulst, C. Engelbrecht, P. Hesen, K. Velitsikakis, and C. Lakenbrink, "Resonances due to long hvac offshore cable connections: studies to verify the immunity of dutch transmission network," in *2015 IEEE Eindhoven PowerTech*, pp. 1–6, IEEE, 2015.

[48] J. T. Bialasiewicz and E. Muljadi, "The wind farm aggregation impact on power quality," in *IECON 2006-32nd Annual Conference on IEEE Industrial Electronics*, pp. 4195–4200, IEEE, 2006.

[49] R. King and J. B. Ekanayake, "Harmonic modelling of offshore wind farms," in *IEEE PES General Meeting*, pp. 1–6, IEEE, 2010.

[50] M. McGranaghan and G. Beaulieu, "Update on iec 61000-3-6: Harmonic emission limits for customers connected to mv, hv, and ehv," in *Transmission and Distribution Conference and Exhibition*, pp. 1158–1161, 2006.

[51] Ł. Kocewiak, C. Álvarez, P. Muszynski, J. Cassoli, and L. Shuai, "Wind turbine harmonic model and its application–overview, status and outline of the new iec technical report," in *14th International Workshop on Large-Scale Integration of Wind Power into Power System as well as on Transmission Networks for Offshore Wind Power Plants*, 2015.

[52] A. H. Soloot, H. J. Bahirat, H. K. Høidalen, B. Gustavsen, and B. A. Mork, "Investigation of resonant overvoltages in offshore wind farms-modeling and protection," in *International Conference on Power Systems Transients (IPST)*, 2013.

[53] M. Cheah, *Offshore wind integration through high voltage direct current systems.* PhD thesis, Cardiff University, 2017.

[54] G. Levačić, I. Uglešić, B. Jurišić, and B. Filipović-Grčić, "Influence of cables on power transmission network frequency response," *Tehnički vjesnik: znanstveno-stručni časopis tehničkih fakulteta Sveučilišta u Osijeku*, vol. 20, no. 1, pp. 1–8, 2019.

[55] J. Sun, "Impedance-based stability criterion for grid-connected inverters," *Power Electronics, IEEE Transactions on*, vol. 26, pp. 3075 – 3078, 12 2011.

[56] L. Harnefors, A. G. Yepes, A. Vidal, and J. Doval-Gandoy, "Passivity-based controller design of grid-connected vscs for prevention of electrical resonance instability," *IEEE Transactions on Industrial Electronics*, vol. 62, no. 2, p. 702–710, 2015.

[57] L. Greedy and T. Schlemmer, *66 kV Systems for Offshore Wind Farms.* 2015.

[58] Prysmian, "High voltage cables."

[59] *Chapter 7. Impedance and Filters. A Way to Analyze RC Circuits. Retrieved at: https://web.stanford.edu/class/archive/engr/engr40m.1178/reader/chapter7.pdf.*

[60] L. Soder and M. Ghandhari, *Static Analysis of Power Systems.* 2015.

[61] Y. Amirnaser, *Voltage - sourced converters in power systems: modeling, control, and applications.* IEEE Press, 2012.

[62] "Renewable energy: Moving towards a low carbon economy. retrieved at: https://ec.europa.eu/energy /en/topics/renewable-energy."

[63] *Automation Library. Retrieved at: https://hvdc.ca/uploads/knowledge_base/ automationlibraryreference4_6_2.pdf?t=1536325095.* Aug 2018.